LATE EOCENE SEA SURFACE TEMPERATURES: INSIGHTS FROM *CRASSOSTREA GIGANTISSIMA*

by

MATT JARRETT

(Under the Direction of Chris Romanek)

ABSTRACT

Isotopic temperatures from Late Eocene (35±0.5Ma) *Crassostrea gigantissima*(Finch, 1824) agree well with a steady Middle to Late Eocene cooling trend seen in previously published isotope data from mollusks and benthic foraminifera. Oysters were collected from along the Savannah River at Griffins Landing in Burke County Georgia to address paleotemperatures during the Late Eocene. Specimens underwent sclerochronological analysis by high resolution microdrilling for carbon and oxygen isotope content. Prior to drilling, cathodoluminescence as well as thin section petrography was performed to assure pristine material. Results from 177 $\delta^{18}O_{calcite}$ analyses from the left valves of three shells range from -2.45‰ to 0.57‰ (PDB), and suggest average annual temperature of ~19ºC and an average annual range of ~15º to 23ºC. Compared to modern Georgia Coast temperatures, Late Eocene climate was similar during winter and 2ºC - 8ºC cooler during summer. Data also show agreement with 35Ma temperatures from the Gulf Coastal Plain.

INDEX WORDS: Late Eocene, Paleoclimates, Sclerochronology, Crassostrea

LATE EOCENE SEA SURFACE TEMPERATURES: INSIGHTS FROM *CRASSOSTREA GIGANTISSIMA*

by

MATT B. JARRETT

B.S., Georgia Southwestern State University, 2005

A Thesis Submitted to the Graduate Faculty of The University of Georgia in Partial Fulfillment of the Requirements for the Degree

MASTER OF SCIENCE

ATHENS, GEORGIA

2009

LATE EOCENE SEA SURFACE TEMPERATURES: INSIGHTS FROM *CRASSOSTREA GIGANTISSIMA*

by

MATT JARRETT

Major Professor: Christopher S. Romanek

Committee: Bruce Railsback
Doug Crowe

Electronic Version Approved:

Maureen Grasso
Dean of the Graduate School
The University of Georgia
August 2009

TABLE OF CONTENTS

Page

LIST OF TABLES

Page

LIST OF FIGURES

Page

Chapter 1

Introduction

The fossil record preserves some of the best evidence in support of evolution as well as the fullest and most accurate record of climatic and environmental change throughout earth's history (Zalasiewicz, 2006). The study of these climatic changes as well as the potential drivers and possible effects on ancient flora, fauna, and sea level is called paleoclimatology (Keller, 1982; Miller et al. 1987; Sloan and Barron, 1992; Greenwood and Wing, 1995). Understanding the effects of temperature is important because biological processes such as growth rate, metabolism, and reproduction are somewhat dependent on temperature (Vermeij, 1978). This is especially important for invertebrate marine fauna because their body temperature is dependent on ambient water temperature (Valentine, 1973).

Two important metrics of paleoclimatology are: 1) mean annual temperature (MAT) and 2) mean annual range in temperature (MART). Both variables strongly influence the geographic distribution of marine organisms. Corals, for example, are not well suited for climates in which the MAT is below approximately 20-22ºC (Valentine, 1973). On the other hand, because certain biological processes are influenced by temperature, there is usually an 'optimal' temperature range (MART) in which a given species is adapted to live (Valentine, 1973).

The study of paleoclimatology was revolutionized during the mid-twentieth century by the pioneering work of Epstein et al. (1953) who demonstrated that the

oxygen isotope content of calcite was dependent upon the water temperature at which the calcite formed. Epstein's work provided a quantitative basis upon which paleoclimate determinations could be made. Emiliani (1955) and Shackleton and Opdyke (1973) capitalized on the newly developed quantitative techniques by examining the oxygen isotope composition of benthic foraminifera of deep sea cores. These early works evaluated broad scale temperature changes through time. Following these early studies, planktonic and benthic foraminifera from deep sea cores were a staple of paleoclimate research (Shackelton and Boersma, 1981; Miller et al., 1987; Zachos et al., 1994), although they rarely yield temperature information at the sub-annual level (i.e., MART). Sub-annual temporal resolution in temperature may be resolved using a technique called sclerochronology which is defined as: "the study of physical and chemical variations in the accretionary hard tissues of organisms, and the temporal context in which they formed" (Jones et al., 2007). Mollusks are especially useful in this regard because they generally grow shell throughout the year (Jones and Quitmyer, 1996; Goodwin et al., 2003), thereby providing a high resolution record of seasonal environmental information.

Eocene Climatology

In the period of time spanning from the Middle Eocene to the Early Oligocene, the earth underwent many tectonic events which shaped the climatic and oceanic circulation system we see today. Of the more important events was the establishment of the Antarctic Circumpolar Current (ACC), which developed in the southern hemisphere with the opening of the Drake Passage when Australia and Antarctica separated (Kennett, 1977). The establishment of the ACC resulted in rapid cooling of the southern hemisphere.

Prior to the opening of the passage (Early Eocene), global ocean temperature was sufficiently warm to preclude the formation of ice at the poles even in winter (Prothero, 1994). This Early Eocene "greenhouse world" deteriorated with a major cooling event at the boundary between the Middle and Late Eocene and was accompanied by a minor transgression in sea level (Hansen, 1987). The onset of Late Eocene cooling is marked by a major extinction in tropical foraminifera followed by an equatorial migration of mid-latitude fauna (Keller, 1982). Mid-latitude foraminifera persisted in the equatorial regions until a second cooling event occurred in the Late Eocene when these fauna were replaced by cooler, mid-high latitude species (Keller, 1982). In the transition from the Eocene to the Oligocene, the greatest cooling occurred at the poles while the lower latitudes experienced only minor cooling (Zachos et al., 1994).

These events resulted in significant extinction events and faunal turnovers (Hansen, 1987; Prothero, 1994; Haasl and Hansen, 1996). Although this is the most climatically unstable time interval recognized in the Paleogene (Keller, 1982), it is not expressed in the fossil record as a single abrupt event, but rather several sequences of faunal abundance change (Miller, 1992).

Coastal Plain Paleoclimate Studies

The Coastal Plain units of the Southeastern U.S. comprise one of most studied Paleogene marine shelf sections in the world due to the exceptional preservation of aragonitic mollusks (Palmer, 1937; Palmer and Brann, 1965; 1966; Toulmin, 1977). Two prominent studies have examined Eocene paleoclimates using fossils collected in the Southeastern U.S., and both used mollusks from the Gulf Coastal Plain (GCP). In the first study, Andreasson and Schmitz (2000) determined seasonal temperatures for the

early Middle Eocene (43 ma) for comparison with data from correlative beds deposited at higher latitudes. Andreasson and Schmitz (2000) showed that early Middle Eocene GCP summer temperatures were similar to the present, with winter temperatures being 7-8ºC higher than today. A comparison of MAT data from Andreasson and Schmitz (2000) and modern sea surface MAT data for the gulf coast (Kobashi and Grossman, 2003) indicates that MAT in the early Middle Eocene was 1-2ºC warmer than the present. Andreasson and Schmitz (2000) also showed that at higher latitude (North Atlantic), average temperatures (MAT), were 8-10ºC higher during the early Middle Eocene compared to the present North Atlantic, with the range in temperature (seasonality) being similar. Also, temperature data from Andreasson and Schmitz (2000) were higher than temperatures predicted by Eocene climate model simulations based on atmospheric CO_2 concentrations (Sloan, 1994; Sloan and Rea, 1995). The goal of Andreasson and Schmitz (2000), was to examine paleoclimate over a latitudinal gradient using average paleotemperatures and paleotemperature ranges. This is a valuable exercise because latitudinal gradients in temperature allow for a better understanding of global energy distributions over time and space.

In the second study, Kobashi et al. (2001) addressed Eocene paleotemperature discrepancies between the predictions of low latitude temperatures based on computer simulations (as described above) and those inferred from the oxygen isotope composition of foraminifera. The computer models predicted that Eocene temperatures were warmer than at present, while the foraminifera record suggested cooler temperatures than at present. Kobashi et al. (2001) addressed this problem by comparing foraminiferal sea-surface temperature (SST) estimates with data from isotope profiles of GCP mollusks.

Their isotopic temperatures showed that the gulf coast was warmer than the present (by 4-5ºC MAT). This estimate is consistent with the mollusk records of Andreasson and Schmitz (2000) as well as fish otolith data from Ivany et al. (2003). Kobashi et al. (2001) concluded that a thermally less stratified ocean during the Eocene easily overturned during winter cooling which resulted in a higher sea-surface nutrient content. As a result, foraminiferal productivity shifted towards the winter months rather than the summer. Mollusk data from Kobashi et al. (2001) showed warmer low-latitude temperatures than the present paired with significantly elevated winter temperatures in the Early Eocene. These results are in agreement with computer models of atmospheric CO_2 concentrations which suggests that elevated CO_2 levels would induce winter warming more-so than summer warming.

The results of the two prior studies help to resolve discrepancies between foraminifera $\delta^{18}O$ and model predictions as well as shed some light on how latitude global energy transport influence physical and biological oceanographic processes.

Historical Overview

While the previous two studies characterized paleoclimate from GCP stratigraphic sections (Figure 1.1), very little climatological work has focused on Atlantic Coastal Plain (ACP) sections. The Atlantic Coastal Plain is historically significant in the beds and fossils it contains. Prior to an 1824 essay by English Geologist John Finch, the coastal plain units of the southeastern U.S. had been simply regarded as 'Alluvium' (Howe, 1937). Finch, however, divided the coastal plain into seven major divisions, one of which was named Calcaire Ostrée for the large oysters it bore which are now known as *Crassostrea gigantissima* (Finch, 1824; Howe, 1937). Along the Georgia/South

Figure 1.1

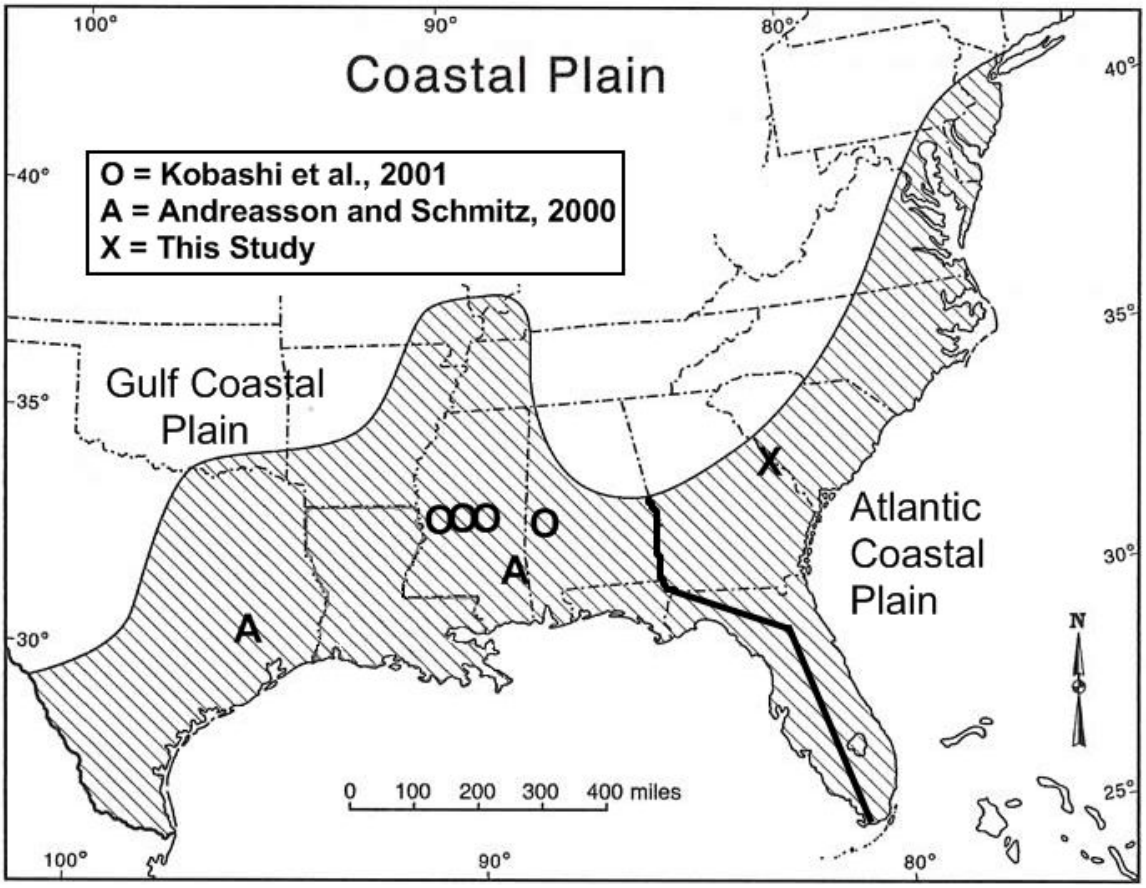

Figure 1.1 - Locality map for prior studies of paleoclimate using mollusks and current study. The thick black line through Florida and between Alabama and Georgia represents the generally accepted division between the Atlantic and Gulf Coastal Plains.

Carolina coastal plain, one of the most historically relevant geological localities is Shell Bluff, just south of Augusta, GA, along the Savannah River. The beds at Shell Bluff were visited by William Bartram in 1791 and Charles Lyell in 1842 (Howe, 1937). These oyster-bearing beds, which gave Shell Bluff its' name, also outcrop ~16 miles to the southeast along the Savannah River at Griffins Landing (Howe, 1937). Oysters collected from this locality form the basis of a paleoclimate investigation described below.

Stratigraphic Framework of Study Area

The Griffins Landing site is part of the Barnwell Group which was deposited during the Late Eocene (Figure 1.2). The dominant lithology of the Barnwell Group is quartz sand. The sands range in grain size from very fine to very coarse and they locally contain gravel lenses and mixtures of pebbles. Sorting can range from very well to very poor (Huddlestun and Hetrick, 1986). The Barnwell Group ranges as far west as Dooly and Crawford Counties in Central Georgia, and as far east as Lexington and Orangeburg counties in South Carolina. Updip, the Barnwell Group pinches out at the fall line while downdip, a facies change occurs in Screven and northern Effingham Counties where it grades into the Ocala Group. In Central Georgia, this change occurs in the southernmost parts of Houston, Pulaski, Dooly, and Bleckley counties (Huddlestun and Hetrick, 1986).

The Barnwell Group is divided into three formations: the Clinchfield Formation, the Dry Branch Formation, and the Tobacco Road Formation (Figure 1.3). The Clinchfield formation is characterized by four separate members, the Riggins Mill Member, the Treadwell Member, the Albion Member and the Utley Limestone. The Clinchfield Formation is dominantly quartz sand in Central Georgia where it consists of the Riggins Mill and Treadwell Members (Huddlestun and Hetrick, 1986). In Eastern

Figure 1.2

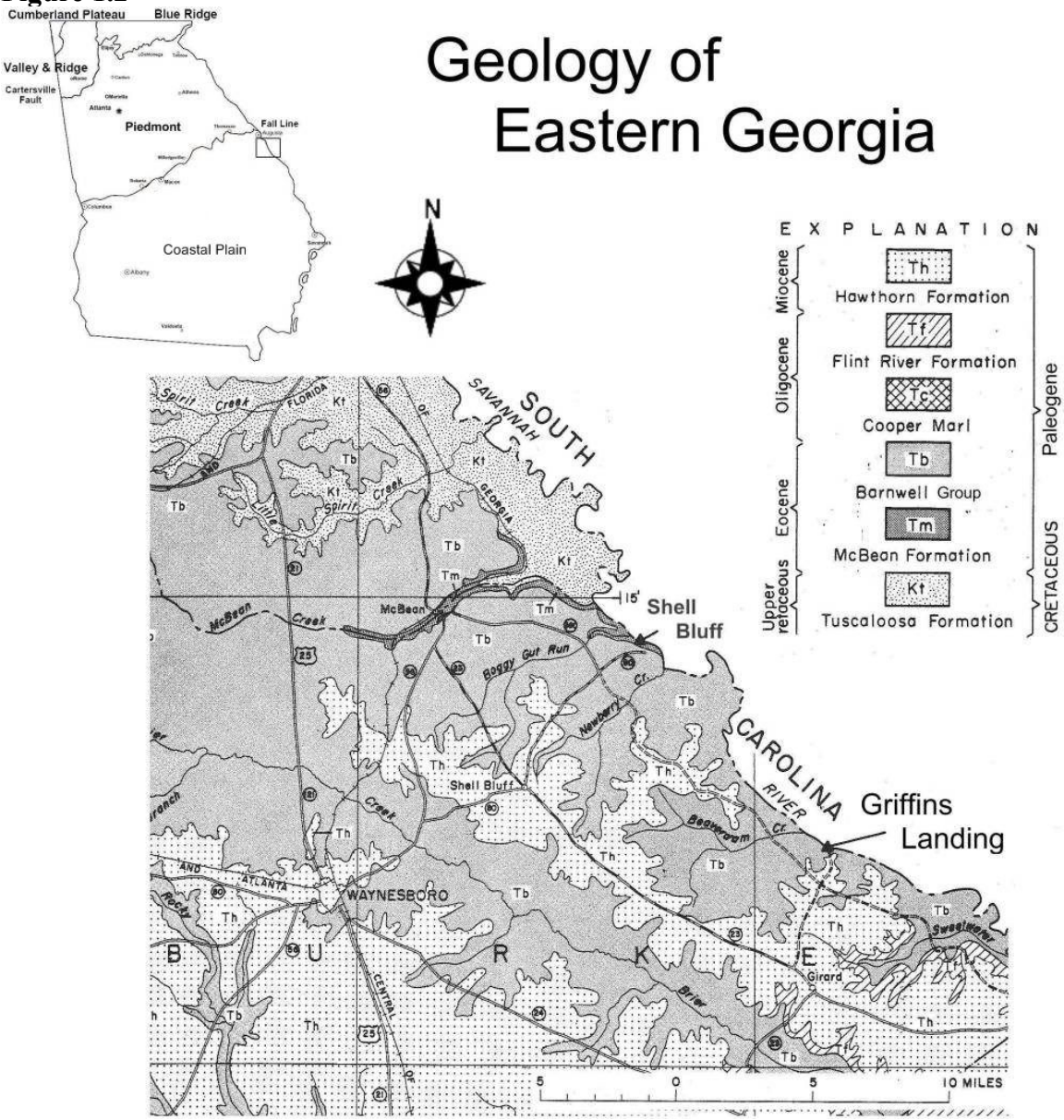

Figure 1.2 - General geologic map showing location of primary collection site at Griffins Landing. Map is adapted from Herrick et al. (1967).

Figure 1.3

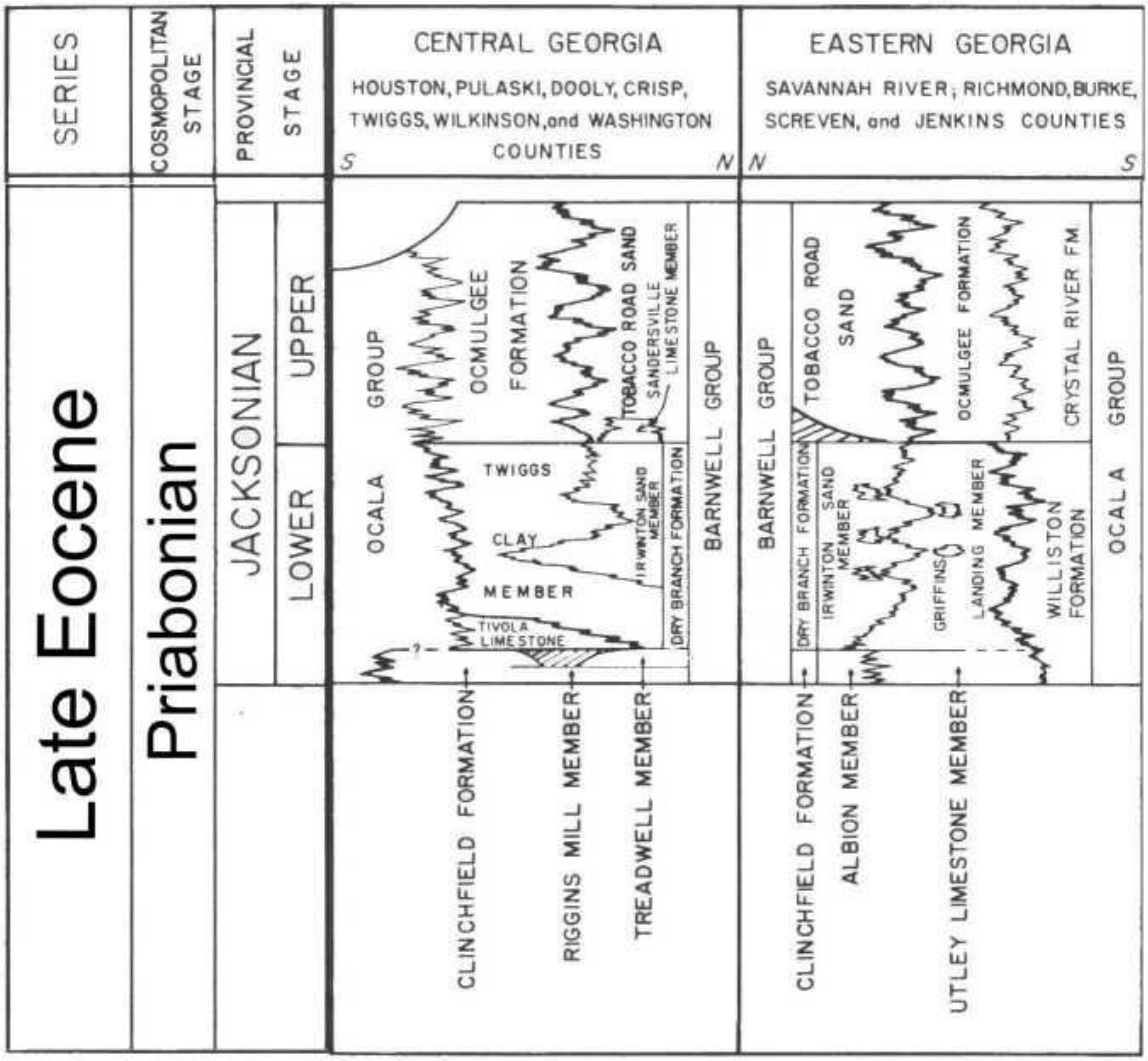

Figure 1.3 - Correlations for Late Eocene Barnwell Group between Central and Eastern Georgia. Adapted from Huddlestun and Hetrick, (1986).

Georgia (east of the Ogeechee river), the Clinchfield is less sandy where it consists of the Albion Sand Member (updip) and the Utley Limestone (downdip) (Huddlestun and Hetric, 1986). The Dry Branch Formation is characterized by three interfingering members, the Twiggs Clay Member, the Irwinton Sand Member, and the Griffins Landing Member. The Twiggs Clay Member is dominant in the west while the Irwinton Sand Member extends from central Georgia to Eastern Georgia. The Griffins Landing Member forms the base of the Dry Branch in Eastern Georgia and does not extend into Central Georgia (Huddlestun and Hetrick, 1986). The Tobacco Road Formation is not divided into members and is predominantly sand with other lithic components being only locally significant (Huddlestun and Hetrick, 1986). The Tobacco Road Sand extends as far west as southeastern Houston County and reaches its eastern limit in Aiken, northern Barnwell, and northern Orangeburg Counties in South Carolina (Huddlestun and Hetrick, 1986). The northernmost extent is in the vicinity of the fall line. A facies change occurs downdip in the Central Savannah River Area of Georgia where the Tobacco Road grades into the Ocala Group in Screven County.

The Griffins Landing Member (GLM) is the stratum of interest for this study and is a well-sorted, massive to vaguely and rudely bedded, calcareous sand (Huddlestun and Hetrick, 1986). In eastern Georgia near the vicinity of the Savannah River, the Irwinton Sand and Griffins Landing Members interfinger so complexly that distinguishing between the two in the field is difficult (Huddlestun and Hetrick, 1986). The bulk of many of the bluffs along the Savannah River in East Central Georgia consist of the Irwinton Sand Member, which outcrops as a buff-white calcareous argillaceous sand with local occurrences of ophiomorpha burrows. Microfossil analysis places the Griffins

Landing Member within calcareous nanoplankton zones NP 19-20 (Laws et al., 1992; Harris et al., 1993) and foraminifera zone P16; therefore, based on the timescale of Berggren et al. (1995), the Griffins Landing Member is ~35±0.5 million years old. Local abundances of the giant oyster *Crassostrea gigantissima* can be found in these outcrops and consist of oysters found in both life position and random orientation (Huddlestun and Hetrick, 1986).

Griffins Landing Member Paleoenvironment

Paleoenvironmental interpretations of the Griffins Landing Member (GLM) vary but all consider the depositional environment to be a marginal coastal marine setting (Zullo and Kite, 1985; Fallaw and Price, 1992; Thayer and Harris, 1992). Planktonic foraminifera identified from the GLM in core material from the Department of Energy's Savannah River Site (SRS) reveal evidence of some open ocean influence while foraminifera collected from Crassostrea-bearing beds exposed along the Savannah River indicate a bay or lagoonal environment (Fallaw and Price, 1992). Thayer and Harris (1992) suggest the GLM was deposited in relatively clear waters of normal marine salinity as indicated by faunal elements, with the presence of abraded gravel and sand sized skeletal allochems, which suggest alternations between high energy and quiet water deposition in which mud accumulated. Based on barnacle data, the GLM was deposited in a subtidal to inner shelf environment (Zullo and Kite, 1985). These paleoenvironmental interpretations serve as a testament to known environmental variability that occurs in near-shore settings (Prothero and Schwab, 2004).

Crassostrea gigantissima

In the updip areas at the base of the GLM, oyster beds of *Crassostrea gigantissima* are common (Huddlestun and Hetrick, 1986). *C. gigantissima* (Finch, 1824), is thought to be the evolutionary ancestor of the American oyster *C. virginica* (Lawrence, 1995). Significantly larger in size than its descendant, the length of *C. gigantissima* has been recorded at up to 26 inches (Figure 1.4). Significant thickening of the left valve by the formation of chambers is commonly observed in cut sections (Lawrence, 1995). Life spans of ~11 years have been estimated from Oligocene specimens (Kirby, 2000). *C. gigantissima* was once regarded as an index fossil for the 'Jackson Group' (Late Eocene), but the presence of the oyster in the Late Oligocene deposits of North Carolina do not support this conclusion (Lawrence, 1995).

Ontogenetic Analysis

It is important to understand life history traits of *C. gigantissima* before any paleoclimatic analysis of their shells is undertaken. This can be done by the examination of annual growth patterns in their shells. Annual growth patterns expressed in the shells of extant species of the eastern oyster (*Crassostrea virginica*) can be found within a portion of the shell of the left valve called the chondrophore (Figure 1.5). In some specimens, annual growth patterns are expressed within the chondrophore as small morpholigical ridges and valleys that give this area of the shell a 'washboard' appearance (Kent, 1988; Lawrence, 1988). Prior studies have interpreted these patterns to represent annual growth in the sense that the small morphological ridges represent warmer months of the year while the valleys represent cooler months (Kent, 1988; Lawrence, 1988). This hypothesis has been supported through the use of oxygen isotopes in both recent,

Figure 1.4

Figure 1.4 - *Crassostrea gigantissima* specimen shown beside a 24" crowbar for scale. This specimen is broken at the ventral margin.

Figure 1.5

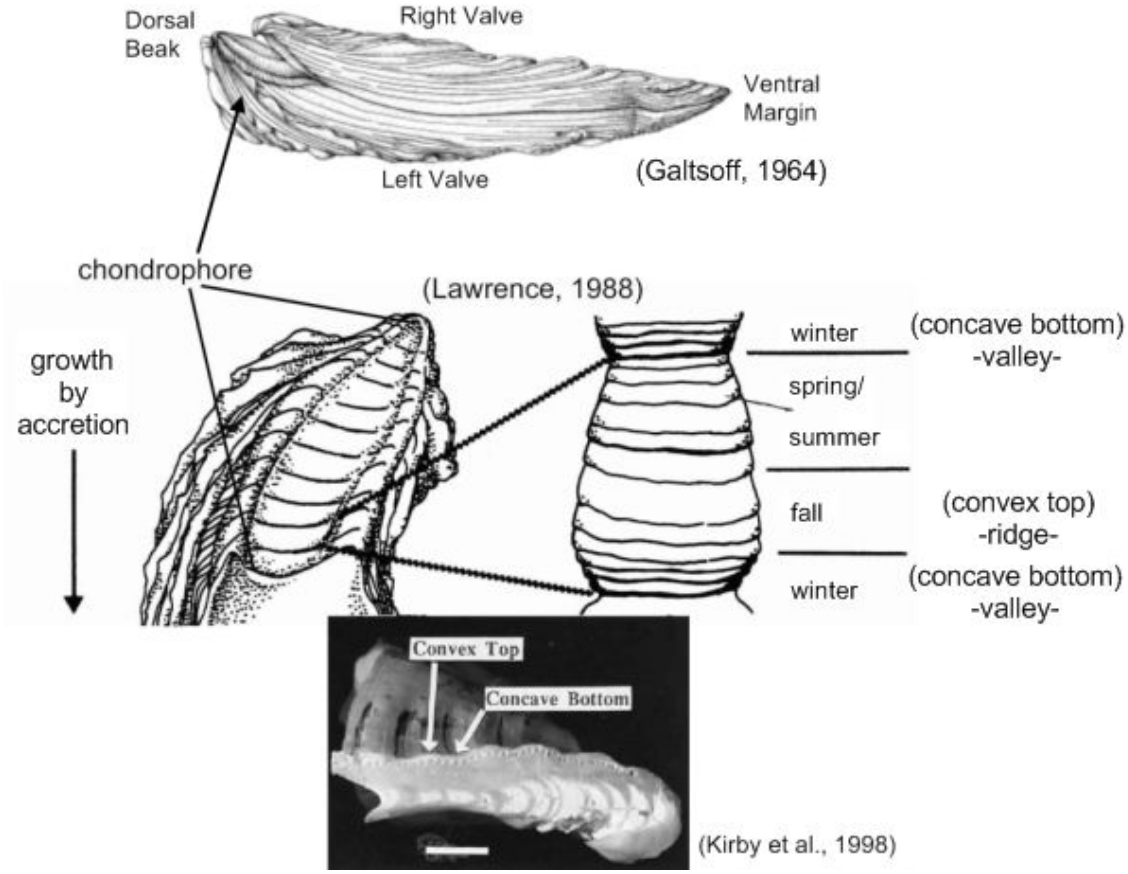

Figure 1.5 – Anatomical features of *Crassostrea gigantissima* with a detailed view of the chondrophore area of the left valve of an oyster including a cross section cut parallel to growth direction shown at the bottom for emphasis. Convex tops represent ridges while concave bottoms represent valleys. Kirby (1998; 2000) suggests that ridges represent summer growth while valleys represent winter growth.

and fossil *Crassostrea* (Andrus and Crowe, 2000, Kirby, 2000). The examination of these features has been applied to archaeological studies of ancient shell middens for the determination of both age and season of capture (Kent, 1988; Lawrence, 1988; Custer and Doms, 1990; Andrus and Crowe, 2000).

Shell Mineralogy and Microstructure

Accurate paleoclimate interpretations can only be obtained if the shells being sampled are unchanged since the time of deposition. This can be evaluated by the examination of *C. gigantissima* shells under thin section petrography. *C. gigantissima,* secretes a shell of both foliated and chalky calcite (Kirby, 2000). The chondrophore consists primarily of foliated calcite which has a fibrous microstructural appearance when examined under thin section petrography and can be recognized by the presence of sweeping extinction across visible parallel growth bands (Taylor et al., 1969).

Experimental Rationale

To aid in our understanding of Late Eocene climate along the Atlantic Coastal Plain, specimens of the giant oyster *Crassostrea gigantissima* (Finch, 1824) were collected from Griffins Landing along the Savannah River for paleoclimate analysis. Following collection in the field, shells were prepared and examined to evaluate the integrity of the shell using a procedure described below. If the chondrophore of the left valve of individual specimens was determined to be unaltered, the shell was serially sampled for carbon and oxygen isotope analysis producing a record that spans several years of growth for each individual. This strategy facilitated the examination of annual seasonality (MART) as well as average annual temperatures (MAT) for the Late Eocene of the ACP.

Of important relevance to this study, previous research has confirmed that oyster calcite is secreted in oxygen isotopic equilibrium with seawater (Surge, 2001). Measured $\delta^{13}C$ and $\delta^{18}O$ values were used to further assess the diagenetic character of each sample by comparing the $\delta^{13}C$ and $\delta^{18}O$ values from specimens to measured values from associated carbonates of known diagenetic origin. In addition, $\delta^{13}C$ and $\delta^{18}O$ values were also used in the determination of paleoenvironment through comparison with $\delta^{13}C$ and $\delta^{18}O$ values from modern mollusks collected in known environments. Oxygen isotope profiles were used in the reconstruction of paleotemperatures. MAT was determined by taking the overall average $\delta^{18}O$ value from unaltered samples from each profile to calculate average temperatures which were then averaged using all the shells collected at that study site together. MART was determined in a similar way by taking both the single most negative and most positive $\delta^{18}O$ values from each to calculate a minimum winter and maximum summer temperature. Calculated temperatures were compared to modern Atlantic Coast sea-surface temperatures and were placed within the context of the current Eocene paleotemperature data from the GCP for comparison of Late Eocene ACP and GCP paleotemperatures.

Research Objectives:

1. Identify *C. gigantissima* shells at Griffins Landing that contain unaltered material that may be used in the study of paleoclimate.
2. Define the environment of deposition from isotope composition.
3. Construct shell isotope profiles and link the isotopic record to other periodic structures in the shell.
4. Interpret paleotemperatures and determine MAT and MART.
5. Compare paleotemperatures between ACP and GCP sections.
6. Place MAT and MART of the Late Eocene of the ACP within a framework of climate change established by other studies of the Southeastern US and other low latitude settings.

Chapter 2

Stable Isotope Geochemistry

The analysis of the stable isotopes of carbon and oxygen are applied to a broad array of studies of carbonate minerals (Hoefs, 1997; Fry, 2006; Griffiths, 2006). There are three stable isotopes of oxygen: ^{16}O, ^{17}O, and ^{18}O. The most common isotope is ^{16}O which comprises about 99.763% of the oxygen on earth, followed by ^{18}O which accounts for 0.1995%, and ^{17}O which accounts for 0.0375% (Hoefs, 1997). There are two stable isotopes of carbon: ^{12}C and ^{13}C. The relative abundance of carbon isotopes is approximately 98.9% and 1.1% for ^{12}C and ^{13}C, respectively (O'Leary, 1988).

While carbon and oxygen isotope abundances remain relatively constant in nature, the slight differences in mass between the isotopes of these elements give rise to small differences in their relative abundances among materials because compounds can exchange isotopes during physicochemical and biological processes (Hoefs, 1997). The exchange of isotopes between reactants and products at equilibrium produces predictable distribution patterns, which can be described by a quantitative relationship referred to as an 'isotope effect'. In other reactions, isotope fractionation does not reach an equilibrium condition and isotope distributions depend on the reaction rates of the isotopically substituted molecules; these relationships can be defined quantitatively in an analogous fashion as a 'kinetic effect' (Eby, 2004). During kinetically controlled processes, the products are preferentially enriched in the isotope of lower relative mass.

An example of an isotope effect can be demonstrated by the evaporation of water into a closed space at 100% relative humidity (i.e., an equilibrium state exists between liquid and gaseous water). Both the forward (evaporation) and the backward (condensation) reaction occur at equal rates (i.e., no net flux of mass in either direction), yet the oxygen isotope ratios of each phase are distinct. This is because at a given temperature the vapor pressures differ between molecules of water of different relative mass. As a result, water vapor will be enriched in ^{16}O compared to liquid water (Eby, 2004).

Alternatively, a kinetic effect is observed when water evaporates in an open space at <100% relative humidity. As the water evaporates, the liquid phase becomes preferentially enriched with respect to ^{18}O compared to the equilibrium condition (isotope effect) because the molecules of water containing ^{16}O evaporate preferentially without a significant back (condensation) reaction.

The stable isotope composition of natural materials is often characterized using a convention termed 'delta notation' (Hoefs, 1997). To obtain delta values, the ratio of the stable isotopes of an element in a sample (R_{samp}) are divided by the ratio of a known standard (R_{std}) and the quotient is expressed in parts per thousand or 'per mill' units ('‰'; Hoefs, 1997) using the equation: $\delta = (R_{samp} / R_{std} - 1) * 1000$. The isotope of lower relative abundance is placed in the numerator of R while the more common isotope is placed in the denominator. The standard used will depend on the element being analyzed and the interests of the researcher. There are two standards used in oxygen isotope studies of carbonate minerals: Vienna Peedee Belemnite (VPDB) and Vienna Standard Mean Ocean Water (VSMOW), while carbon isotope studies use VPDB (Hoefs, 1997).

Oxygen Composition of Natural Waters

By definition, the global mean $\delta^{18}O$ value for seawater is 0‰ (SMOW). Surface ocean water is relatively well mixed, so this value is nearly constant throughout the world (Epstein and Mayeda, 1953; Hoefs, 1997). Evaporative processes occurring near the equator produce air masses that contain water vapor depleted in ^{18}O relative to seawater. As these air masses are driven towards the poles, a decrease in temperature results in condensation of the vapor (Faure, 1998), resulting in the preferential removal of ^{18}O in rainwater. With continual condensation, northward moving water vapor becomes progressively depleted in ^{18}O. This process is described as Rayleigh Distillation and results in a predictable latitudinal decrease in the $\delta^{18}O$ value of atmospheric water (Faure, 1998). The $\delta^{18}O$ value for freshwater of rivers and lakes is variable and generally a reflection of the $\delta^{18}O$ value of the rainfall in the drainage area as well as being lower in $\delta^{18}O$ value marine water (Hoefs, 1997)(Figure 2.1).

Temporal Changes in the $\delta^{18}O$ Value of Seawater

The $\delta^{18}O$ value of seawater ($\delta^{18}O_{sw}$) can be modified on a global scale when water is removed from the system and stored in the form of polar ice. If this water experiences Rayleigh Distillation prior to storage as polar ice, a significant portion of ^{16}O can be removed from the world's oceans leading to an increase in the average $\delta^{18}O$ value for seawater. Estimation of the change in the $\delta^{18}O$ value of seawater ($\delta^{18}O_{sw}$) throughout earth's history has been aided in large part through the study of benthic foraminifera in deep sea cores. The accuracy of these estimates rests in the fact that during the Cenozoic the deep ocean does not experience seasonal, latitudinal, and geographical variations in temperature that are commonly expressed in surface ocean waters (Lear et al., 2000).

Figure 2.1

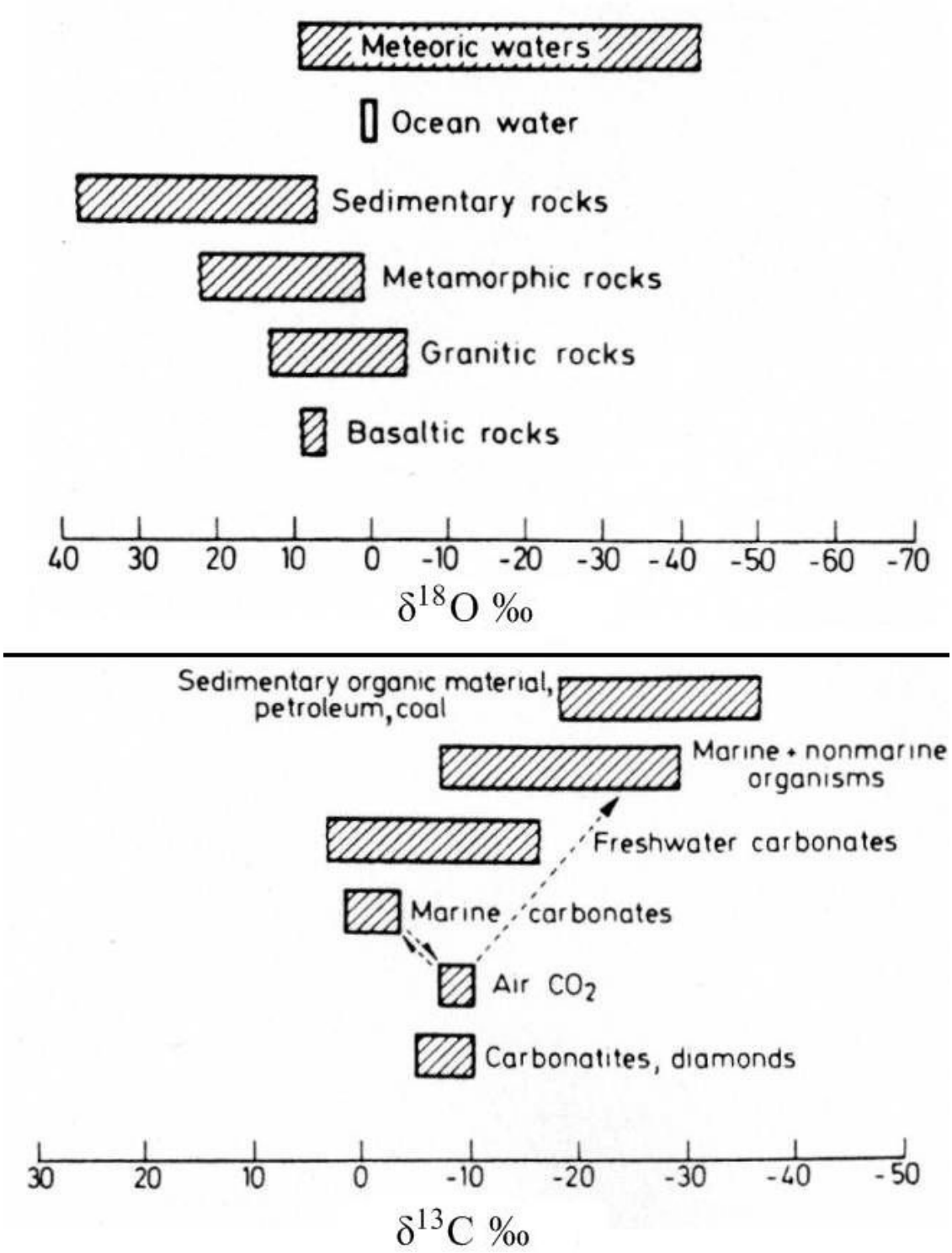

Figre 2.1 - Variations in the $\delta^{18}O$ and $\delta^{13}C$ values of natural materials. Note the difference in scales. Adapted from Hoefs (1997).

Attempts to constrain $\delta^{18}O_{sw}$ values for the Cenozoic Era have been made by assuming a minimum temperature value of 1-2ºC for bottom water temperatures in an ice-free world (Miller et al., 1987; Zachos et al., 1994). Using this temperature and a $\delta^{18}O_{sw}$ of 0‰, an equilibrium $\delta^{18}O$ value can be calculated for foraminifera of ~2.1‰ PDB for 1ºC (Zachos et al., 1994). Positive departures from this value can be attributed to an increase in the $\delta^{18}O$ value of seawater as a result of an increase in ice volume (Miller et al., 1987; Zachos et al., 1994). This technique and others (see below) may be used to estimate $\delta^{18}O_{sw}$ values for past periods in earth's history.

The prospect of calculating more accurate $\delta^{18}O$ values for seawater has been enhanced through the works of Zachos et al. (1994) and Lear et al. (2000). To extract $\delta^{18}O_{sw}$ values from the $\delta^{18}O$ value of benthic foraminifera, Mg/Ca ratios of shell carbonate were used to independently calculate paleotemperatures. This enabled Lear et al. (2000) to pair calculated Mg/Ca temperatures with the $\delta^{18}O$ values of the benthic foraminifera to independently determine the $\delta^{18}O$ value of seawater over time (Lear et al., 2000).

Zachos et al. (1994) observed that the $\delta^{18}O$ value of seawater not only varies with time but also with latitude. They gathered $\delta^{18}O$ values of surface seawater from the southern hemisphere at various latitudes to characterize the latitudinal dependence of $\delta^{18}O_{sw}$ values. Their best-fit function is:

$$\mathbf{\delta_{sw} = 0.576 + 0.041x - 0.0017x^2 + 1.35e\text{-}5x^3}$$

where x is latitude (between 0 and 70 degrees). Andreasson and Schmitz (2000) and Kobashi et al. (2001) (see Chapter 1) used the Cenozoic $\delta^{18}O_{sw}$ data presented by Lear et al. (2000) to constrain a global average value for $\delta^{18}O_{sw}$ which was then corrected for

latitude using the correction shown above from Zachos et al. (1994). The latitude specific value for $\delta^{18}O_{sw}$ was then used calculate paleotemperatures from the $\delta^{18}O$ values of shell carbonate. This technique can be applied to the calculation of a value of $\delta^{18}O_{sw}$ for the Late Eocene for this study. Griffins Landing is at ~33º latitude which returns a correction factor of 0.56‰ if this value is then added to the global average $\delta^{18}O_{sw}$ value for the Late Eocene (-0.9‰), the calculated $\delta^{18}O$ value for seawater that will be used in this study is -0.34‰.

Carbon Isotopes

Dissolved inorganic carbon (DIC) is the cumulative sum of the inorganic carbon species dissolved in water. It includes: aqueous carbon dioxide ($CO_{2(aq)}$), carbonic acid ($H_2CO_{3(aq)}$), bicarbonate ion ($HCO_3^-{}_{(aq)}$), and carbonate ion ($CO_3^{-2}{}_{(aq)}$). The $\delta^{13}C$ value of DIC can vary greatly in natural waters because of the distinct $\delta^{13}C$ values for carbon sources that contribute to the DIC pool and variability in pH. In marine systems, the main sources of carbon for DIC are carbonate minerals and atmospheric CO_2. Marine limestones generally have a $\delta^{13}C$ value around 0‰ (Hoefs, 1997), while atmospheric CO2 has a $\delta^{13}C$ value around -7‰ (Libes, 1992). The $\delta^{13}C$ value for marine DIC generally ranges from ~0 to 2‰ and this is due primarily to the buffering and exchange capacity of carbonate minerals in contact with marine water (Hoefs, 1997).

In freshwater environments, there are three main sources of carbon that control the $\delta^{13}C$ value of DIC ($\delta^{13}C_{DIC}$): variation and abundance of plant types in the drainage area, underlying bedrock, and atmospheric CO_2 (Geary et al., 1992). Plant material in a drainage basin is relatively enriched in ^{12}C compared to other DIC sources due to the discrimination against ^{13}C in the process of carbon fixation during photosynthesis

(O'Leary, 1988). The photosynthetic pathway used by a plant will affect the $\delta^{13}C$ value of its tissues. For example, the $\delta^{13}C$ value of C_3 plant tissue ranges from -23‰ to -34‰ (PDB), while C_4 plants generally range from -6‰ to -16‰ (Faure, 1998). Processes such as bacterial metabolism can oxidize plant material to CO_2, which can then dissolve in water forming DIC that is relatively enriched in ^{12}C when compared to other DIC sources (Faure, 1998). Carbon is also added to freshwater through rock weathering reactions because rainwater combines with atmospheric CO_2, forming a weak carbonic acid solution with a pH of ~5.7 which then reacts with rocks to produce DIC which has a $\delta^{13}C$ value that is relatively high compared to respired plant material (Railsback et al., 1996). For example carbonate rocks have $\delta^{13}C$ values that typically vary around 0 ± 3‰ (Hoefs, 1997). Atmospheric CO_2 is a minor source for carbon in freshwater systems and the equilibration between aqueous and gaseous CO_2 enriches the water in ^{13}C compared to the gas phase by about 7‰ (Hoefs, 1997). Overall, freshwater DIC has a more negative and variable $\delta^{13}C$ value than marine DIC because of the contribution of respired CO_2 from organic matter (Figure 2.1).

Mollusk Shell Carbonate

Shell secretion by mollusks is accomplished by an organ called the mantle which produces shell carbonate from the extrapallalial fluid (EPF) which is a mixture of biological and ambient fluids (Ponder and Lindberg, 2008). Due to biological fluid exchange that takes place during respiration and feeding, the percentage of various constituents, including DIC, in EPF can vary temporally (McConnaughey and Gillikin, 2008). Oxygen, on the other hand, is derived entirely (but not always) from ambient fluids because environmental water is the most dominant source of oxygen for the EPF.

It follows then, that the oxygen isotopic composition of mollusk shell carbonate is affected by the isotope composition of the ambient water while the carbon isotope composition is affected by both environmental and biological fluids.

The incorporation of oxygen isotopes within shell carbonate is controlled to some extent by a temperature dependent fractionation, which means that the $\delta^{18}O$ value of mollusk shells can serve as a valuable source of paleotemperature data. Epstein et al. (1953) were the first to develop the calcite paleotemperature equation, which can be used to calculate the "isotope temperature" of formation of calcite, provided the $\delta^{18}O$ value of the water from which the calcite precipitated is known:

$$\mathbf{t^{o}C = 16.5 - 4.3\delta + 0.14\delta^{2}}$$

where δ is obtained by subtracting the $\delta^{18}O$ value of water ($\delta^{18}O_w$) from the $\delta^{18}O$ value of the calcite ($\delta^{18}O_c$) sample. Using this equation, Epstein et al. (1953) showed that a negative correlation exists between the $\delta^{18}O$ value of calcite and temperature (0.23‰/°C) when the $\delta^{18}O$ value of water remains constant.

On the other hand, the carbon isotope composition of mollusk shells is primarily controlled by the $\delta^{13}C$ value of ambient DIC and DIC derived from the respired metabolic carbon that resides in bodily fluids (i.e. EPF). Nevertheless, it has been well documented that the $\delta^{13}C$ value of shell carbonate fluctuates to a varying degree with the $\delta^{13}C$ value of ambient DIC (Krantz et al., 1987; Geary et al., 1992; Wang et al., 1995; Andreasson et al., 1999; Surge and Lohman, 2001; Surge et al., 2003). One important factor that affects the $\delta^{13}C$ value of shell carbonate generated from DIC is the isotope fractionathion between HCO_3^- (the primary C-bearing species in ambient waters and biological fluids) and shell calcite (~1‰) or aragonite (2.7‰) (Romanek et al., 1992; Klein et al., 1996). It

should be noted though, that shell $\delta^{13}C$ values are typically a few ‰ lower than theoretical estimates derived using DIC-solid carbonate fractionation factors due to the incorporation of metabolic CO_2 (termed 'vital effects') into the shell (McConnaughey and Gillikin, 2008).

Paleoenvironmental Determination

Stable isotope data from mollusks can be viewed within the context of the information provided to potentially discern information about the environments in which they lived. This is an important concept in paleoclimate studies because in normal marine environments where variability in the value of seawater $\delta^{18\backslash}O$ is relatively low, variations in the $\delta^{18\backslash}O$ values of mollusk shells will primarily record changes in temperature. This contrasts with estuarine environments where large scale shifts in the $\delta^{18\backslash}O$ value of water may occur through freshwater-seawater mixing. As such, $\delta^{18}O$ values of shell are related to temperature but moreso the $\delta^{18}O$ value of water in substantive ways. Without an accurate estimate of the $\delta^{18}O$ of estuarine waters, unreasonable and or inaccurate paleotemperature calculations could easily result.

The stable isotope values of mollusk shells that lived in fresh water attest to the relative depletion of ^{18}O and ^{13}C in meteoric water compared to seawater (Hudson, 1977; Shanahan et al., 2005). Freshwater-seawater mixing alters the carbon and oxygen isotope composition of estuarine waters to an extent that is dependent on the mixing ratio (Kirby, 2000). Key fingerprints of freshwater-seawater mixing are concurrent negative excursions in both the $\delta^{13}C$ and $\delta^{18\backslash}O$ value of mollusk shell carbonate. This works especially well if the freshwater component is relatively low in $\delta^{18\backslash}O$ and $\delta^{13}C$ value

compared to the marine component of the mixed (estuarine) water (i.e., at higher latitudes) (Gillikin et al., 2004).

To discern the paleoenvironmental inferences that may be made from the isotope composition of mollusk shells, stable isotope data were obtained from both published literature and through donations of unpublished data. These data were derived from the shells of ~85 live specimens that were collected from known environments. Two types of comparisons were made using either: 1) the average oxygen and carbon isotope composition or 2) the range in values observed in a single shell. Average values were calculated from all the analyses of an isotope profile of a single shell while ranges were calculated by subtracting the single most negative value from the single most positive value of a profile.

Average isotope values from modern mollusks are compared in Figure 2.2. Mollusks from marine environments have a tendency to have relatively positive average $\delta^{13}C$ and $\delta^{18}O$ values. Relatively few marine shells plot in the region defined by negative average in both $\delta^{13}C$ and $\delta^{18}O$ values, while all estuarine shells plot within this region. Four shells from a lagoonal environment are included and they all have average $\delta^{18}O$ values near 0‰ and positive average $\delta^{13}C$ values. The effect of freshwater-seawater mixing in estuaries tends to drive the average $\delta^{13}C$ and $\delta^{18}O$ values of mollusk shell carbonate to more negative values compared to shell material deposited in normal marine environments (Figure 2.2). This effect is partially mitigated by the temperature dependence on the $\delta^{18}O$ value of calcite which results in higher $\delta^{18}O$ values as the average temperature of deposition decreases.

Figure 2.2

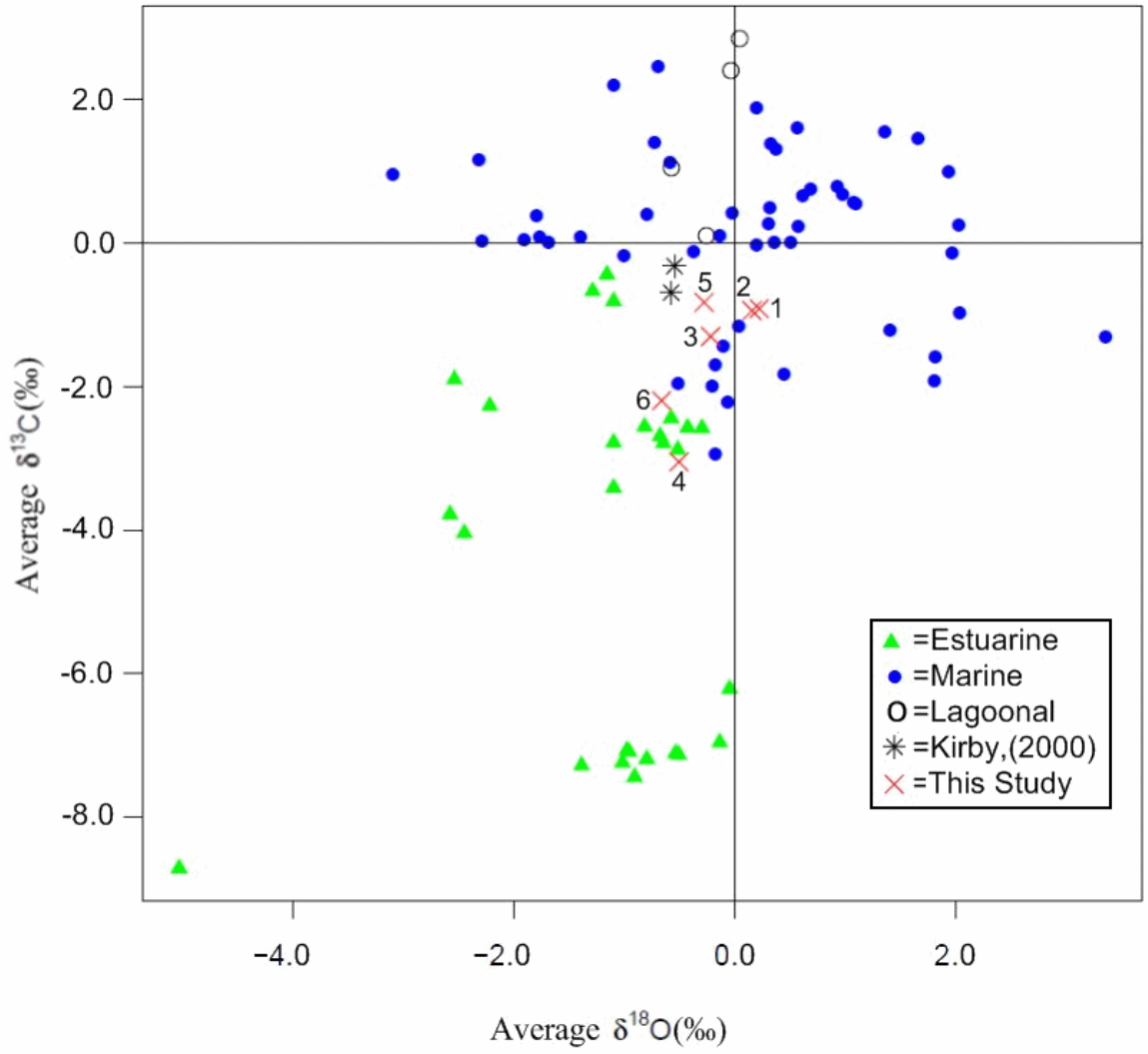

Figure 2.2 - Average $\delta^{13}C$ and $\delta^{18}O$ values from stable isotope profiles of individual mollusk shells. Values from marine environments are represented by blue circles, estuarine shells are represented by green triangles and lagoonal environments are represented by open circles. Asterisks represent data from Kirby et al. (2000). The numbered X's represent data from this study (see Table 4.1). Data used are provided in Appendix 3. Note that in plotting average values for data from Kirby (2000), +0.4‰ was added to the $\delta^{18}O$ value to correct for the difference in Oligocene seawater (-0.4‰) compared to modern oceans (Zachos et al., 1996). Likewise, +0.9‰ was added to the $\delta^{18}O$ value data of this study to correct for differences between Late Eocene seawater (-0.9‰) and modern oceans.

In Figure 2.3, ranges of $\delta^{13}C$ and $\delta^{18}O$ values from individual shells are compared for the same data. Estuarine mollusks tend to have greater ranges in $\delta^{13}C$ and $\delta^{18}O$ values compared to mollusks from normal marine environments. There is however, a field of overlap between estuarine and marine shells that was not observed in Figure 2.2. Shells from lagoonal environments fit within a narrow band of ranges of $\delta^{18}O$ values (~2‰) while showing greater variation in the range of $\delta^{13}C$ values. The relationships expressed in Figure 2.3 are controlled in large part by larger scale fluctuations in both the $\delta^{13}C$ and $\delta^{18}O$ values of most estuarine waters compared to marine environments. Range in $\delta^{18}O$ shell values are partially mitigated by latitude in that range will be higher for environments that have a wider seasonality in temperature (higher latitudes vs tropics which have narrower seasonalities).

Paleoecology

Isotopic variations recorded in mollusk shell profiles may be used to address questions of paleoecological significance too. For example, Kirby (2000) studied isotopic variability within shells of Late Oligocene specimens of the extinct oyster *Crassostrea gigantissima* to address the possible role of paleoenvironment in the evolution to its much smaller descendant *C. virginica*. In comparing isotope profiles of *C. gigantissima* to *C. virginica*, Kirby found that *C. gigantissima* had more narrow seasonal ranges in both $\delta^{13}C$ and $\delta^{18}O$ values as well as more positive average $\delta^{13}C$ and $\delta^{18}O$ values. Kirby also compared the number of oxygen isotope cycles in a profile to the length of the isotope profile to determine and compare growth rates and life spans between *C. gigantissima* and *C. virginica*. He found that *C. gigantissima* and *C. virginica* had similar growth rates while *C. gigantissima* lived longer and underwent

Figure 2.3

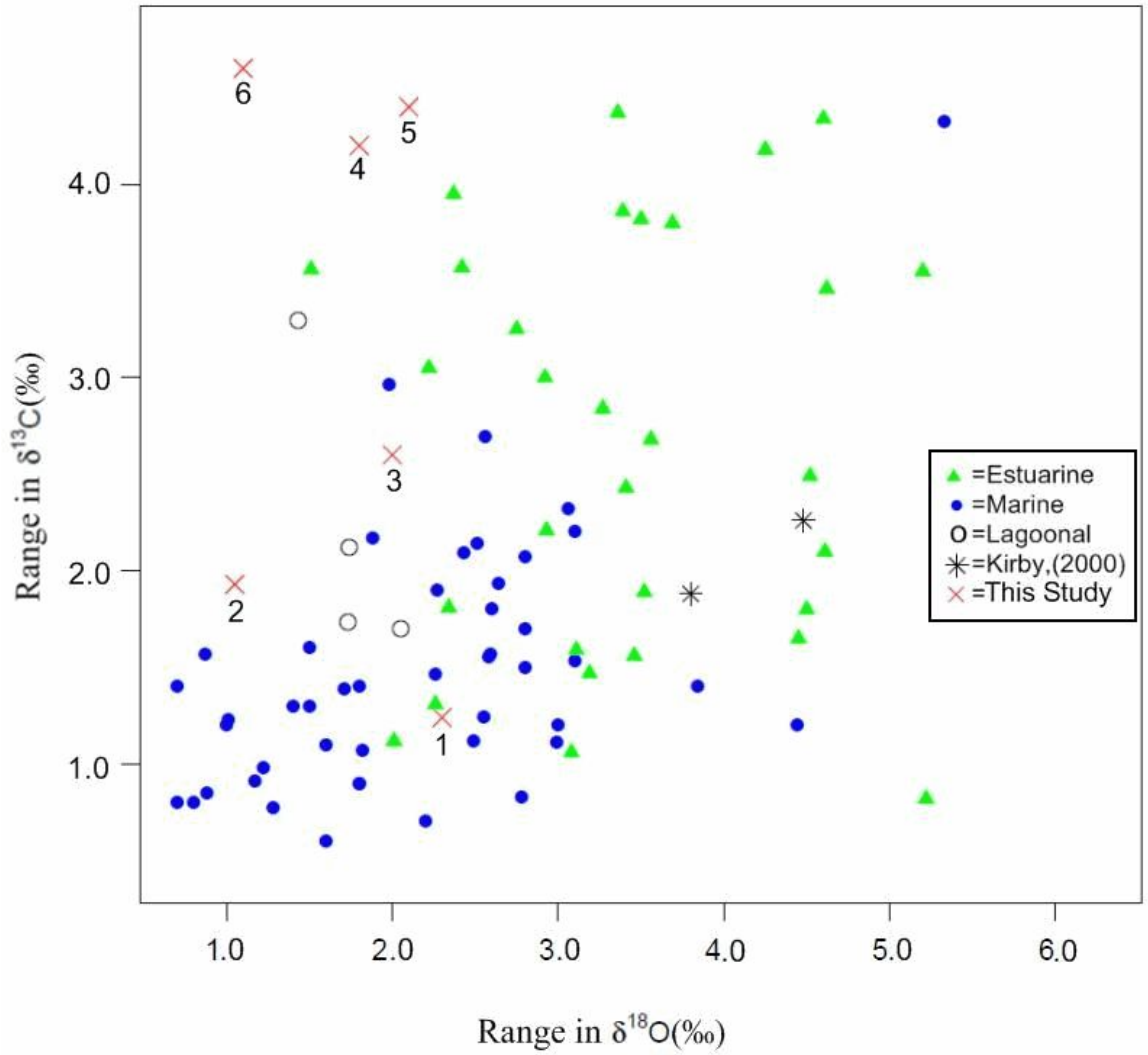

Figure 2.3 - Ranges of $\delta^{13}C$ and $\delta^{18}O$ values from stable isotope profiles of individual mollusk shells. Values from estuarine environments are represented with green triangles, marine shells are represented by blue circles and lagoonal shells are represented by open circles. Fossil *C. gigantissima* data from Kirby et al. (2000) are represented by asterisks. The numbered X's represent data from this study (see Table 4.1). The data used are provided in Appendix 3.

more shell thickening than *C. virginica.* From these data, Kirby concluded that *C. gigantissima* lived in a more fully marine habitat than modern *C. virginica* which live prmarily in estuaries. The higher rate of shell thickening measured in *C. gigantissima* supported this conclusion because faster shell thickening would be required due to higher predation pressures from drilling gastropods in fully marine environments.

Kirby (2000) also suggested an alternative technique in assessing paleoenvironmental information using oxygen isotope profiles from mollusk shells. He assumed that calcification ceased in mollusks seasonally due to stresses caused by temperature extremes. A typical pattern of calcification cessation due to temperature stress may be recognized in a $\delta^{18}O$ profile as transient excursions in either the most positive or negative portion of the oxygen isotope cycles of a profile (Figure 2.4). Kirby assumed that calcification ceased in *Crassostrea gigantissima* at the same temperature that extant *Crassostrea* cease calcification (T=10ºC) (Kirby, 2000). In this way, Kirby could ascribe an invariant and consistent temperature (10ºC) to each most positive $\delta^{18}O$ value of a cycle at a growth cessation throughout an oxygen isotope profile. Using these paired temperatue-$\delta^{18}O_{shell}$ estimates, Kirby could calculate the $\delta^{18}O$ value of the water in which an individual lived. Using this method, Kirby was able to compute the extent to which the $\delta^{18}O$ value of seawater changed throughout the ontogeny of any particular shell.

Kirby (2000) compared a pattern of winter cessation in most positive $\delta^{18}O$ values for shells of *C. gigantissima* and *C. virginica*. The *C. gigantissima* profiles showed a range of most positive values of less than 1‰ (0.81‰ for BQ-1 and 0.52‰ for BQ-2), while a *C. virginica* sample (Miss-1) displayed a range of most positive values of 1.55‰.

Figure 2.4

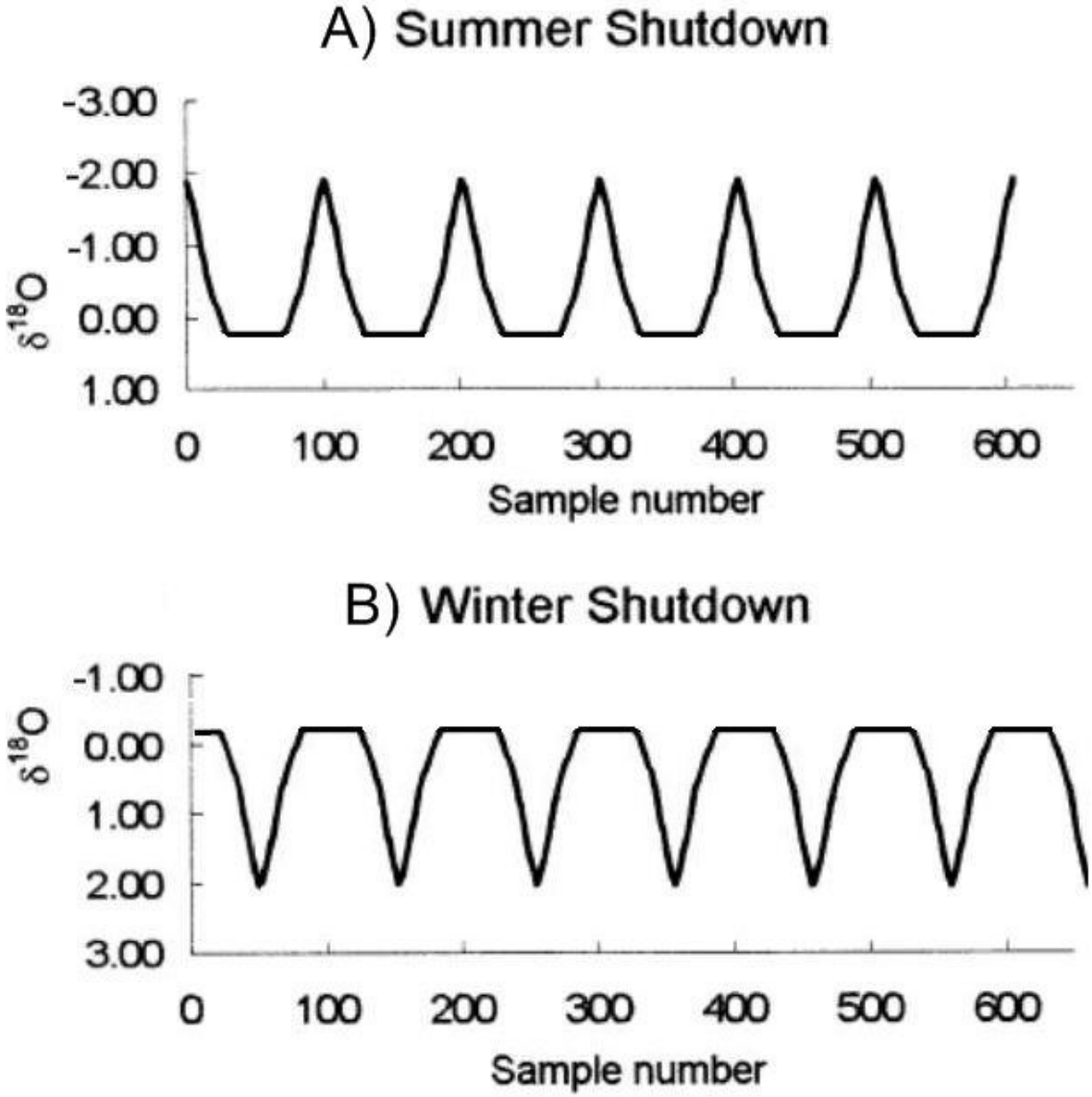

Figure 2.4 - Typical shape for isotope profiles exhibiting signs of calcification cessation. Note the inverted Y-axis so that temperature increases upwards. Adapted from Goodwin et al. (2003).

The latter value is similar to the range of most positive $\delta^{18}O$ values (1.6‰) estimated from oxygen isotope profiles of *C. virginica* reported in Surge et al. (2001). Surge collected her specimens in an estuarine environment. The greater range of most positive $\delta^{18}O$ values for *C. virginica* was interpreted by Kirby to be the result of the larger fluctuating $\delta^{18}O$ values for water in an estuarine environment compared to that of the normal marine environment.

It should be noted, however, that calcification cessation my not occur universally at a consistent invariant temperature in all environments or in all species. In some environments temperatures, may not be cold enough in winter to preclude shell growth. As well, different species may have different tolerances to temperature and what may force calcification to cease in one species may not have the same effect on another.

Diagenesis

Diagenetic processes can compromise the integrity of oxygen or carbon isotope data stored in the calcareous hard parts of marine organisms. Diagenesis encompases the physical or chemical changes that occur to sediments or rocks after deposition (Scholle, 2003). Diagenesis can affect the shells of mollusks at the sea floor after (and sometimes even before) an organism's death (Scholle, 2003). Once diagenesis has occurred, the isotopic information stored in the shells may reflect (in part or total) the composition of the fluids that altered them. When calcium carbonate undergoes chemical exchange with diagenetic fluids, both minor (Mg, Sr) and trace elements (Na, Mn, Fe, Zn) may be incorporated or extracted from the solid because the chemistry of the fluids involved in diagenesis are usually different from the waters in which the carbonates formed (Veizer, 1983; Al-Aasm and Veizer, 1986). In the typical case of meteoric diagenesis of carbonate

minerals, Sr and Na concentrations decrease in diagenetic calcite while Mn, Fe, and Zn increase (Brand and Veizer, 1980). With regard to oxygen isotopes, a typical effect of diagenesis is to increase the $\delta^{18}O$ value of the fluid and decrease the $\delta^{18}O$ value of the altered minerals/rocks involved (Kharaka and Thorsden, 1992).

Cathodoluminescence of carbonate minerals can be used to map areas where certain trace elements are present (Budd et al., 2000). The elements Mn, Cu, and Zn are activators, meaning they produce luminescence when a carbonate mineral is bombarded with a cathode ray (electrons) under specific conditions (Budd et al., 2000). Iron is an activator, but at relatively high concentration, it can quench luminescence as well (Budd et al., 2000). This technique can be used with caution to identify some altered materials, although the absence of luminescence does not always indicate an absence of alteration.

Thin Section Petrography

Careful examination of mineral fabrics can provide additional evidence for diagenetic alteration. As stated in Chapter 1, the shells of *Crassostrea gigantissima* are composed of chalky and foliated low-magnesian calcite. The original mineral frabric contains a foliated microstructure which is easy to recognize in thin section because extinction in cross polarized light sweeps across foliations as the stage of a petrographic microscope is rotated (Taylor et al., 1969). Recrystallized (diagenetically altered) carbonate appears blocky in thin section (e.g., sparry calcite) and it does not display the characteristic sweeping extinction of the primary fibrous fabric of *C. gigantissima* (Scholle, 2003).

Chapter 3

Methods

Shell Selection and Preparation

Fossil oysters were collected at Griffins Landing, located ~30 miles south of Augusta along the Savannah River in Burke County, Georgia. Prior to sampling, the bluffs at Griffins Landing were measured and described to establish a stratigraphic framework for this study (Figure 3.1; Appendix 1). Lateral positions of the outcrops where the shells were collected are shown in Figure 3.2.

The outcrops from which shells were collected consisted primarily of kaolinitic clays with a minor sand component. Two types of shell orientation were noted during sample collection: 1) life position, 2) random orientation. Shells in life position were recognized in outcrop as being both upright (dorsal beak pointing down section and ventral margin facing upward) and articulated (both valves together) (Figure 3.3). It was important to collect shells in life position as it is likely they were not transported and are accurate representatives of the environment in which they lived. All specimens were collected from within the outcrop (Bed 2, see Figure 3.1) by prying several inches into the outcrop with a crowbar, chisel, and rock hammer. Only articulated shells were collected once verified as being in life position. Many of the shells within Bed 2 had readily observable bioerosion on their ventral margins from either clionid sponges or boring bivalves (most likely *Lithophaga sp.*).

Figure 3.1

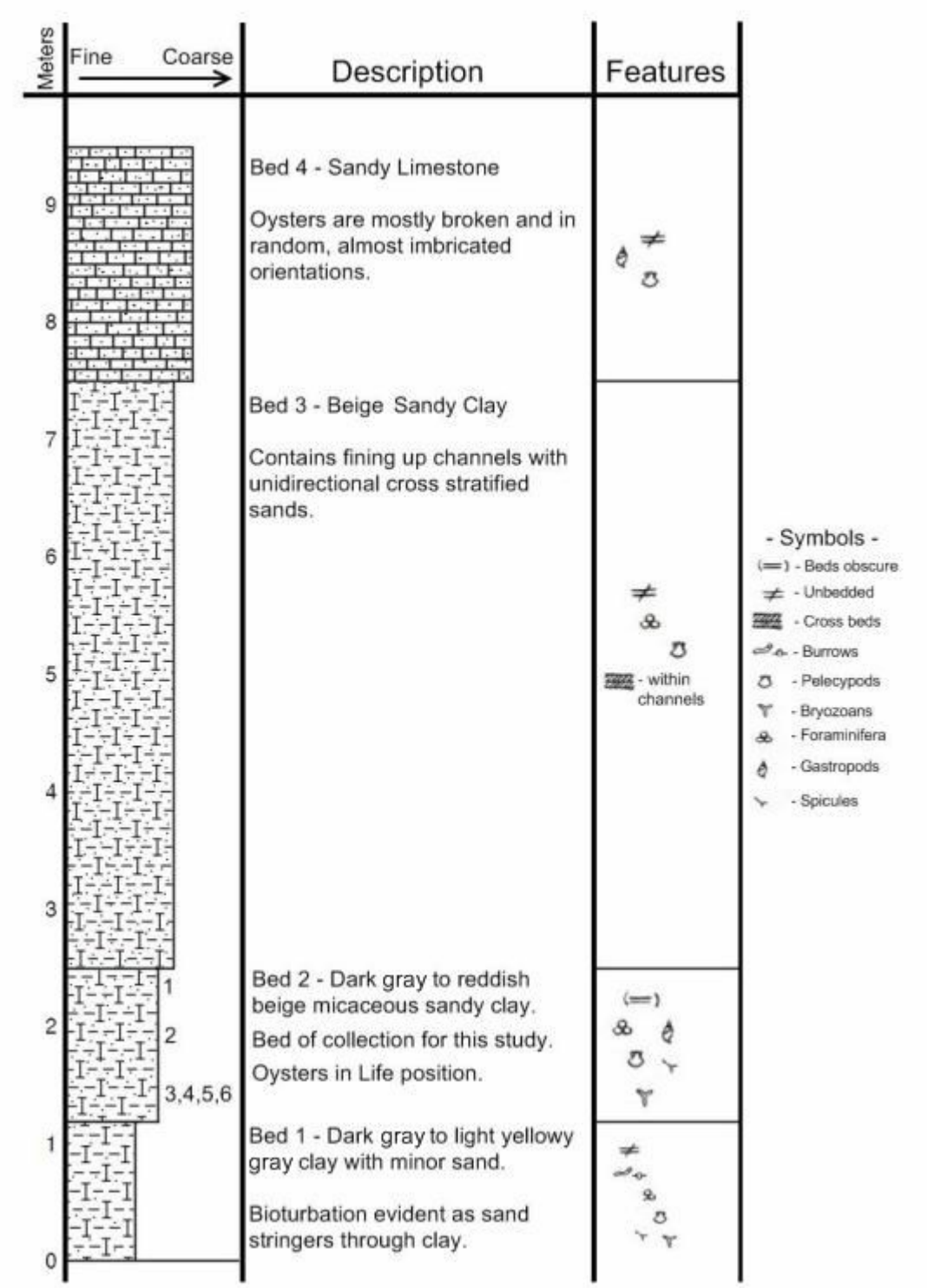

Figure 3.1 - Generalized stratigraphic section for the bluffs along the Savannah River at the Griffins Landing locality. Note that the zero meter mark represents river level while the numbers in the stratigraphic column show relative positions from which shells were collected. Symbols shown on the right are from Compton (1985).

Figure 3.2

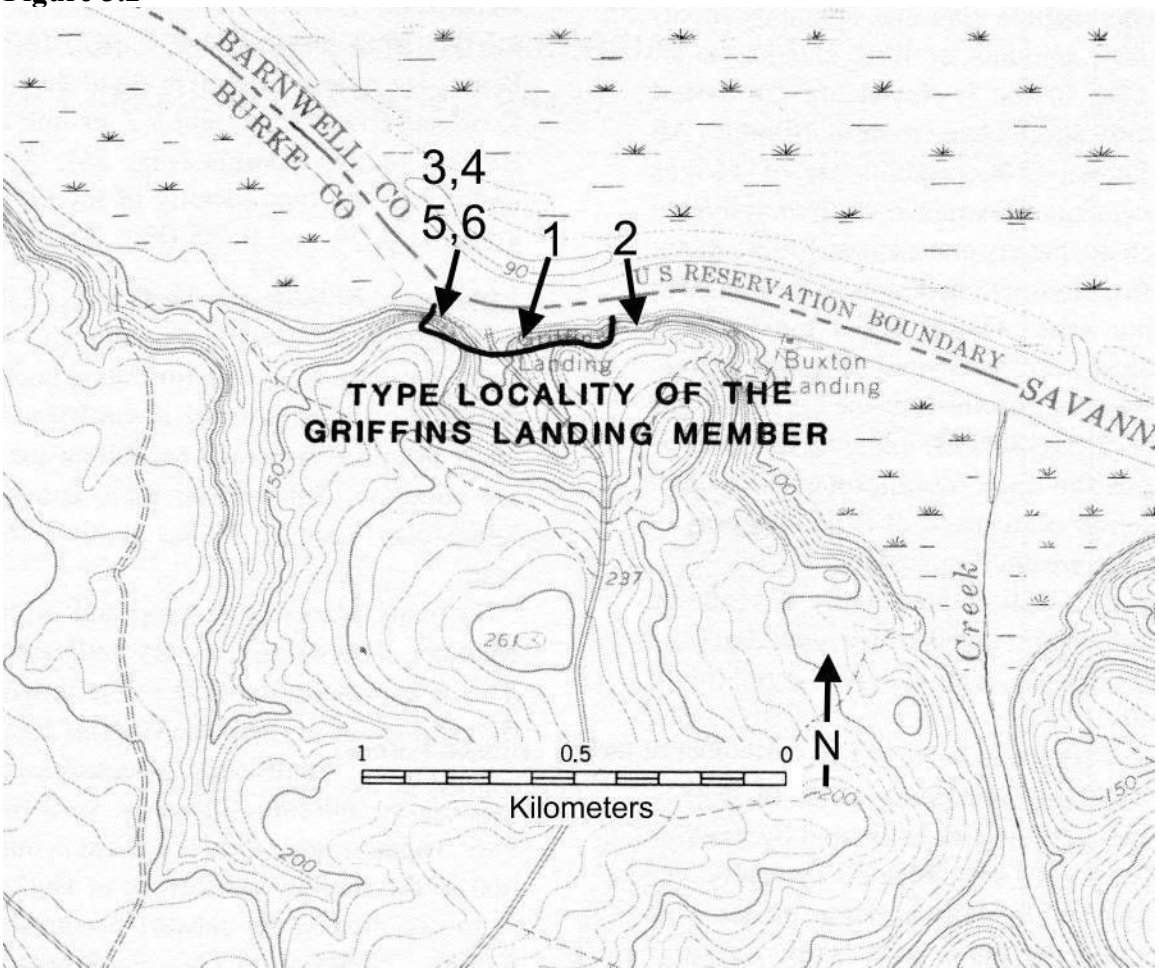

Figure 3.2 - Locality map of Griffins Landing showing the relative lateral positions along the outcrop of each shell. Adapted from Huddlestun and Hetrick (1986).

Figure 3.3

Figure 3.3 - Shells in life position at Griffins Landing. These shells are interpreted to be in life position because they are all oriented in the same direction with all dorsal beaks pointing towards the bottom of the image (down section).

All shells used in the determination of paleoclimate for this study were collected from Bed 2 as shown in Figure 3.1. Relative stratigraphic positioning of each collected shell was such that Shells 3,4,5, and 6 were collected from an oyster reef that was at the stratigraphically lowest position in bed 2. Shell 2 wsa collected stratigraphically above this and shell 1 was collected from near the top of Bed 2 (Figure 3.1). Collection sites for samples varied laterally along the river. Moving from west to east along the river, in the order of collection sites: Shells 3,4,5, and 6 were collected at 33º 6.976N / 81º 42.273W, Shell 1 was collected at 33º 6.949N / 81º 42.234W, and Shell 2 was collected at 33º 6.988N / 81º 42.109W (coordinates based on WGS 84) (Figure 3.2).

Once shells were removed from outcrop, they were taken back to the lab and cleaned of external material with a soft brush under tap water. Then, the right and left valves were separateed by prying them apart using a flathead screwdriver and the left valve was saved for further analysis. A pictoral representation of the entire process that is described as follows is shown in Figure 3.4

Methods for the preparation of shells for isotope analysis were similar to those of Kirby (1998, 2000). In the laboratory, shells were cut using a watercooled rock saw. The first step was to separate the chondrophore from the rest of the shell. The separated chondrophore was then cut radially through the center in a direction that was perpendicular to the external growth lines and parallel to growth direction. This resulted in two halves of the chondrophore. The sectioned halves were cleaned under running tap water with a soft brush and the cut faces were polished using lapwheels in a stepwise fashion from coarse to fine grit (320, 450, 600). The polished surfaces were mounted onto 2x1-inch glass slides using epoxy. Thin sections were made by cutting away excess

Figure 3.4

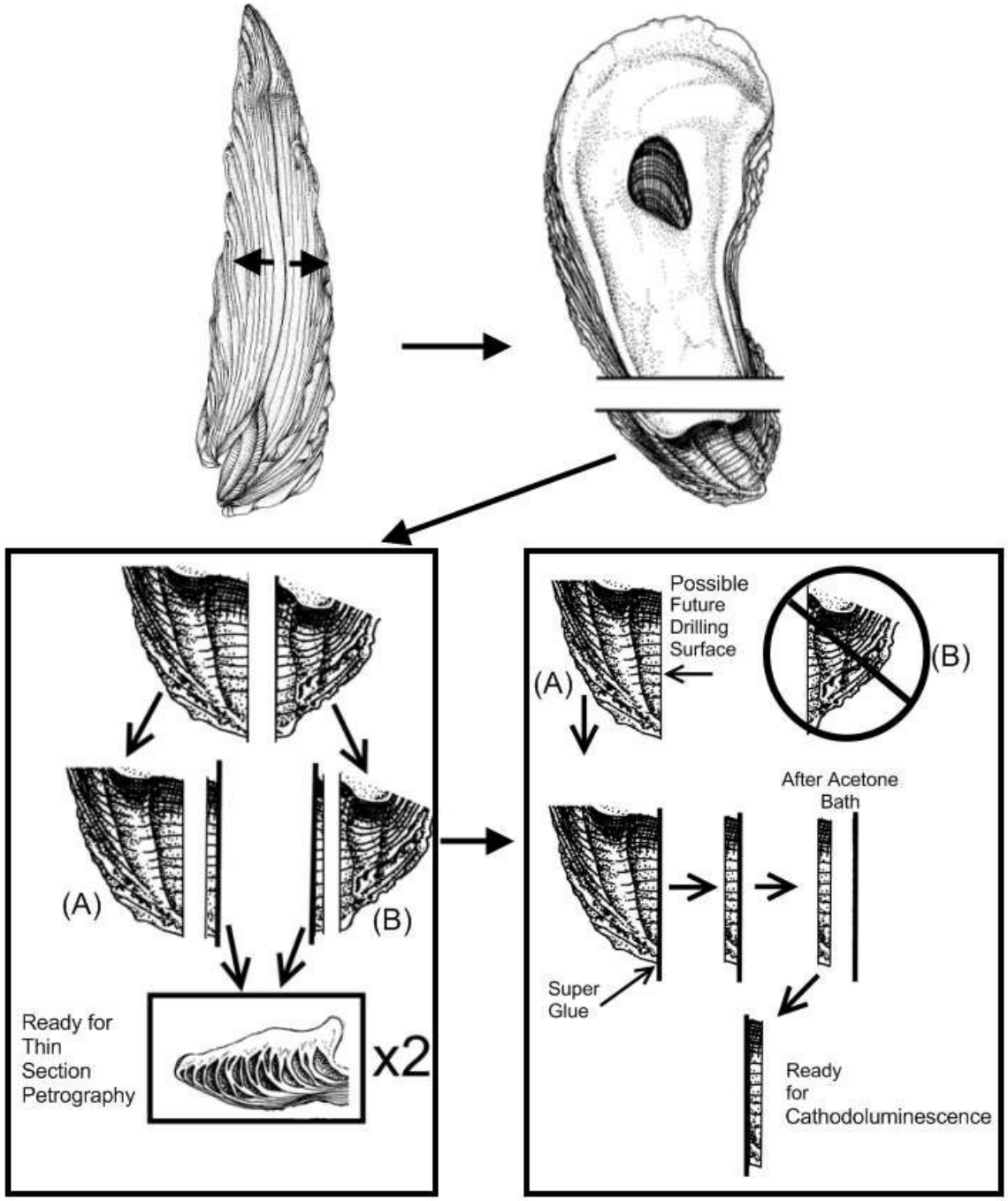

Figure 3.4 - Summary of the technique used to prepare shells for stable isotope analysis. Pictures adapted from Galtsoff et al. (1964).

material parallel to the slide leaving a ~2 mm thick billet on the slide [the remaining shell material (A & B) was set aside for later analysis] and then grinding the mounted section to ~30 micron thickness. Using this methodology two thin sections were prepared from each chondrophore and each was observed under transmitted light microscopy to determine which section was more suitable for further analysis.

The cut surface of the excess material from a selected thin section (e.g., 'A' in Figure 3.4) was lightly polished on a lapwheel and fixed to a 2x1-inch glass slide using super glue. After grinding down this second section to a thickness of ~6-7 mm, the section was soaked in acetone to remove the glass slide and to dissolve away any super glue. The ground face was then allowed to dry and re-glued to a glass slide using a two part room temperature curing epoxy such that the side of the section not glued to the glass surface consisted of material that was in closest proximity to its complimentary thin section made earlier.

Each thin section was viewed in transmitted light by optical microscopy to examine shell microstructure. Foliated microstructure was verified by the presence of crystal fibers aligned in parallel foliations that have sweeping extinction (Figure 3.5). Once foliated microstructure was identified, the complimentary section was viewed and photographed under cathodoluminescence using an ELM 3UR Nuclide cold Cathodoluminoscope. For best luminescence, atmospheric pressure in the luminoscope was maintained at approximately 65-75 torr. Sections that did not display luminescence were chosen for microdrilling. In total, 25 shells were processed in this manner, from which 6 displayed primary shell microstructure and non-luminescent characteristics. The thick sections of these 6 shells were selected for further stable isotope analysis.

Figure 3.5

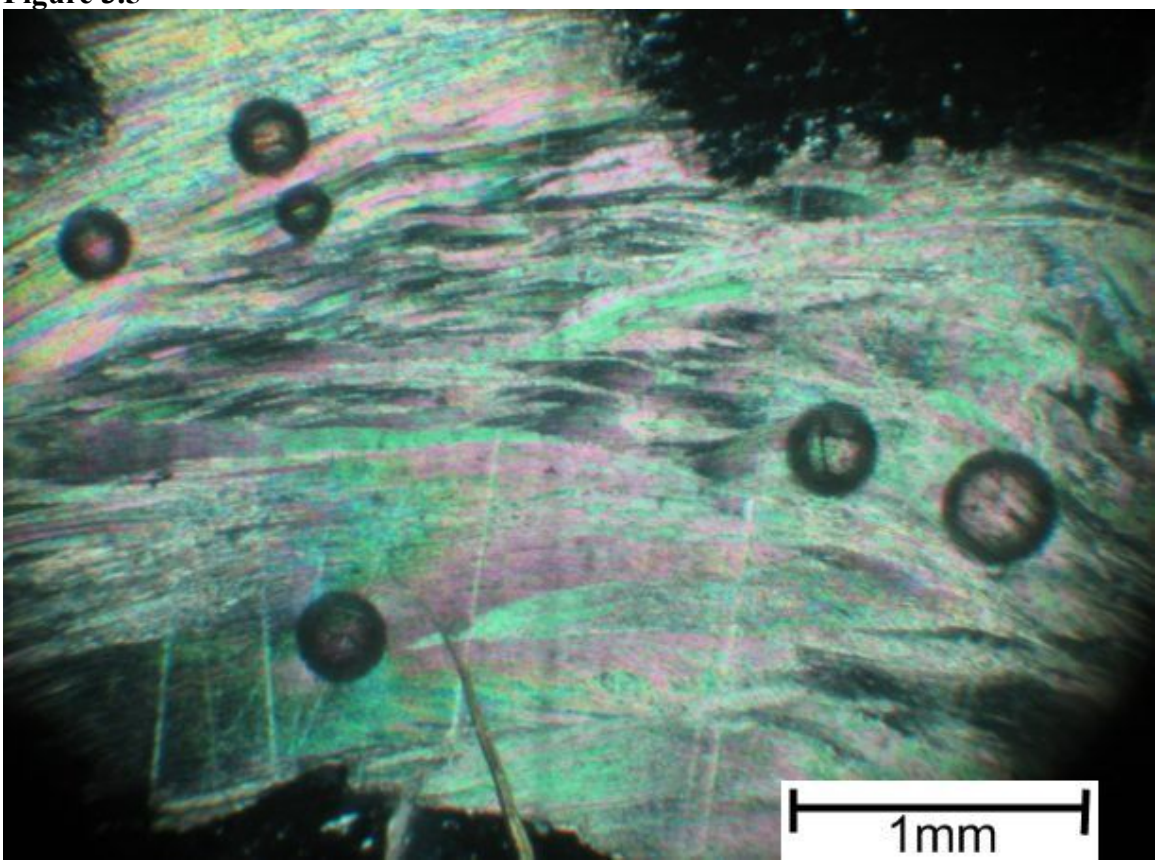

Figure 3.5 - Primary foliated microstructure of a *C. gigantissima* specimen collected at Griffins Landing. This photomicrograph was taken under cross-polarized light at a magnification of 40x.

Drill Procedures

Because the outer surface of the chondrophore was typically recrystallized in all samples, material was targeted below the surface of the chondrophore for stable isotope analysis (Figure 3.6). This area of the sections typically displayed growth bands that are easily distinguished as alternating light and dark bands in transmitted or reflected light.

Samples of shell carbonate were collected by drilling grooves parallel to growth bands using a Merchantek Micromill with a 0.5mm dental bit. Each groove was drilled ~1-1.5 mm in length and <0.5 mm depth into the shell removing approximately 100-150 μg of carbonate using a standard high spatial resolution milling technique (Dettman, 1995). Sequential samples were collected along a profile from the dorsal beak to the ventral margin of the chondrophore (Figure 3.6), producing a time series of samples from younger to older portions of the shell. Sampling resolution was ~3 samples per millimeter.

To better understand the isotopic significance of shell material, a small number of samples were collected from each shell that were recognized as luminescent under cathodoluminescence, and samples of dogtooth sparry calcite that coated the internal shell chambers of some shells. Additional dogtooth spar samples were also obtained from additional shells collected at the Griffins Landing that were not used in the study of paleoclimates as additional data for the analysis of diagenetic alteration.

Isotope Analysis

Each powdered sample was collected using a razor blade and dental microspatula. Samples were gently transferred to a small square of weighing paper to record sample mass using a digital microbalance (±0.1ug). Each sample was then placed in an

Figure 3.6

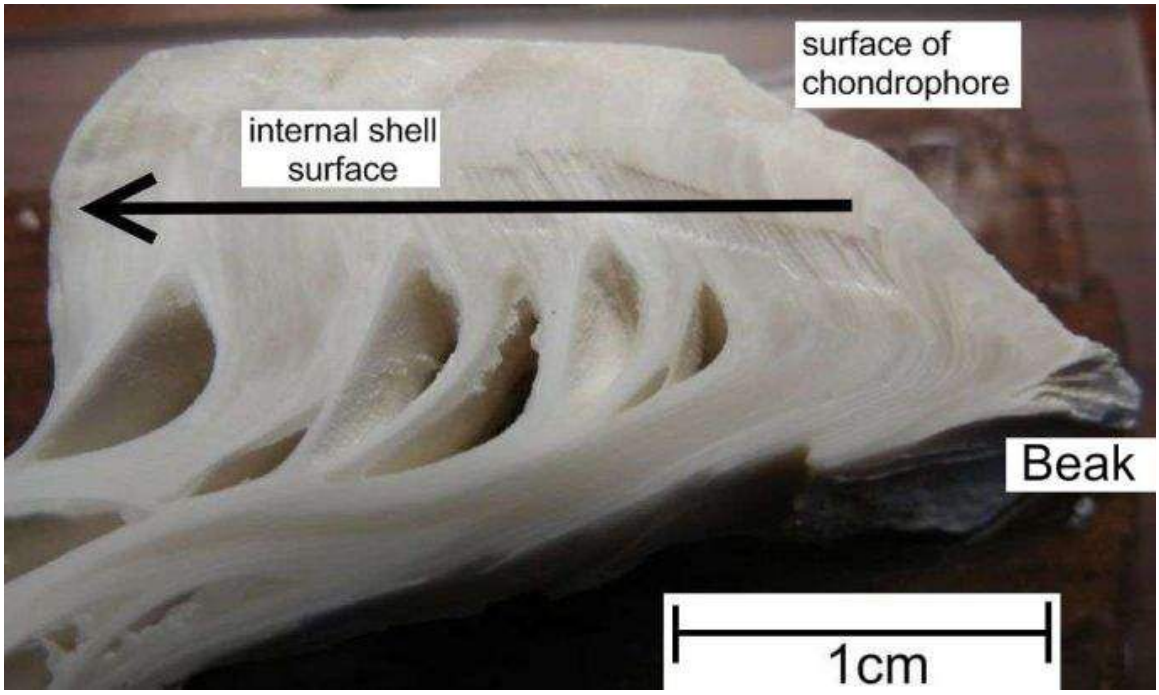

Figure 3.6 - Photograph of the cut and polished thick section from Shell 3 that was sampled for stable isotope analysis. The arrow indicates the direction of ontogenetic growth. Primary (unaltered) material was sampled serially from the ontogenetically youngest to the ontogenetically oldest portion of each shell (right to left).

exetainer™ vial for stable isotope analysis at the University of Georgia's Savannah River Ecology Laboratory (SREL).

Exetainer vials were flushed with He to remove atmosphere and then reacted with 8-10 drops of 104% orthophosphoric acid at 25ºC using a ThermoQuest Gasbench II peripheral device attached to a $Delta_{plus}$ XL isotope ratio mass spectrometer. All isotope data are reported in the conventional δ notation (‰ units), using the NBS-19 standard ($\delta^{18}O = -2.20$, $\delta^{13}C = -1.95$) to calibrate samples to Vienna Peedee Belemnite (VPDB) (Craig, 1957). Standards were run between every fifth sample in a sequence. The precision achieved for NBS-19 was ±0.17 ‰ for $\delta^{18}O$ and ±0.14 ‰ for $\delta^{13}C$ (~n=8-15) for each suite of samples analyzed from each shell.

Ontogenetic Analysis

Sixteen additional shells were collected in the field which displayed readily distinguishable morphological ridges and valleys on the external surface of the chondrophore. The distance between each adjacent ridge, was measured for each shell using a digital caliper to estimate the average yearly growth rate for *C. gingantissima* from the study area. Measurements were made from ridge to ridge because valleys tended to be broad while ridges were more narrow, yielding a more precise length measurement. A total of 96 annual cycle distances were measured, from which an average annual cycle length was determined. The average growth rates for the chondrophores of these additional specimens was compared to the average growth rates obtained from the six sampled specimens. The average growth rate for the chondrophore of each specimen used in this study was obtained by dividing the length of the drilled profile by the number of oxygen isotope cycles within each profile to obtain an average

growth rate in mm/yr. The length of each isotope profile was obtained using a measuring tool available in the micromill software by measuring the distance of lines that were perpendicular to drill groove sets on each shell. The cumulative length of these measurements represents the length of the drilled profile.

Paleotemperature Determination

The paleotemperature equation of Epstein et. al. (1953) was used to calculate isotope temperatures. The isotopic composition of seawater was determined using the Cenozoic $\delta^{18}O_{water}$ curve developed by Lear et al. (2000) in combination with the estimated age (35 ±0.5 ma) of the Griffins Landing Member. Because the Lear curve provides a global mean oxygen isotope composition, this value was corrected for latitude using the relation described earlier by Zachos et al. (1994). The value for Late Eocene seawater use for paleotemperature estimates in this study was -0.34‰.

Data Analysis

All plots were made using programs written for the R-Package for Data Analysis and Graphics (Appendix 4). Isotope data were connected by generating a smoothed connecting line using a cubic spline interpolation method for all of the profiles. All figures and profiles presented in this study can be re-produced using the provided code in Appendix 4.

Chapter 4

Results

Diagenetic Alteration

All the shells that were analyzed in this study experienced some form of diagenetic alteration. Sparry dogtooth calcite coatings were observed on the surface of most internal shell chambers indicating secondary infilling of calcite that displayed bright orange luminescence (Figure 4.1). Furthermore, in all specimens, the outer surface of the chondrophore was translucent in appearance and displayed a distinct blocky fabric in thin section (Figure 4.2), which was clearly recrystallized. Surprisingly, this blocky material was nonluminescent in most specimens (Figure 4.3). For many sections that were deemed inappropriate for further analysis, the shell displayed notable bright orange luminescence that was indicative of diagenetic alteration (Figure 4.3).

Only non luminescent shell material was selected for the shells that were sampled in this study. These portions of the shells also had visible growth bands in polished cut sections (see Figure 3.6). In this section, unaltered portions of shell displayed the characteristic sweeping extinction and fibrous appearance of primary calcite (see Figure 3.5).

Isotope Profiles

In total, over 100 shells were examined at the outcrop prior to locating a suitable collection site which contained a sufficient number of thick-shelled oysters in life position for the study. A subset of these shells was taken to the laboratory, where they

Figure 4.1

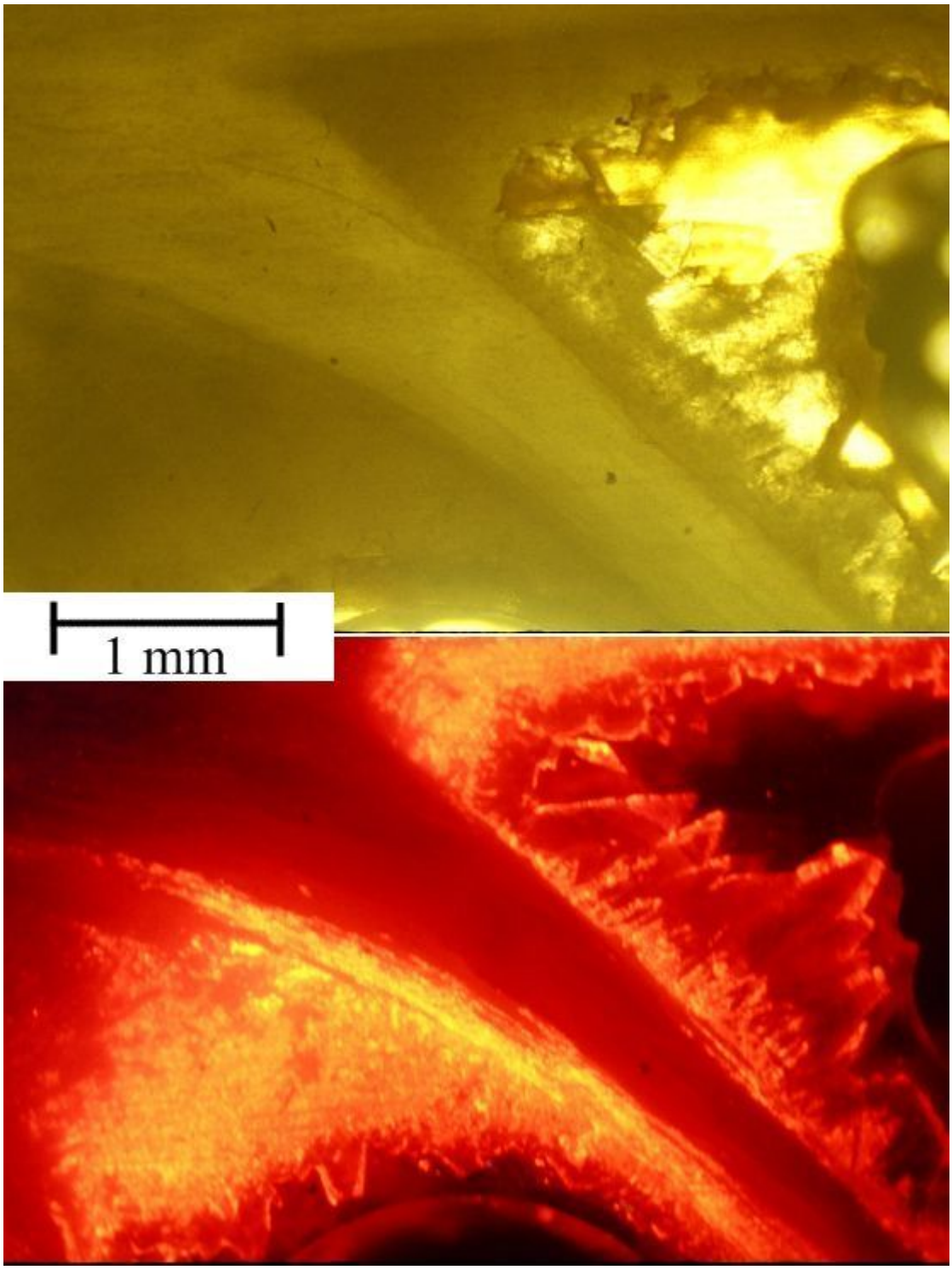

Figure 4.1 - Dogtooth spar within internal shell chambers of shell 1. Top picture was photographed under transmitted light while the bottom picture shows the characteristic bright orange luminescence of dogtooth spar under cathodoluminescence. Both photos show the same portion of shell. Magnificaton was 40x.

Figure 4.2

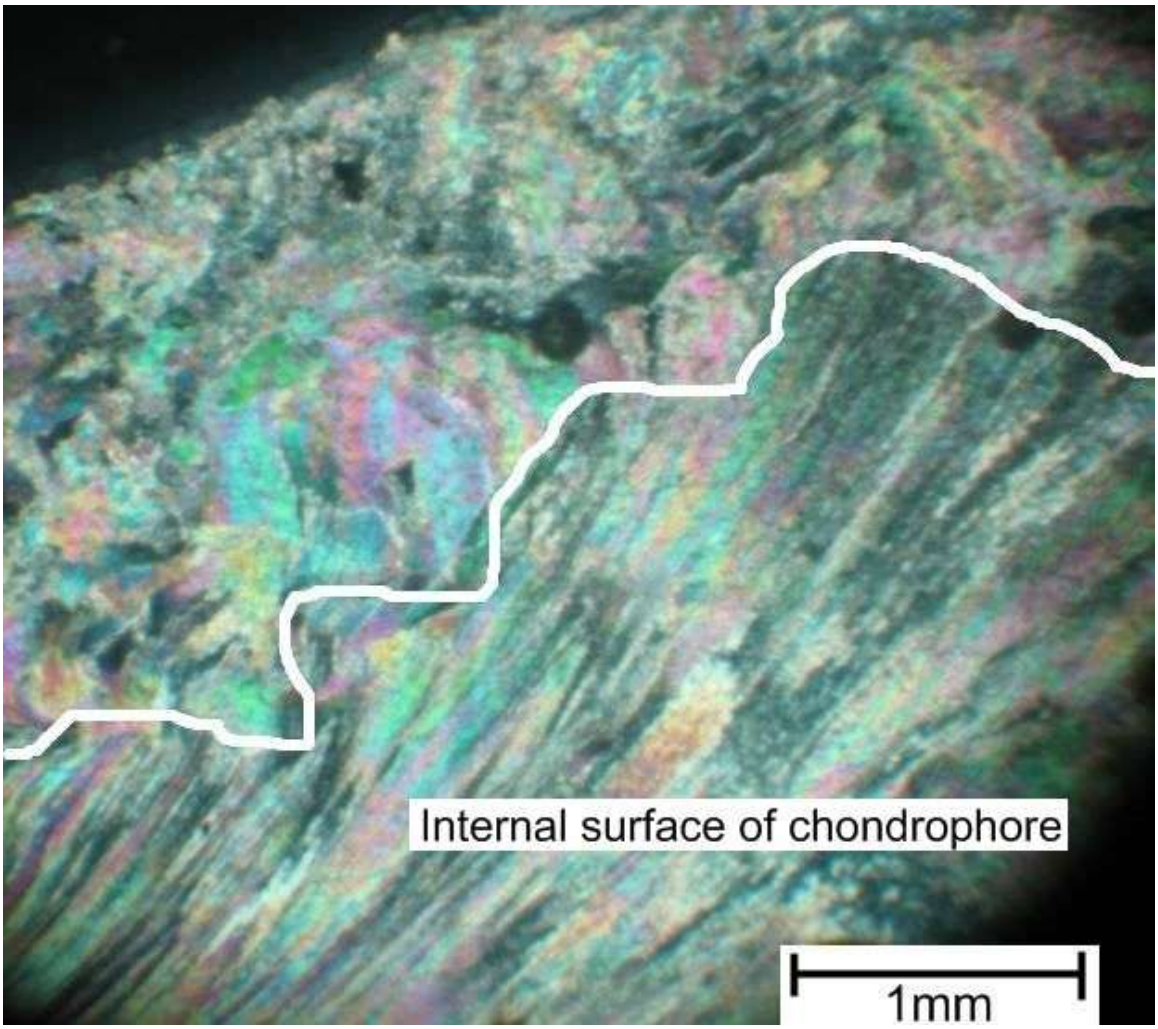

Figure 4.2 - Thin section photograph taken from Shell 4 showing an interface between primary foliated fabric (below) and blocky spar (above) at the translucent surface layer of the chondrophore (white line demarcates transition). Magnification was 40x.

Figure 4.3

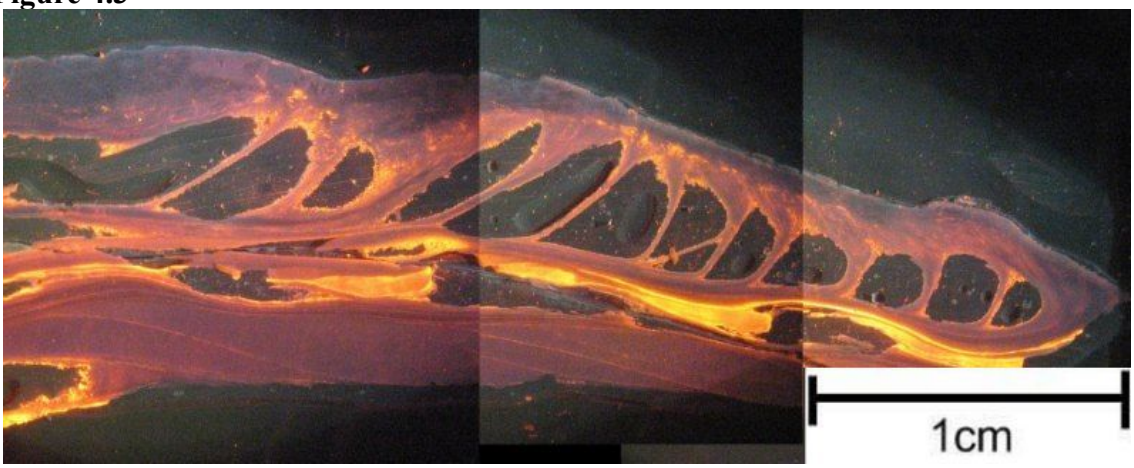

Figure 4.3 - Photograph showing the cathodoluminescence of a shell section that was not selected for further analysis. Note the non-luminescence of a recrystallized surface layer in this section.

were disarticulated and cleaned, followed by preparation of thick and thin sections for cathodoluminescence and fabric analysis. Based on these analyses, six shells were sufficiently unaltered to be sampled for isotope analysis. From these shells, sequential samples of unaltered shell material were collected. After stable isotope analysis of these samples, carbon and oxygen isotope profiles were constructed.

Isotope profiles were constructed by plotting the position of each drilled sample along the chondrophore transect in millimeters along the x-axis. Distances were determined by measuring perpendicular to drilled groove sets as outlined in Chapter 3. Ontogenetically younger shell material is plotted from left to right forming a time series for each graph. Oxygen and carbon isotope values are plotted on the y-axis. Oxygen isotope values are plotted with more negative $\delta^{18}O$ values increasing towards the top of the plot so that paleotemperatures increase upwardly. Paleotemperatures were calculated from the $\delta^{18}O$ values of calcite using a $\delta^{18}O_{sw}$ value of -0.34‰ for Late Eocene seawater as described in Chapter 2.

Annual cycles in the oxygen isotope profiles were determined using a program written in the R language. A visual representation of the output is shown in Figure 4.4. The program works by first overlaying a smoothed curve to the oxygen isotope profile from which isotope values can then be calculated for any position along the profile. A smoothed curve overlay is necessary for this process to remove noise from the $\delta^{18}O$ profile because scanning along a non-smoothed profile would result in multiple values that fit the criteria for a most positive value within each suite of most positive values in a $\delta^{18}O$ cycle. The y-coordinate values that made up the data used to draw the curve, were scanned by the computer from left to right to identify points that represented the most

Figure 4.4

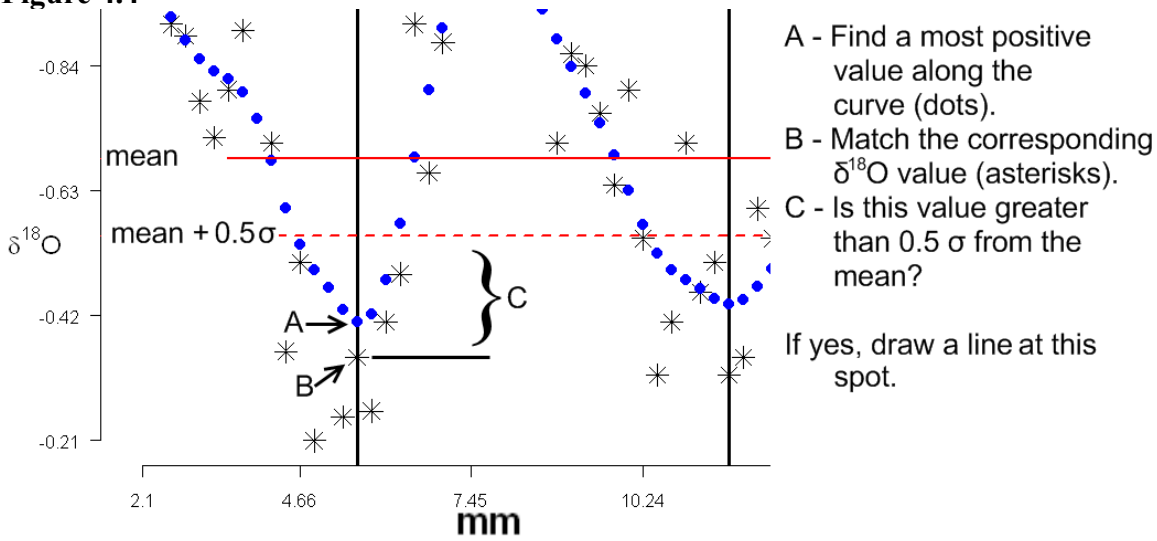

Figure 4.4 - Visual representation of the model used by the computer to pick oxygen isotope cycles. The dotted blue line represents the curve used to determine the most positive $\delta^{18}O$ value for each cycle on the curve (curve is not displayed on isotope plots).

positive values within each dip of the smoothed curve. Once the data points that represented the most positive values of the theoretical curve were identified, the corresponding $\delta^{18}O$ values within the actual $\delta^{18}O$ profile were identified using these points. The most positive $\delta^{18}O$ values were then compared to a value that was one half of a standard deviation from the mean $\delta^{18}O$ value. A cycle was delimited only if the selected most positive value was greater than one half of a standard deviation from the mean. Once the cycle positions were picked along the profile, vertical black lines were drawn for each one.

The isotope profiles for each shell are plotted in Figures 4.5 through 4.10. Isotope profiles are presented at the top of each figure with a cathodoluminescence image of the sampled section below it. The cathodoluminescence image shows the location of each drilled sample as a numbered solid red line and the location from which diagenetic sub-samples were taken are marked with a 'Rx' symbol. Morphological ridges, when observed on the surface of the chondrophore, were also marked on the image with a letter and marked on the isotope profiles with a dashed vertical line.

Average $\delta^{13}C$ and $\delta^{18}O$ values were obtained by determining the mean value of all analyses in each profile (raw data are reported in Appendix 2) and are reported ± (1σ) standard deviation (Table 4.1). Ranges in isotope values are reported by subtracting the minimum value from the maximum value of each profile. Isotope temperature ranges are reported by substituting the minimum and maximum $\delta^{18}O$ values of a profile and the $\delta^{18}O$ value for Late Eocene seawater (-0.34‰) into the paleotemperature equation of Epstein et al. (1953). The most positive $\delta^{18}O$ value for each $\delta^{18}O$ cycle was determined and marked by a red X. The most negative $\delta^{18}O$ value for each cycle was determined and

Table 4.1 - Summary statistics for all the data collected for six unaltered shells.

	Shell 1	(n=34)	Shell 2	(n=74)	Shell 3	(n=69)	Shell 4	(n=47)
	$\delta^{13}C$	$\delta^{18}O$	$\delta^{13}C$	$\delta^{18}O$	$\delta^{13}C$	$\delta^{18}O$	$\delta^{13}C$	$\delta^{18}O$
Min =	-1.60	-1.49	-2.17	-1.26	-2.68	-2.45	-4.86	-2.27
Max =	-0.40	0.57	-0.24	-0.21	-0.09	-0.40	-0.75	-0.48
Rng =	1.20	2.06	1.93	1.05	2.59	2.04	4.11	1.79
Avg =	-1.01	-0.70	-0.91	-0.68	-1.31	-1.13	-3.04	-1.40
StDev=	0.32	0.45	0.30	0.26	0.65	0.46	1.17	0.50
Min-T =		**12.68°C**		**15.94°C**		**16.78°C**		**17.11°C**
Max-T =		**21.63°C**		**20.57°C**		**26.18°C**		**25.33°C**
Rng-T =		**8.95°C**		**4.63°C**		**9.40°C**		**8.21°C**
Avg-T =		**18.08°C**		**18.00°C**		**19.99°C**		**21.27°C**
StDevT =		**1.96**		**1.14**		**2.10**		**2.30**

	Shell 5	(n=70)	Shell 6	(n=23)
	$\delta^{13}C$	$\delta^{18}O$	$\delta^{13}C$	$\delta^{18}O$
Min =	-3.51	-2.35	-4.61	-2.11
Max =	0.95	-0.27	0.03	-1.05
Rng =	4.46	2.08	4.65	1.06
Avg =	-0.82	-1.18	-2.20	-1.57
StDev=	1.15	0.52	1.53	0.34
Min-T =		**16.22°C**		**19.61°C**
Max-T =		**25.17°C**		**24.54°C**
Rng-T =		**9.49°C**		**4.93°C**
Avg-T =		**20.24°C**		**22.02°C**
StDevT =		**2.37**		**1.58**

	Most Positive $\delta^{18}O$ Values					
	Shell 1	**Shell 2**	**Shell 3**	**Shell 4**	**Shell 5**	**Shell 6**
Rng =	0.90	0.11	0.20	0.40	0.50	0.10
Avg =	0.15	-0.27	-0.50	-0.66	-0.50	-1.05
StDev=	0.45	0.06	0.10	0.15	0.22	0.07
AvWin=	14.46°C	16.20°C	17.19°C	17.63	17.20°C	19.62°C
StDev=	1.89	0.24	0.43	0.36	0.94	0.32
	(n=3)	**(n=3)**	**(n=3)**	**(n=5)**	**(n=4)**	**(n=2)**

	Most Negative $\delta^{18}O$ Values					
	Shell 1	**Shell 2**	**Shell 3**	**Shell 4**	**Shell 5**	**Shell 6**
Rng=	0.67	0.21	1.20	0.40	0.80	0.30
Avg=	-1.06	-0.97	-1.73	-2.18	-1.93	-1.87
StDev=	0.30	0.09	0.51	0.19	0.42	0.15
AvSum=	19.69°C	19.25°C	22.75°C	24.87°C	23.72°C	23.39°C
StDev=	1.38	0.41	2.42	0.91	1.99	0.72
	(n=4)	**(n=4)**	**(n=4)**	**(n=4)**	**(n=3)**	**(n=3)**

marked in a similar way. Average summer and winter temperatures were determined by calculating a temperature from each most negative and positive $\delta^{18}O$ value respectively, and averaging the data. The summary statistics for each shell are reported in Table 4.1, summary statistics for all diagenetically altered material are reported in Table 4.2. Carbon and oxygen isotope values for each shell are regressed in Figure 4.11.

Isotope profiles and a cathodoluminescence photo of the drilled section from shell 1 are shown in Figure 4.5. Luminescence was observed along the drilled profile beginning at approximately sample #35, but no recrystallized mineral fabrics were observed in thin section over the area of the drilled profile. Carbon and oxygen isotope values from shell 1 average -1.01 ± 0.32‰ (n=34) and -0.70 ± 0.45‰ (n=34), and have ranges of 1.20‰ and 2.06‰, respectively. There are three to four cycles in the oxygen isotope profile that are not correlated with the $\delta^{13}C$ values (R^2=0.01) (Figure 4.11). The most positive $\delta^{18}O$ values within the profile have an average of 0.15 ± 0.45‰ (n=3) and a range of 0.90‰. The most negative $\delta^{18}O$ values within the profile have an average of -1.06 ± 0.30‰ (n=4) and a range of 0.67‰. There are four distinct morphological ridges (A-D) on the surface of the chondrophore which nearly coincide with the most negative $\delta^{18}O$ values of each cycle. Isotopic temperatures indicate an annual temperature range from ~13º to 22ºC with an average annual temperature of ~18º ± 2.0ºC (n=34). Average winter and summer temperatures were 14º ± 1.4ºC (n=3), and 20º ± 1.4ºC (n=4), respectively. Internal chambers within shell 1 were infilled with secondary dogtooth sparry calcite and one sample of recrystallized carbonate, noted by its bright orange luminescence, was drilled from shell 1 and had a $\delta^{13}C$ value of 0.22‰, and a $\delta^{18}O$ value of -0.66‰.

Table 4.2 - Summary statistics for all the data from diagenetic sub-sampling. Rx-recrystallized calcite, DTS-dogtooth spar, Lm-luminescent calcite, Rnd-DTS-additional samples of dogtooth spar collected (see Chapter 3).

	Shell 1 Rx	(n=1)	Shell 3 Rx	(n=5)	Shell 4 DTS	(n=3)
	$\delta^{13}C$	$\delta^{18}O$	$\delta^{13}C$	$\delta^{18}O$	$\delta^{13}C$	$\delta^{18}O$
Min =	0.22	-0.66	-3.85	-3.31	-5.54	-2.94
Max =	0.22	-0.66	-2.06	-2.78	-4.44	-2.22
Rng =	0.00	0.00	1.80	0.53	1.10	0.72
Avg =	0.22	-0.66	-2.00	-2.33	-4.92	-2.52
StDev=	0.00	0.00	2.31	1.60	0.56	0.38

	Shell 6 Lm	(n=10)	Shell 6 Rx	(n=5)	Rejected (Sh 6)	(n=37)	Shell 6 DTS	(n=10)
	$\delta^{13}C$	$\delta^{18}O$	$\delta^{13}C$	$\delta^{18}O$	$\delta^{13}C$	$\delta^{18}O$	$\delta^{13}C$	$\delta^{18}O$
Min =	-4.44	-3.12	-1.86	-1.87	-5.11	-2.77	-6.95	-3.29
Max =	-0.61	-1.57	-0.81	-1.36	-1.86	-1.16	-5.59	-2.79
Rng =	3.82	1.55	1.05	0.50	3.25	1.61	1.37	0.50
Avg =	-3.20	-2.28	-1.20	-1.57	-4.38	-2.28	-6.29	-3.04
StDev=	1.14	0.45	0.41	0.21	0.53	0.30	0.48	0.17

	Rnd-DTS	(n=10)	ALL Rx	(n=11)	ALL DTS	(n=23)
	$\delta^{13}C$	$\delta^{18}O$	$\delta^{13}C$	$\delta^{18}O$	$\delta^{13}C$	$\delta^{18}O$
Min =	-8.30	-3.47	-3.85	-3.31	-8.30	-3.47
Max =	-4.63	-1.96	0.22	-0.66	-4.44	-1.96
Rng =	3.67	1.51	4.07	2.65	3.86	1.51
Avg =	-6.83	-3.11	-1.67	-2.11	-6.35	-3.00
StDev=	1.02	0.45	1.17	0.87	0.97	0.38

Figure 4.5

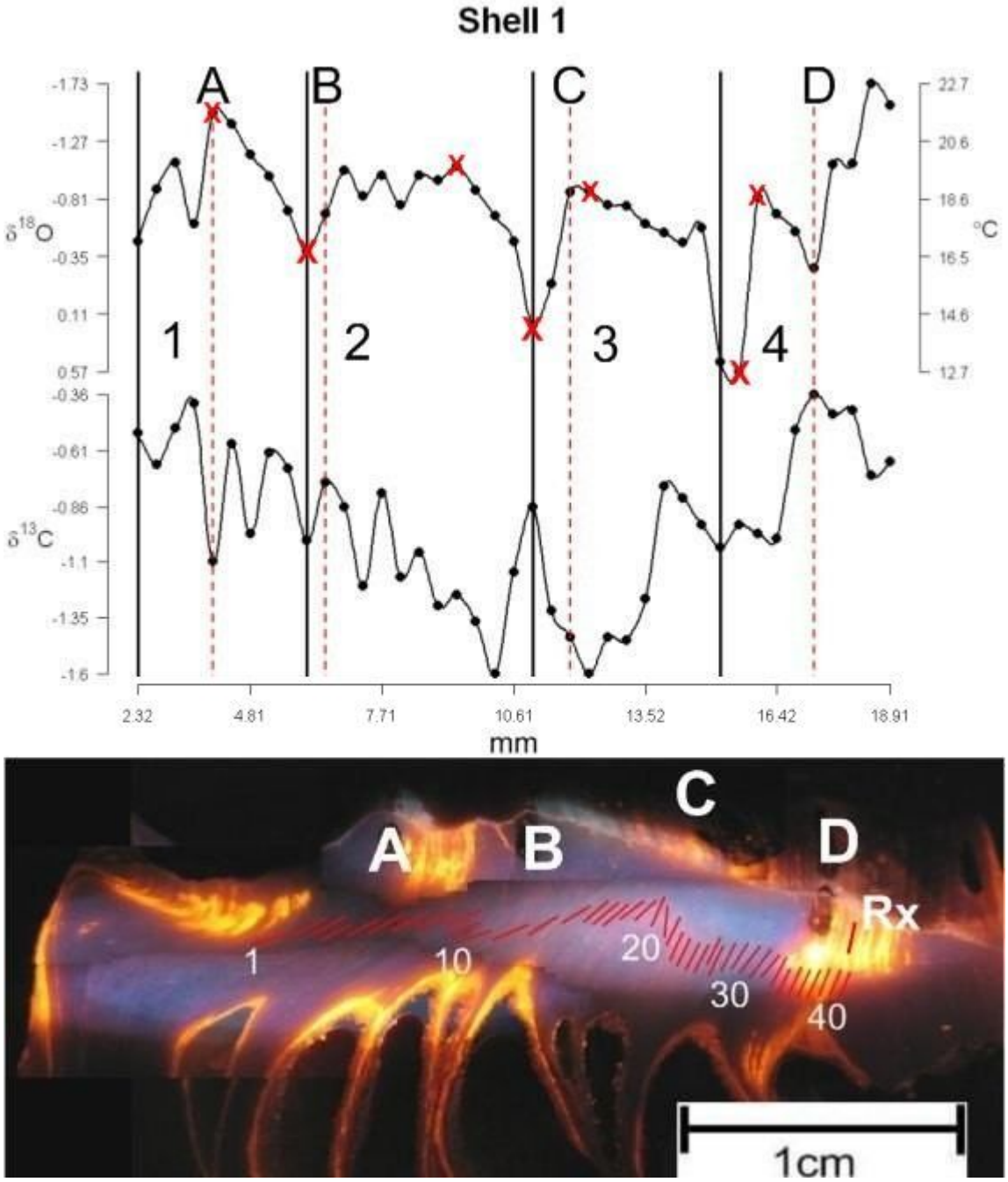

Figure 4.5 - Isotope profiles for shell 1 showing both the carbon and oxygen isotope profiles. Y axis for oxygen isotopes is inverted so that paleotemperature increases upwardly. An image of the section viewed under cathodoluminescence is provided in the bottom panel. Red lines on image indicate locations of drilled samples. Letters demarcate locations of morphological ridges as do dotted lines on the $\delta^{18}O$ profile. Solid vertical lines represent divisions between cycles. X's show the most positive and most negative values.

Isotope profiles and a cathodoluminescence photograph of the drilled section from shell 2 are shown in Figure 4.6. There was little to no luminescence along the drilled profile and no recrystallized mineral fabrics were observed in thin section except within the vicinity of where the chip is broken. Carbon and oxygen isotopes from shell 2 average at -0.91 ± 0.3‰ (n=74), and -0.68 ± 0.26‰ (n=74), and have ranges of 1.93‰ and 1.05‰, respectively. There are three to four cycles in the oxygen isotope profile that are not correlated with the $\delta^{13}C$ values (R^2=0.07) (Figure 4.11). The most positive $\delta^{18}O$ values within the profile have an average of -0.27 ± 0.06‰ (n=3), and a range of 0.11‰. The most negative $\delta^{18}O$ values within the profile have an average of -0.97 ± 0.09‰ (n=4), and a range of 0.21‰. There were four distinct morphological peaks on the surface of the chondrophore of shell 2 (A-D) which nearly coincided with the most negative $\delta^{18}O$ values of each cycle. Isotopic temperatures indicate an annual temperature range from ~16º to 21ºC, with an average temperature of 18º ± 1.14ºC (n=74). Average winter and summer temperatures were 16º ± 0.2ºC (n=3) and 19º ± 0.4ºC (n=4) respectively. Internal chambers within shell 2 were infilled with a thin rim of secondary dogtooth sparry calcite. There were no diagenetic sub-samples collected from shell 2.

Isotope profiles and a cathodoluminescence photo of the drilled section from shell 3 are shown in Figure 4.7. There were a few bands of dull luminescence but no recrystallized mineral fabrics were observed in thin section over the area of the drilled profile. Carbon and oxygen isotopes from shell 3 average at -1.31 ± 0.65‰ (n=69), and -1.13 ± 0.46‰ (n=69), and have ranges of 2.59‰ and 2.04‰, respectively. There were three to four cycles in the oxygen isotope profile that are not correlated with the $\delta^{13}C$ values (R^2=0.03) (Figure 4.11). The most positive $\delta^{18}O$ values within cycles of the $\delta^{18}O$

Figure 4.6

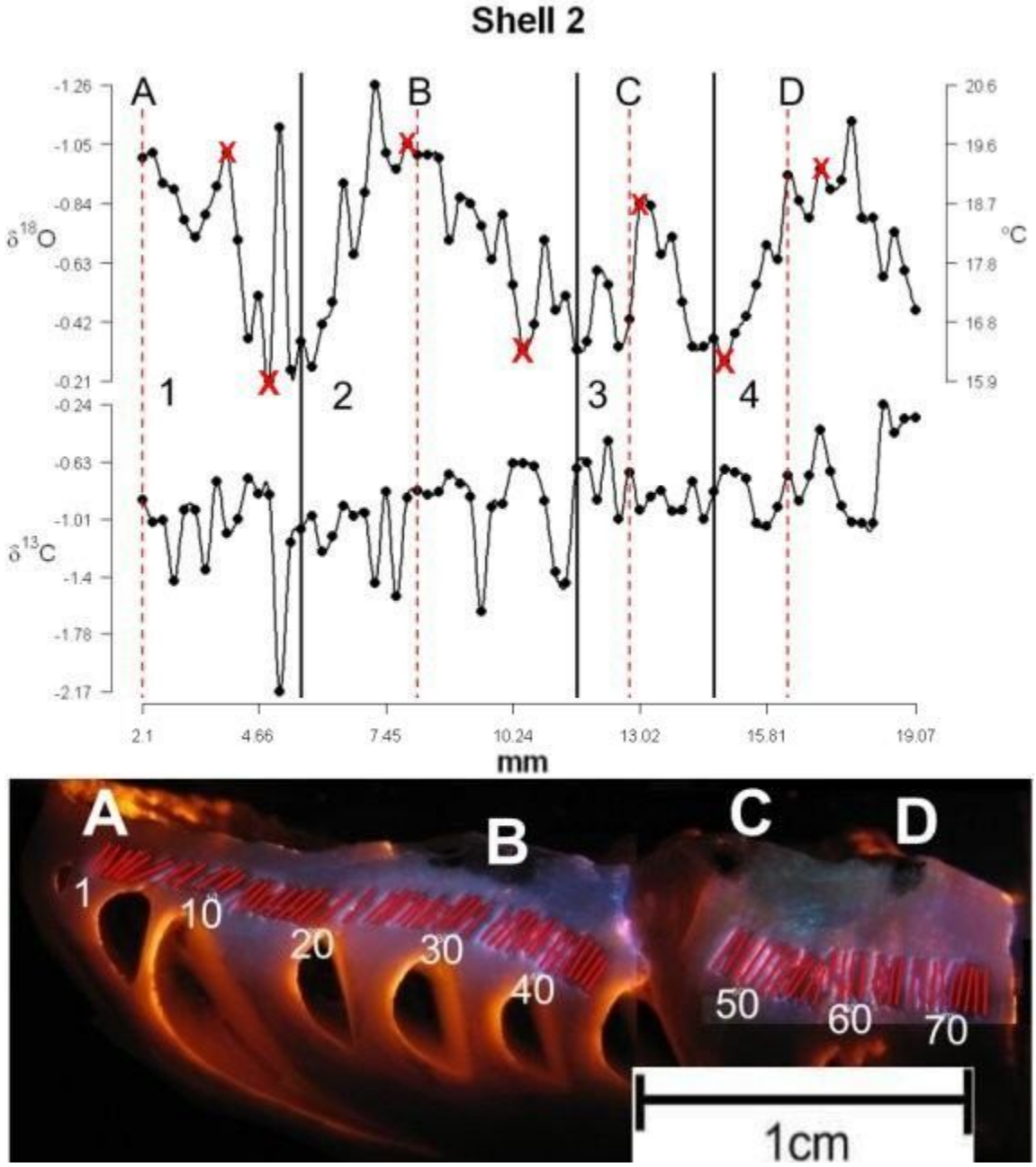

Figure 4.6 - Isotope profiles for shell 2 showing both the carbon and oxygen isotope profiles. Y axis for oxygen isotopes is inverted so that paleotemperature increases upwardly. An image of the section viewed under cathodoluminescence is provided in the bottom panel. See Figure 4.5 for definition of displayed features.

Figure 4.7

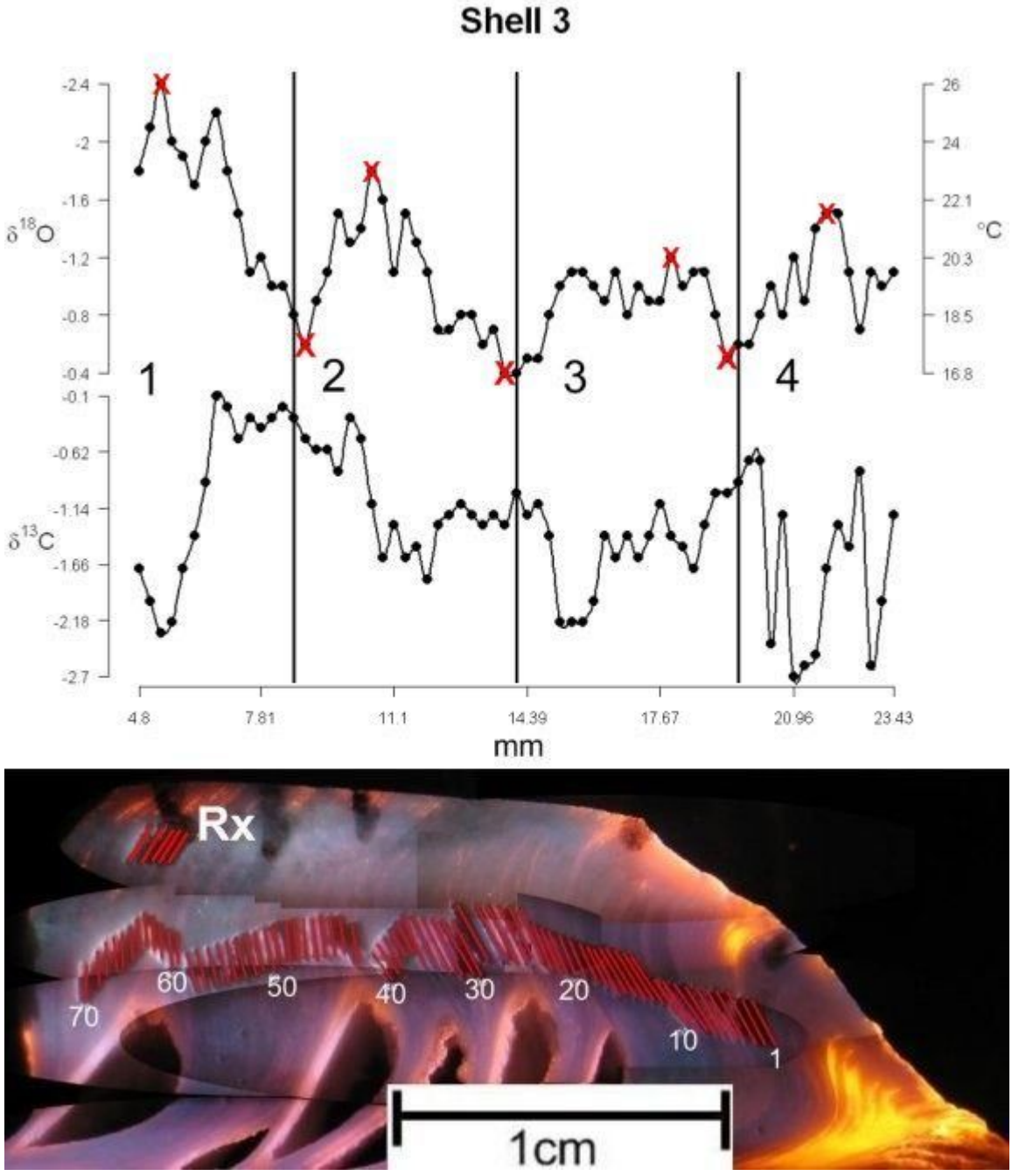

Figure 4.7- Isotope profiles for shell 3 showing both the carbon and oxygen isotope profiles. Y axis for oxygen isotopes is inverted so that paleotemperature increases upwardly. An image of the section viewed under cathodoluminescence is provided in the bottom panel. See Figure 4.5 for definition of displayed features.

profile have an average of -0.50 ± 0.10‰ (n=3), and a range of 0.20‰. The most negative $\delta^{18}O$ values within the profile have an average of -1.73 ± 0.51‰ (n=4), and a range of 1.20‰. There were no distinct morphological ridges on the surface of the chondrophore of shell 3. Isotope temperatures indicate an annual temperature range from ~17º to 26ºC, with an average temperature of 20º ± 2.1ºC (n=69). Average winter and summer temperatures were 17º ± 0.4ºC (n=3), and 23º ± 2.4ºC (n=4), respectively. Internal chambers within shell 3 were infilled with a thin rim of secondary dogtooth sparry calcite. Samples of recrystallized calcite drilled from shell 3 have an average $\delta^{13}C$ and $\delta^{18}O$ value of -2.00 ± 2.31‰ (n=5) and -2.33 ± 1.60‰ (n=5), with ranges of 1.80‰ and 0.53‰, respectively.

Isotope profiles and a cathodoluminescence photo of the drilled section of shell 4 are shown in Figure 4.8. There were a few bands of dull luminescence and no recrystallized mineral fabrics were observed in thin section over the area of the drilled profile. Carbon and oxygen isotopes from shell 4 average at -3.04 ± 1.17‰ (n=47), and -1.40 ± 0.50‰ (n=47), and have ranges of 4.11‰ and 1.79‰, respectively. There are four cycles in the oxygen isotope profile that are positively correlated with the $\delta^{13}C$ values (R^2=0.66) (Figure 4.11). The most positive $\delta^{18}O$ values within cycles of the $\delta^{18}O$ profile have an average of -0.66 ± 0.15‰ (n=5) and a range of 0.40‰. The most negative $\delta^{18}O$ values within the profile have an average of -2.18 ± 0.19‰ (n=4) and a range of 0.40‰. There were no distinct morphological ridges on the surface of the chondrophore of shell 4. Isotopic temperatures indicate an annual temperature range from ~17º to 25ºC with an average temperature of 21º ± 2.3ºC (n=47). Average winter and summer temperatures were 18º ± 0.4ºC (n=5) and 25º ± 0.9ºC (n=4), respectively.

Figure 4.8

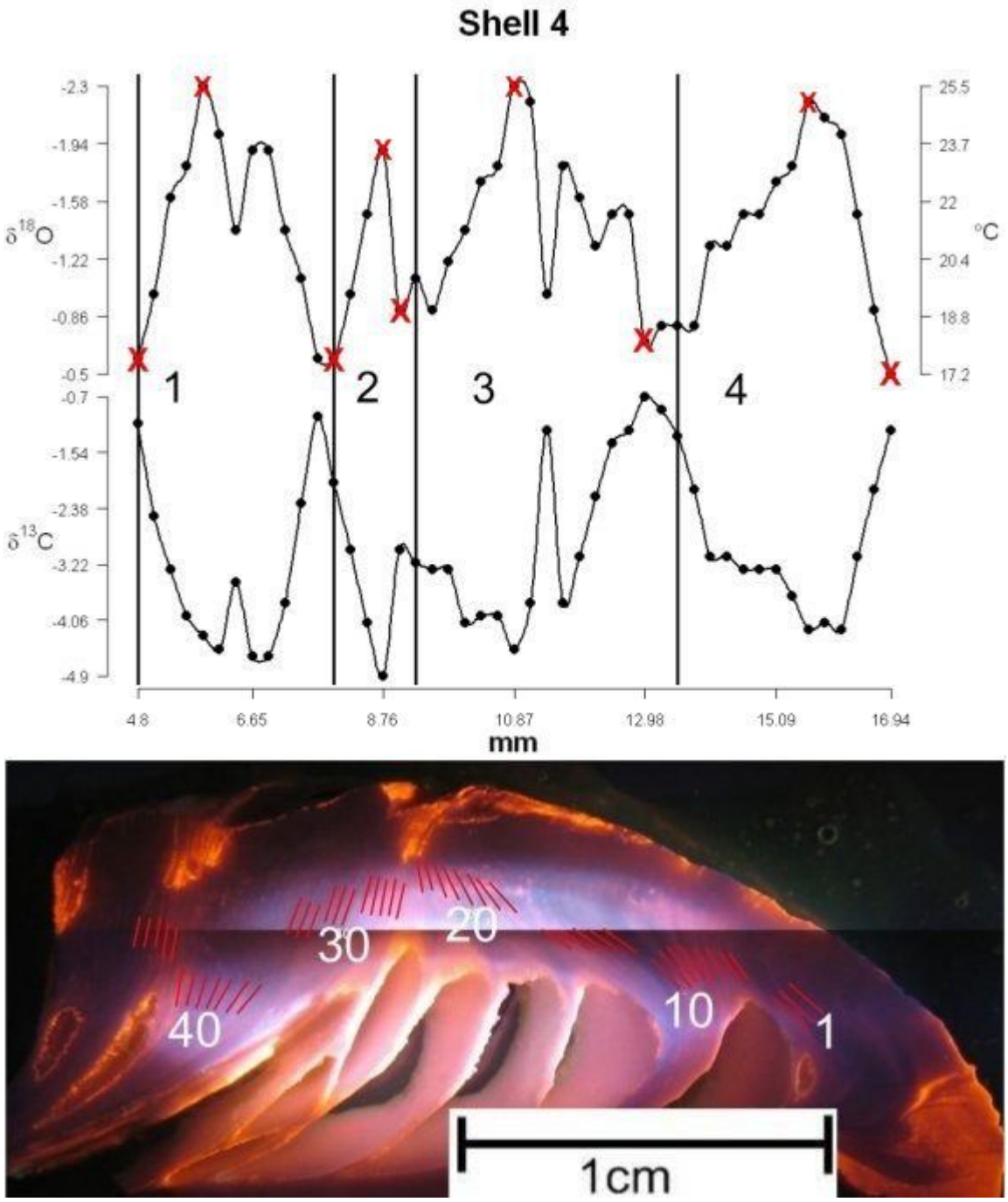

Figure 4.8 - Isotope profiles for shell 4 showing both the carbon and oxygen isotope profiles. Y axis for oxygen isotopes is inverted so that paleotemperature increases upwardly. An image of the the section viewed under cathodoluminescence is provided in the bottom panel. See Figure 4.5 for definition of displayed features.

Internal chambers within shell 4 were infilled with a rim of secondary dogtooth sparry calcite. These dogtooth spar samples have an average $\delta^{13}C$ and $\delta^{18}O$ value of -4.92 ± 0.56‰ (n=3), and -2.52 ± 0.38‰ (n=3), with ranges of 1.1‰ and 0.72‰, respectively.

Isotope profiles and a cathodoluminescence photo of the drilled section of shell 5 are shown in Figure 4.9. There are a few bands of dull luminescence towards the middle of the profile and towards the ventral end but no recrystallized microfabrics were observed in the thin section from where samples were collected. Carbon and oxygen isotopes from shell 5 average at -0.82 ± 1.15‰ (n=70), and -1.18 ± 0.52‰ (n=70), and have ranges of 4.46‰ and 2.08‰, respectively. There are three cycles in the oxygen isotope profile that are positively correlated with the $\delta^{13}C$ values (R^2=0.78) (Figure 4.11). The most positive $\delta^{18}O$ values within the $\delta^{18}O$ cycles the profile have an average of -0.50 ± 0.22‰ (n=4), and a range of 0.50‰. The most negative $\delta^{18}O$ values within the profile have an average of -1.93 ± 0.42‰ (n=4), and a range of 0.80‰. There were three morphological ridges on the surface of the chondrophore which nearly coincide with the most negative $\delta^{18}O$ value of each cycle. Isotopic temperatures indicate an annual temperature range of ~16º to 25ºC, with an average annual temperature of 20º ± 2.4ºC (n=70). Average winter and summer temperatures were 17º ± 0.94ºC (n=4), and 24º ± 2.0ºC (n=3), respectively. Internal chambers within shell 5 were infilled with secondary dogtooth sparry calcite. There were no diagenetic sub-samples collected from shell 5.

Isotope profiles and a cathodoluminescence photo of the drilled section from shell 6 are shown in Figure 4.10. There was a change in the luminescent character coupled with a change from foliated fabric to blocky spar beginning at sample 24 and extending to the end of the profile (sample 60), indicating diagenetic alteration in this portion of the

Figure 4.9

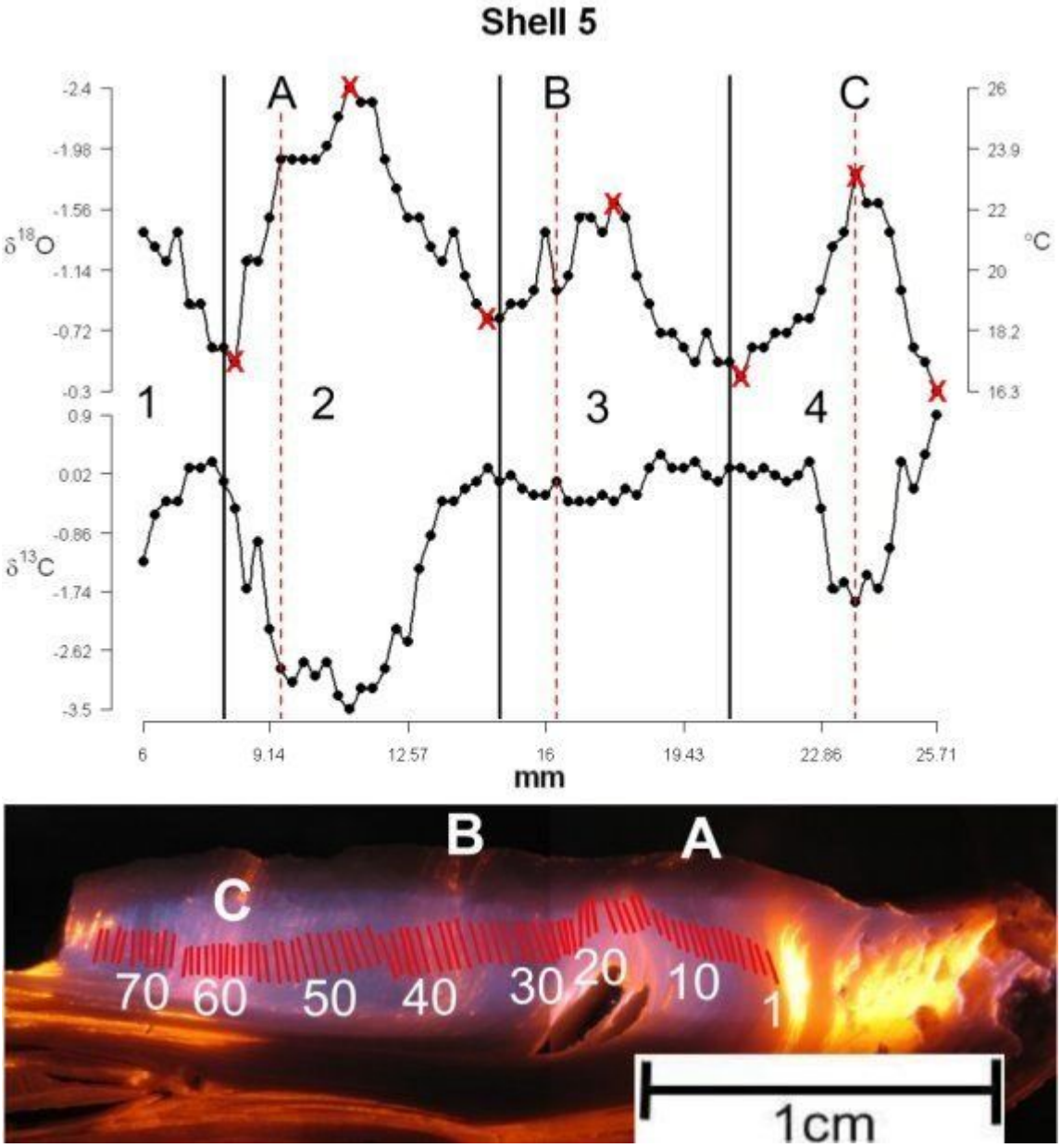

Figure 4.9 - Isotope profiles for Shell 5 showing both the carbon and oxygen isotope profiles. Y axis for oxygen isotopes is inverted so that paleotemperatures increase upwardly. An image of the section viewed under cathodoluminescence is provided in the bottom panel. See Figure 4.5 for definition of displayed features.

Figure 4.10

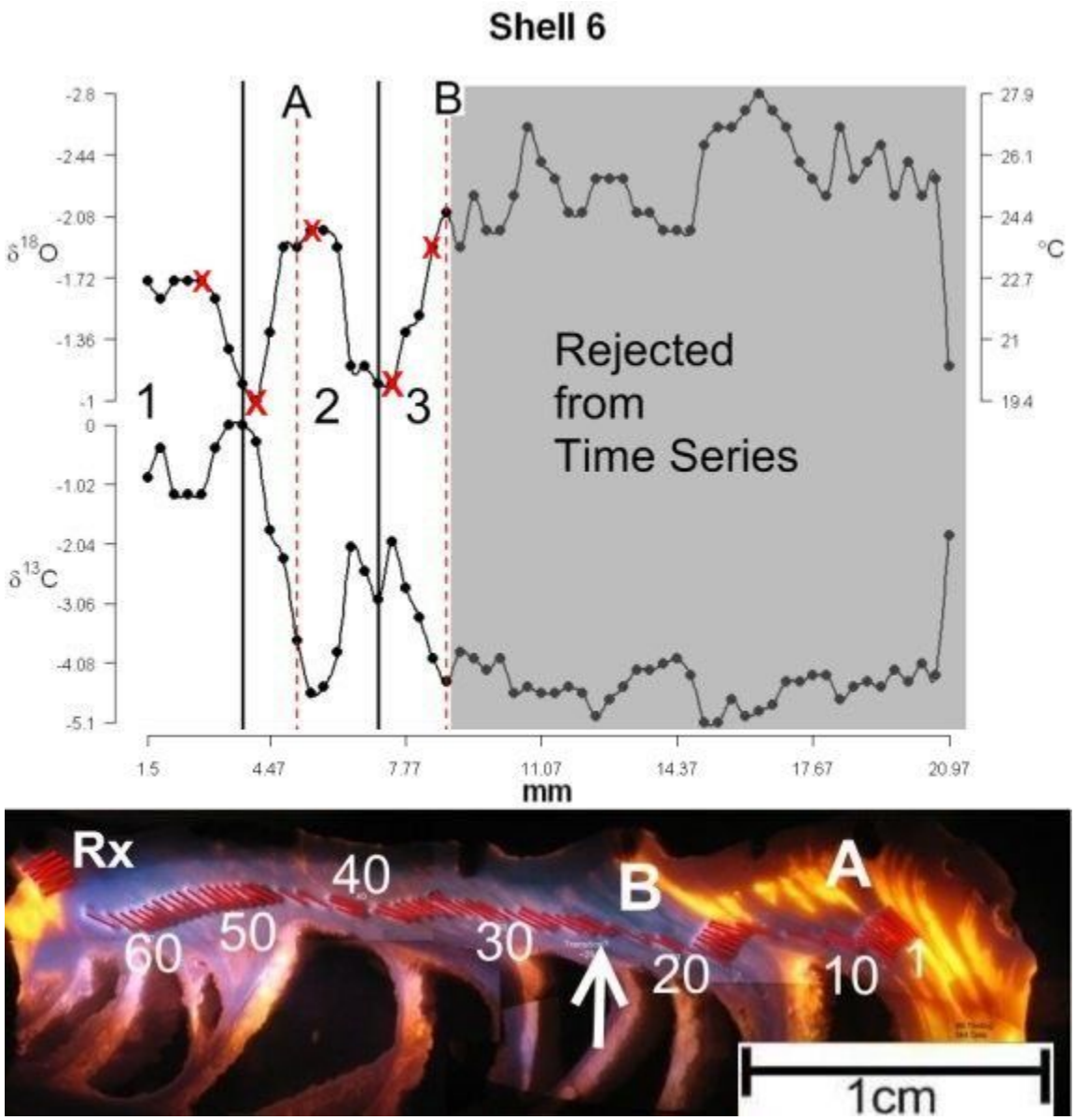

Figure 4.10 - Isotope profiles for Shell 6 showing both the carbon and oxygen isotope profiles. Y axis for oygen isotopes is inverted so that paleotemperature increases upwardly. An image of the section viewed under cathodoluminescence is provided in the bottom panel. Diagenetic samples are shaded gray. See Figure 4.5 for definition of displayed features.

drilled section. Carbon and oxygen isotopes from shell 6 average -2.2 ± 1.53‰ (n=23), and -1.57 ± 0.34‰ (n=23), for the unaltered portion, and have ranges of 4.65‰ and 1.06‰, respectively. There were two cycles in the primary portion of the oxygen isotope profile that are weakly correlated with the $\delta^{13}C$ values (R^2=0.32) (Figure 4.11). The most positive $\delta^{18}O$ values within the unaltered profile have an average of -1.05 ± 0.07‰ (n=2), and a range of 0.10‰. The most negative $\delta^{18}O$ values have an average of -1.87 ± 0.15‰ (n=3), and a range of 0.30‰. There are two distinct morphological ridges on the surface of the chondrophore within the nonluminescent part of the profile which nearly coincide with the most negative $\delta^{18}O$ values of each cycle. Isotopic temperatures indicate an annual temperature range from ~20º to 25ºC, with an average temperature of 22 ± 1.6ºC (n=23). Average winter and summer temperature was 20º ± 0.3ºC (n=2), and 23º ± 0.7ºC (n=3), respectively. Internal chambers within shell 6 were infilled with secondary dogtooth sparry calcite. Rejected samples of luminescent calcite collected from shell 6 (samples 24 - 60 at ~0.8 to 21.0 mm) (Table 4.2) have an average $\delta^{13}C$ and $\delta^{18}O$ value of -4.38 ± 0.53‰ (n=37) and -2.28 ± 0.30‰ (n=37) with ranges of 3.25‰ and 1.61‰, respectively. Samples of recrystallized calcite from shell 6 (Table 2) have an average $\delta^{13}C$ and $\delta^{18}O$ value of -1.20 ± 0.41‰ (n=5) and -1.57 ± 0.21‰ (n=5), with ranges of 1.05‰ and 0.50‰, respectively. Luminescent calcite samples from shell 6 have an average $\delta^{13}C$ and $\delta^{18}O$ value of -3.20 ± 1.14‰ (n=10), and -2.28 ± 0.45‰ (n=10), respectively. Dogtooth spar collected from the internal chambers of shell 6 have an average $\delta^{13}C$ and $\delta^{18}O$ value of -6.29 ± 0.48‰ (n=10) and -3.04 ± 0.17‰ (n=10) with ranges of 1.37‰ and 0.5‰, respectively.

Figure 4.11

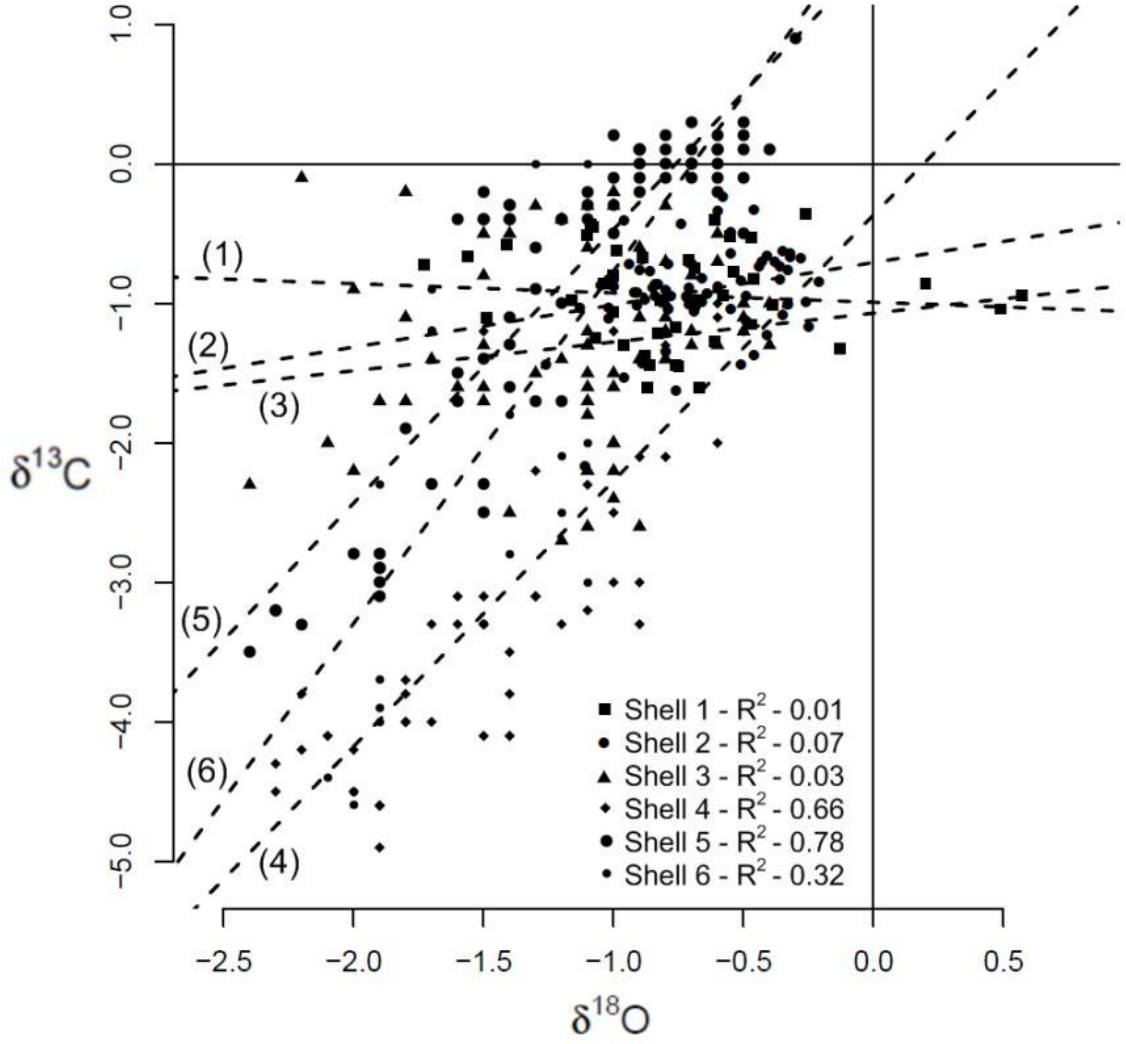

Figure 4.11 - Crossplot of data from each shell sampled for stable isotopes in this study. Regression lines are numbered for each corresponding shell.

Chapter 5

Discussion

Diagenesis

In order to extract paleoenvironmental information from the isotope composition of *C. gigantissima* shells it is important to distinguish diagenetic overprints from primary isotope signals. Diagenetically altered shell material was recognized by: 1) cathodoluminescence and, 2) the presence of a blocky spar mineral fabric. Dogtooth calcite was recognized as a third diagenetic phase that rimmed the surface of internal shell chambers and it displayed bright orange luminescence as well. For the purpose of this discussion, diagenetically altered samples were placed into two broad groupings: 1) recrystallized and luminescent shell material (observed in shells 1, 3, and 6), and 2) dogtooth spar calcite (observed in shells 4, 6 and elsewhere - see Chapter 3). In contrast, primary shell material was recognized by: 1) the lack of cathodoluminescence, and 2) the presence of a primary foliated mineral fabric. Visible growth bands on the surface of cut and polished sections also aided in the identification of primary shell material.

The isotope composition of all the primary and diagenetic shell samples are compared to the field of $\delta^{18}O$ values for Late Eocene low magnesian calcite (LMC from planktonic and benthic foraminifera) and diagenetic soil-related calcites in Figure 5.1. Most of the diagenetic samples (open symbols) have $\delta^{18}O$ values between -3.5‰ and -2.0‰, while most of the primary samples (closed symbols) have $\delta^{18}O$ values between -2.0‰ and 0‰. When considered by shell, the recrystallized sample from shell 1 has a

Figure 5.1

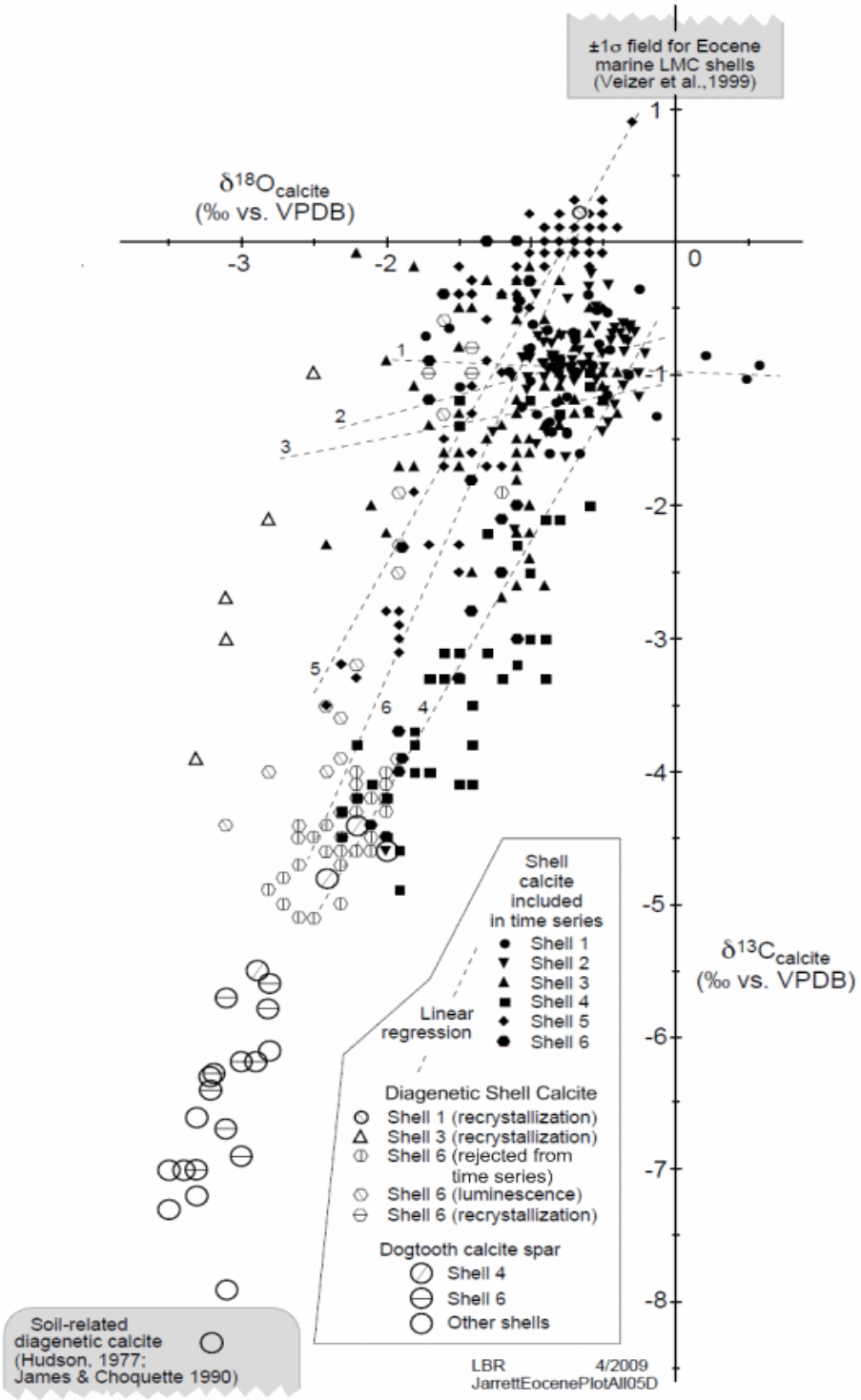

Figure 5.1 - Crossplot of all samples including fields for diagenetic soil-related carbonates (Hudson, 1977; James and Choquette, 1990) and Late Eocene low magnesian calcite (LMC) of marine origin (Veizer et al., 1999).

$\delta^{18}O$ value that is within the range of values for primary shell material. Recrystallized samples from shell 3 have more negative $\delta^{18}O$ values than the primary samples, as do recrystallized samples from shell 6 [luminescence (Lm), recrystallized (Rx) and rejected samples]. Almost all of the dogtooth spar samples have $\delta^{18}O$ values that are lower than the primary samples from an individual shell.

All diagenetic samples have a broad range of $\delta^{13}C$ values from -8.3‰ to 0‰, which contrasts with the primary samples which range from -5.0‰ to 1.0‰. When considered by shell, the recrystallized sample from shell 1 has a $\delta^{13}C$ value which is more positive than all the primary samples from this shell. Recrystallized samples from shell 3 generally have more negative $\delta^{13}C$ values than do the primary samples (avg: -2.0 ± 2.3‰ vs.-1.3 ± 0.7‰), as do the recrystallized samples from shell 6. Almost all the dogtooth spar samples have $\delta^{13}C$ values that are lower than the primary samples.

All of the samples of this study plot between the field for Late Eocene low magnesian calcite (LMC: Veizer et al., 1999) and diagenetic soil-related calcite (Hudson, 1977; James and Choquette, 1990) in Figure 5.1. Most of the primary samples plot close to the LMC field while most of the dogtooth spar plot nearest the diagenetic soil-related calcite field, while the remaining diagenetically altered samples plot with intermediary compositions.

The altered samples may be viewed within the context of open and closed system diagenesis. In open system diagenesis, rock/water ratios are relatively low (Bathurst, 1975), and this results in alternation products that have isotope values similar to the infiltrating diagenetic fluids. In the case of low temperature freshwater alteration, these fluids will be relatively low in $\delta^{18}O$ value due to their meteoric origin. In addition, they

will be relatively low in $\delta^{13}C$ value, especially for formations that have low buffering capacity (i.e., low carbonate content; Hoefs, 1997). In this context, the dogtooth spar samples may have precipitated through open system diagenesis, where void-filling carbonate cements formed from diagenetic fluids seeping through pore spaces (Bathurst, 1975) into the internal chambers of the shells. This interpretation is consistent with the isotope composition of dogtooth spar samples, which plot nearest the field for diagenetic soil-related calcite.

In closed system diagenesis, rock/water ratios can be relatively high, and diagenetic fluids may acquire isotope compositions that are more similar to the rocks through which they flow (Martin et al., 1986). For the case of low temperature diagenesis of shells at Griffins Landing, these fluids may be isotopically similar to the original shell material (Bathurst, 1975; Martin et al., 1986, Martin et al., 1986). This interpretation is consistent with the isotope composition of most of the recrystallized samples in this study.

Primary samples from shell 1, 2, and 3 plot close to the Late Eocene LMC field. The difference in isotopic composition may be attributed to intrinsic differences in the types of samples analyzed in each study (i.e., benthic foraminifera vs. mollusk) or slight differences in the isotope composition of the marine waters from which the samples formed. It is interesting to note that no statistically significant relationship exists between the $\delta^{13}C$ and $\delta^{18}O$ values of these samples.

Curiously, the "unaltered" samples from shells 4, 5, and 6 did not display luminescence or altered fabrics that are the hallmark of diagenetic alteration, yet they display trends in $\delta^{13}C$ and $\delta^{18}O$ values that are similar to the diagenetically altered

samples. Linear regressions of the isotope data for shells 4 – 6, all the recrystallized samples, and the dogtooth spar samples are shown in Figure 5.2 (coefficients for linear regressions and correlation coefficients are presented in Table 5.1). It is clear that samples from shells 4 - 6 display trends similar to the diagenetically altered samples, as well as the mixing line for Late Eocene LMC and diagenetic soil-related carbonates. The slopes for the regression lines of the diagenetic (recrystallized, luminescent, dogtooth) samples range from 1.5 to 2.3 much like the slopes for linear regressions of the data from shells 4 - 6 (1.9 to 2.5; Table 5.1 and Figure 5.2). While the slopes from primary samples from shells 1 -3 range from -0.7 to 0.3. This suggests the possibility that shells 4, 5, and 6 were influenced by diagenetic fluids.

The data from this study are compared to published data for modern *Crassostrea* (Kirby, 2000; Surge and Lohmann, 2001) to better understand the significance of the $\delta^{13}C$ and $\delta^{18}O$ values from the fossil specimens (Figure 5.3: coefficients for regressions and correlation coefficients are presented in Table 5.1). The positive linear relationships displayed by data from Kirby (2000) and Surge and Lohmann (2001) are distinct from the diagenetically altered samples. This is not surprising given that the modern specimens were collected from estuarine environments. The relationships for modern specimens may be reconciled based on the mixing of isotopically distinct freshwater and seawater that commonly occurs in estuarine habitats (see Chapter 2). It follows that there is a tendency for estuarine shells to have a wider range of isotope compositions than marine shells. The analysis of the ranges in isotope composition reported in Figure 2.3 for previous studies of modern shells from marine and estuarine environments support this contention. Also, the data from Kirby (2000) and Surge and Lohmann (2001) are offset

Figure 5.2

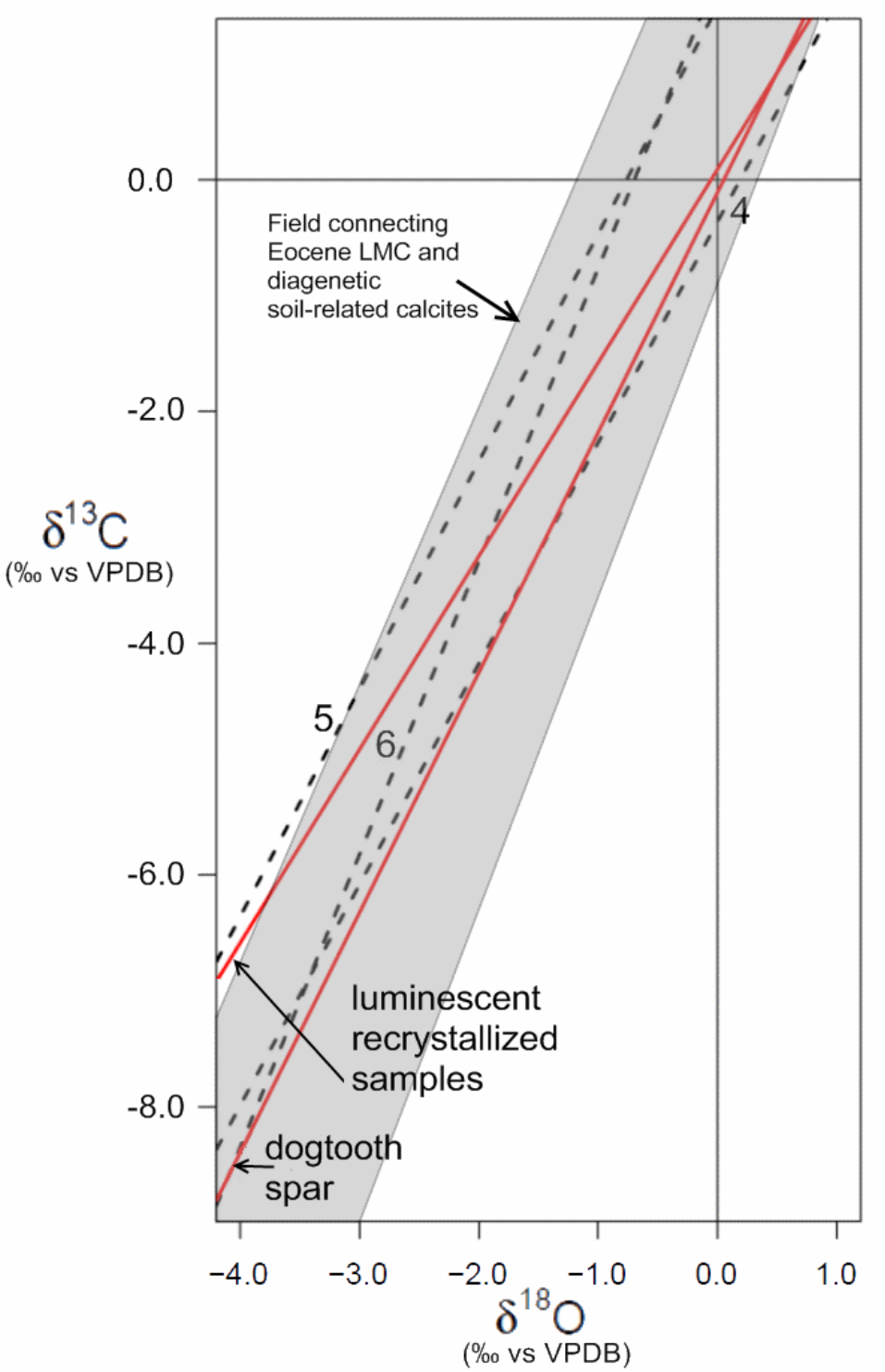

Figure 5.2 - Linear regressions for shells 4, 5, and 6 (dashed lines), and the diagenetically altered samples (solid lines).

Table 5.1 - Regression coefficients [slope (m) and y-intercept (b)] and correlation coefficients (R^2) for linear regression of the $\delta^{13}C$ and $\delta^{18}O$ values from various groups of samples in this and previous studies. Rx - recrystallized samples, Spar - dogtooth spar samples, Rej - rejected from time series, Lum - luminescent samples, Rndm - additional dogtooth spar samples

Sample	R^2	m (slope)	b (y-intercept)	
Shell 1	0.01	-0.70	-0.99	**(n=41)**
Shell 2	0.07	0.30	-0.71	**(n=74)**
Shell 3	0.03	0.21	-10.70	**(n=69)**
Shell 4	0.66	1.90	-0.37	**(n=47)**
Shell 5	0.78	1.96	1.49	**(n=70)**
Shell 6	0.32	2.53	1.76	**(n=23)**
Sh3Rx	0.97	3.39	7.49	**(n=5)**
Sh4Spar	0.99	1.54	-1.05	**(n=3)**
Sh6Rej	0.71	1.49	-0.99	**(n=37)**
Sh6Rx	0.72	1.72	1.56	**(n=5)**
Sh6Lum	0.78	2.27	2.01	**(n=10)**
Sh6Spar	0.39	1.77	-0.89	**(n=10)**
RndmSpar	0.56	1.72	-1.40	**(n=10)**
AllRx	0.35	1.67	0.09	**(n=58)**
AllSpar	0.67	2.07	-0.11	**(n=23)**
Kirby (2000)	0.41	0.43	-2.79	**(n=84)**
S & L (2001)	0.70	0.99	6.38	**(n=284)**

Figure 5.3

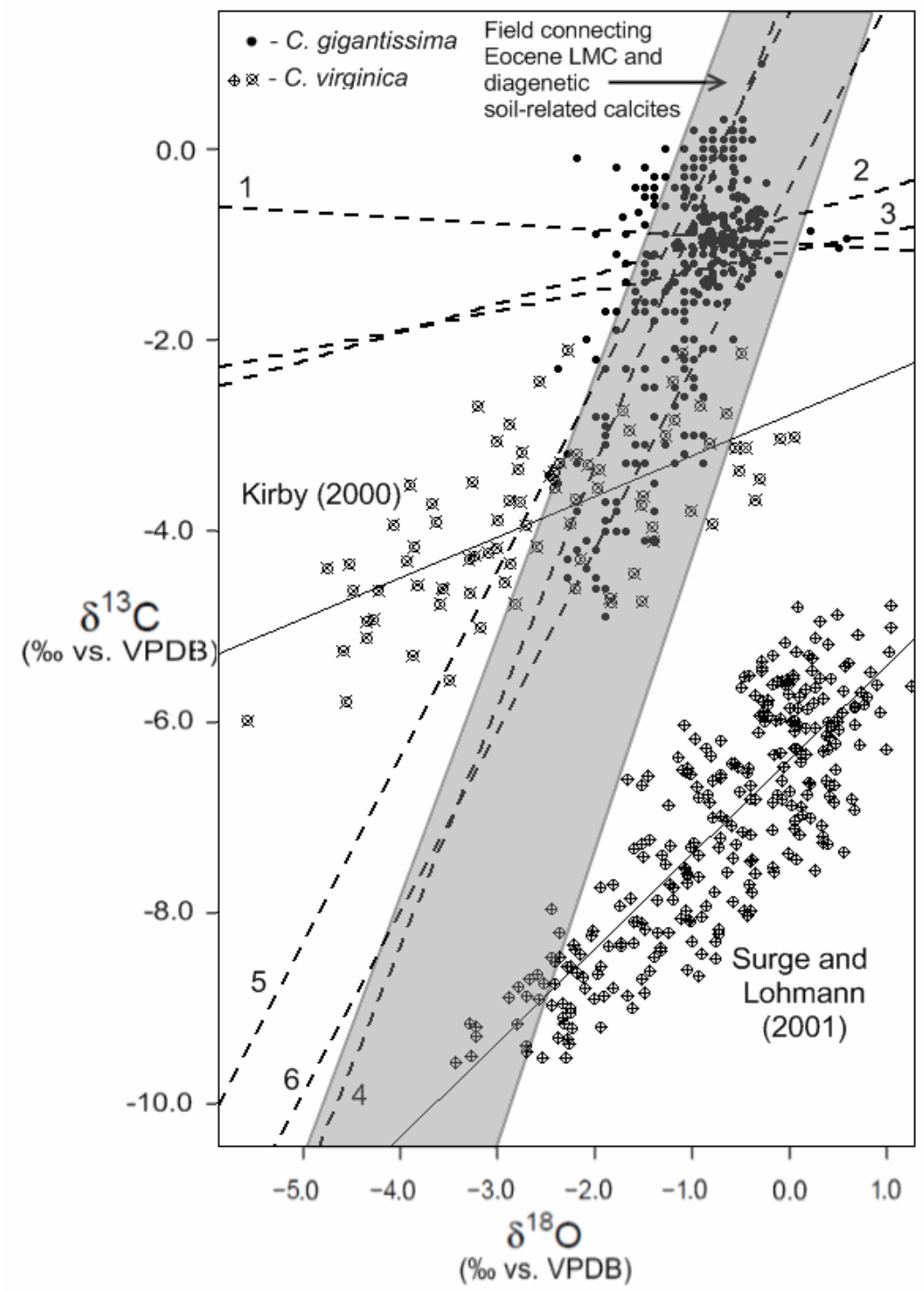

Figure 5.3 - Data from this study are compared to data from modern *Crassostrea virginica* (Kirby, 2000; Surge and Lohmann, 2001). Dashed lines represent correlations of samples from this study while solid lines are correlations for modern *Crassostrea*.

to slightly lower values than the primary samples analyzed from shells 1 – 3, which is consistent with an estuarine origin. On the other hand, while the linear regressions of the isotope data from the modern *Crassostrea* samples are distinct from those of shells 4 – 6, the possibility exists that the data from shells 4 – 6 represent primary material that formed in an estuarine environment, rather than in a secondary diagenetic environment.

This hypothesis may be evaluated by comparing data from shell 3 with shells 4,5, and 6 that were all collected from a single oyster reef. It is expected that samples from shell 3 would display similar isotope values to shells 4 – 6 if they were all primary, and that the trends in the data would be similar. However, not only are the primary samples from shell 3 isotopically distinct from shells 4 -6, these sample display a trend in isotope composition that is distinct from any group of diagenetically altered samples including those shell 3 (Table 5.1; Figure 5.1). The conclusion to be drawn from this analysis is that shells 4 - 6 are diagenetically altered in subtle ways that cannot be detected using cathodoluminescence and thin section petrography.

The fact that shells 4,5, and 6 still retain primary mineral fabrics is perplexing. The possibility exists that minor amounts of diagenetic calcite are infilling small pore spaces in these shells that is undetectable using thin section petrography or cathodoluminescence techniques (Martin et al., 1986). Other studies have documented the preservation of primary fabrics in shells while geochemical data suggest they are diagenetically altered (Martin et al., 1986). Given that the $\delta^{18}O$ values from dogtooth spar samples are similar to primary shell material while their $\delta^{13}C$ values are distinct suggests that $\delta^{13}C$ values may be a sensitive indicator for the freshwater diagenesis of marine shells.

Also troubling is the fact that shells 4 - 6 still retain a cyclical pattern of $\delta^{18}O$ and $\delta^{13}C$ values within the isotope profiles. Given that diagenetic processes should overprint primary isotopic signals, as demonstrated by the recrystallized portion of samples in this study, the presence of cyclicity within the isotope profiles suggests that diagenesis imparted a minor effect on the isotope composition of these shells.

Based on the collective observations presented above, the conclusion is drawn that shells 1, 2, and 3 represent unaltered shells, while shells 4, 5 and 6 are diagentically altered. Therefore only samples from shells 1, 2, and 3 will be used in the paleoclimate analysis which follows.

Paleoenvironmental Implications

Prior interpretations of the environment of deposition for the Griffins Landing Member (GLM) suggests a near-shore normal marine to lagoon setting (Fallaw and Price, 1992; Thayer and Harris, 1992). Because of the variability in paleoenvironmental interpretations (see Chapter 1), the depositional environment of the Griffins Landing Member is vaguely defined. The stable isotope profiles of *C. gigantissima* may provide some additional information to constrain the depositional environment of the GLM. Compared to the carbon and oxygen isotope values from modern shells collected from known environments, the range of isotope compositions for primary material from shells 1,2 and 3 from Griffins Landing plot within the field for a normal marine environment (see Figure 2.2 and 2.3). This interpretation is supported by the lack of a strong linear relationship between the $\delta^{13}C$ and $\delta^{18}O$ values of shells 1,2, and 3 compared to correlated values for shells deposited in an estuarine environment [e.g., data of Kirby (2000) and Surge and Lohmann (2001) in Figure 5.3; Table 5.1).

Modern *Crassostrea* thrive in fringing environments such as estuaries because these environments offer protection from predatory gastropods and bioerosion that are encountered in normal marine environments (Galtsoff, 1964). Evidence for bioerosion by bivalves and clionid sponges, observed in most shells that were collected at Griffins Landing is consistent with the interpretation of a normal marine environment. In addition, published barnacle data from the GLM suggest a subtidal habitat because the morphology of the barnacles suggests that they could not withstand dessication (Zullo and Kite, 1985). This suggests the oysters of this study lived in a subtidal marine environment.

Paleobiological Implications

Ontogenetic Age of Shells

Periodic cycles in the oxygen isotope profiles of mollusk shells are useful in addressing problems involving the age and growth rate of organisms (Kirby, 1998; Jones and Gould, 1999). A prior study of *Crassostrea gigantissima* placed the lifespan of the oyster at ~11 years, based on periodic cycles in the $\delta^{18}O$ profiles of shell carbonate and counts of morphological ridges and valleys on the surface of the chondrophore of individual specimens (Kirby, 2000). Anywhere from three to four annual cycles are recorded in the oxygen isotope profile of the specimens of this study, except for shell 6 which contained two cycles within the primary portion of the shell (see Chapter 4).

To confirm that the cycles reflect annual growth, morphological ridges on the chondrophore of each shell were compared to the oxygen isotope profiles (see Chapter 4). All observed ridges consistently plotted near the most negative $\delta^{18}O$ value of each oxygen isotope cycle of a profile (Figures 4.5 - 4.10). In this regard, ridges represent summer

growth. Based on this, the average yearly growth rate for shells of this study were determined (Table 5.2). The range of values was 2.1 to 7.9 mm/yr and the average growth rate was 4.8 ± 2.0 mm (n=6).

To further evaluate the growth rate of *C. gigantissima,* ridge and valley measurements were taken from 16 additional shells of collected from various locations at Griffins Landing. The average distance between morphological ridges was 5.7 ± 2.1 mm (n=96 ridges) (Table 5.3). This growth rate is indistinguishable from growth rate determined by $\delta^{18}O$ cycles in shells 1 - 6 (using 1 standard deviation). For comparison the data from Kirby (2000) show average annual growth rates of 6.3 and 8.3 mm/yr for *C. gigantissima* (shells BQ-1 and BQ-2, respectively), the average growth rates reported in this study are outside of the standard deviation for the mean from Kirby's data. Kiby's data are distinguishable from our data in that they show higher growth rates than shells from this study. A higher growth rate could be due to a myriad of factors including differneces in habitat, or life history strategies among individuals.

Isotope Profiles and Calcification Cessation

As discussed earlier, Kirby (2000) suggested that the temperature of calcification cessation for *Crassostrea gigantissima* is 10ºC. Given this information, a potential application exists for calculating the isotope composition of Late Eocene seawater using the temperature of cessation of calcification (10ºC) and the average most positive $\delta^{18}O$ value for cycles of the oxygen isotope profile of a shell (see Chapter 2). For shell 1 (Figure 4.5), the most positive $\delta^{18}O$ value of each cycle in the oxygen isotope profile appears as a transient spike similar in form to the idealized structure represented in Figure 2.4B. The average most positive $\delta^{18}O$ value for cycles of the profile is 0.15 ± 0.45‰

Table 5.2 - Growth rate of *C. gigantissima* based on the analysis of cycles in oxygen isotope profiles of shells in this study.

Specimen	Length of Drilled Profile (mm)	Observed Cycles	Average Growth Rate (mm/yr)
Shell 1	16.6	~3.5	4.7
Shell 2	27.6	~3.5	7.9
Shell 3	19	~3.5	5.4
Shell 4	12.4	~4	3.1
Shell 5	20	~3.5	5.7
Shell 6	4.2	~2	2.1
Avg Cycle Length =	**4.8 ± 2.0 mm**	**(n=6)**	

Table 5.3- Measurement of distances between morphological ridges on chondrophores of 16 additional shells collected at Griffins Landing. n= number of ridges observed in a chondrophore of a single shell, units are in millimeters.

	Chon-1	Chon-2	Chon-3	Chon-4
Avg=	5.52	5.21	5.97	6.19
StDev=	1.21	1.95	1.01	2.22
	(n=13)	**(n=11)**	**(n=4)**	**(n=5)**

	Chon-5	Chon-6	Chon-7	Chon-8
Avg=	5.53	6.00	2.85	3.73
StDev=	2.24	2.23	0.35	0.93
	(n=2)	**(n=8)**	**(n=3)**	**(n=6)**

	Chon-9	Chon-10	Chon-11	Chon-12
Avg=	7.42	6.29	5.07	4.43
StDev=	1.91	3.23	1.72	1.23
	(n=5)	**(n=7)**	**(n=3)**	**(n=5)**

	Chon-13	Chon-14	Chon-15	Chon-16
Avg=	6.40	4.05	6.70	7.74
StDev=	0.49	1.66	2.29	0.85
	(n=2)	**(n=6)**	**(n=9)**	**(n=7)**

	Grand Total
Avg=	**5.69**
StDev=	**2.09**
	(n=96)

(n=3; see Table 4.1). If this value is inserted into the paleotemperature equation with a temperature of 10ºC, the calculated isotope composition of seawater is -1.44‰. For the oxygen isotope profile of shell 2 (Figure 4.6), there is no indication of transient positive spikes suggestive of calcification cessation, but the range in the most positive values of $\delta^{18}O$ cycles is only 0.11‰ compared to that of shell 1 (0.90‰). Using the average most positive value of -0.27 ±0.06‰ from shell 2, the calculated $\delta^{18}O$ value for seawater is -1.86‰. The $\delta^{18}O$ profile for shell 3 (Figure 4.7) is similar in form to that of shell 2 with a relatively narrow range of values (0.20‰). Using an average most positive value of -0.5 ± 0.10‰ for this specimen the $\delta^{18}O$ value for seawater is determined to be -2.09‰. These $\delta^{18}O$ values are more negative than the $\delta^{18}O$ values for: 1) local Late Eocene seawater (-0.34‰), 2) global Late Eocene seawater (-0.9‰), or 3) seawater in an ice-free world (-1.2‰) (Miller et al., 1987). This indicates: 1) that temperatures in the Late Eocene at Griffins Landing did not fall below 10ºC, 2) that calcification for *Crassostrea gigantissima* did not cease at 10ºC, or 3) that the depositional environment for Griffins Landing was estuarine rather than normal marine.

Looking at the data from a different perspective, assuming the $\delta^{18}O$ value for seawater is between -0.9‰ and -0.34‰, the most positive values within the cycles of the $\delta^{18}O$ profiles would have to be ~0.69‰ to 1.25‰ to be consistent with a winter cessation temperature of 10ºC. For comparison, the absolute most positive value recorded in any shell of this study was 0.57‰. Assuming that estimates for the $\delta^{18}O$ value of Late Eocene seawater are accurate, and that Griffins Landing is a normal marine habitat, it is most likely that sea-surface temperatures in the Late Eocene did not reach a growth cessation temperature of 10ºC.

Paleoclimate Interpretations

Average Paleotemperature Estimates

The average paleotemperature for the three unaltered shells (1,2,3) was determined for various $\delta^{18}O$ values of seawater in Figure 5.4. Using the local estimate for $\delta^{18}O_{sw}$, of -0.34‰ and the average $\delta^{18}O$ value for shells 1 - 3 (see Table 4.1), average temperature (MAT) of ~18.7 ± 1.1ºC is computed. Seasonality can be obtained by several methods. The combined range of temperatures from all three shells is 12.7 to 26.2ºC, while individually the ranges are: 12.7 to 21.6ºC, 15.9 to 20.6ºC and 16.8 to 26.2ºC respectively (see Table 4.1). Averaging the lowest recorded temperature and highest recorded temperature in each shell results in an overall average seasonal range of ~15 to 23ºC for all samples.

The estimate for the isotope composition of seawater affects the calculation of both MAT and MART as demonstrated in Figure 5.4. If the global $\delta^{18}O$ value for Late Eocene seawater were used (-0.9‰; Lear et al., 2000), calculated paleotemperatures would be 3ºC cooler. Alternatively, if the modern $\delta^{18}O$ value for seawater were used the calculated paleotemperatures would increase by ~1ºC (14-27ºC).

Comparison of Late Eocene and Modern Oceans

Modern sea-surface temperatures recorded off the coast of Georgia at Grays Reef were obtained for the years 1988-2001. Average sea-surface temperature (SST) was 21.8ºC, with a range from 13.6º to 28.5ºC. (Data courtesy of NOAA National Data Buoy Center Station 41008, Grays Reef). Compared to paleotemperatures derived from shells 1-3 using the latitude corrected value for Late Eocene seawater (-0.34‰), Late Eocene sea-surface water temperatures for winter were 1ºC cooler to 3ºC warmer than modern

Figure 5.4

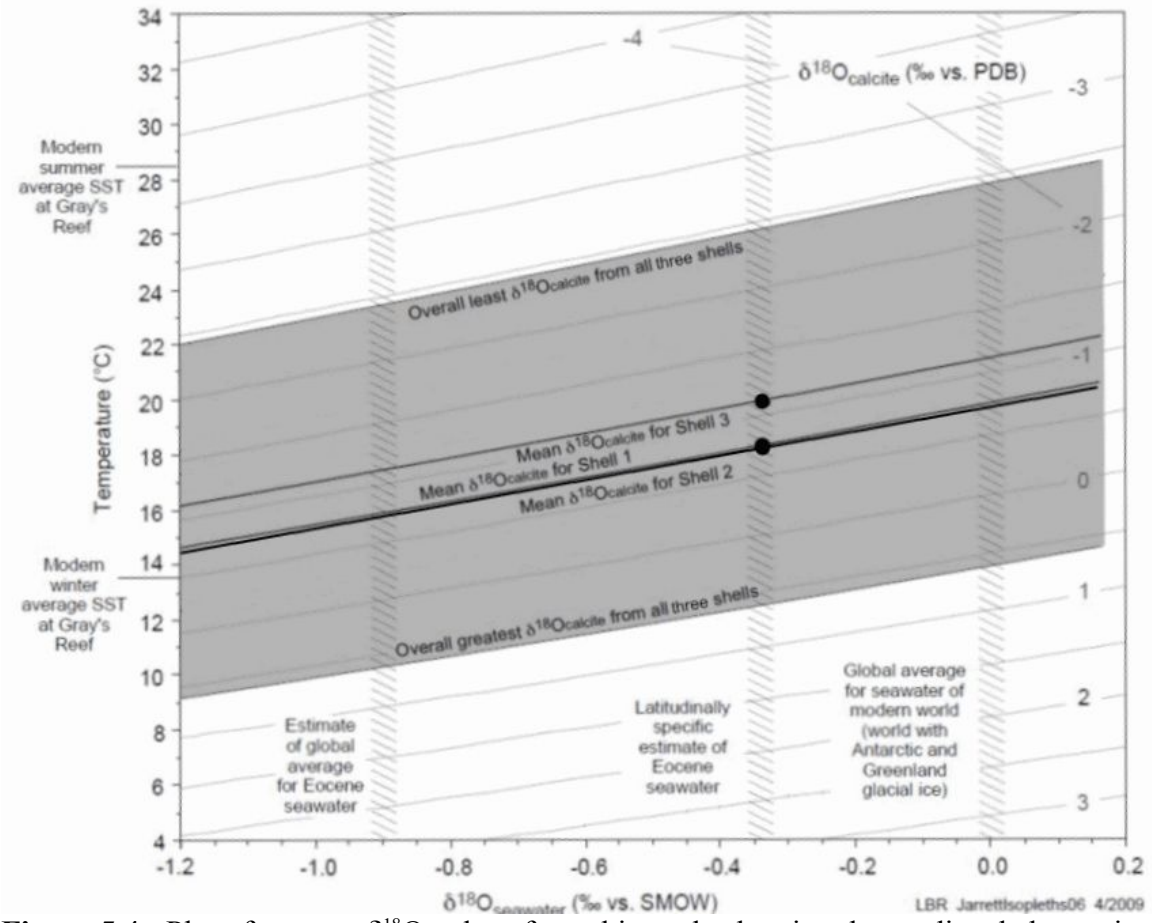

Figure 5.4 - Plot of average $\delta^{18}O$ values from this study showing the predicted change in temperatures for various $\delta^{18}O$ values of seawater. The average $\delta^{18}O$ values for shells 1,2, and 3 are -0.70‰, -0.68‰, -1.13‰, respectively, while the minimum and maximum $\delta^{18}O$ value of all shells (-2.45‰ and 0.57‰) and are used to constrain seasonal maximum and minimum temperatures.

SST and summer temperatures were ~2 to 8ºC cooler than modern SST. Overall, the average Late Eocene SST was ~3ºC lower than modern SST. Such warm modern temperatures probably a result of a vigorous Gulf Stream carrying warm equatorial water northward. However, Frakes et al. (1979) indicate that the Gulf Stream was active during the Eocene as well, although it is uncertain what the temperature of the Gulf Stream was at the time. In summary, the Late Eocene experienced similar winters with somewhat cooler summers than present day conditions along the Georgia coast.

Comparison to Other Eocene Mollusk Studies

Late Eocene paleoclimate determined in this study may be placed within a framework of previous paleoclimate studies reported in the literature. Based on existing Gulf Coastal Plain (GCP) data, the Middle Eocene experienced the warmest average temperature of the epoch (Andreasson and Schmitz, 2000; Kobashi et al., 2001). From here forward, climate steadily cooled leading to an Oligocene glaciation. This viewpoint is supported by the record of benthic foraminifera collected from deep sea cores that demonstrate a steady cooling trend from the Middle Eocene to the Oligocene (Figure 5.5).

The ranges and average paleotemperatures reported in Andreasson and Schmitz (2000) and Kobashi et al. (2001) for Eocene mollusk shells are compared to our data in Figure 5.6 (see Table 5.4 for their data). For comparative purposes, winter and summer temperatures from this study were determined using the methods outlined in their studies, (as detailed in Table 5.4), to facilitate this comparison. Paleotemperatures of ~19º to 28ºC are reported by Kobashi et al. (2001) and 23º to 29ºC by Andreasson and Schmitz (2000), for the Middle Eocene (see Table 5.4).

Figure 5.5

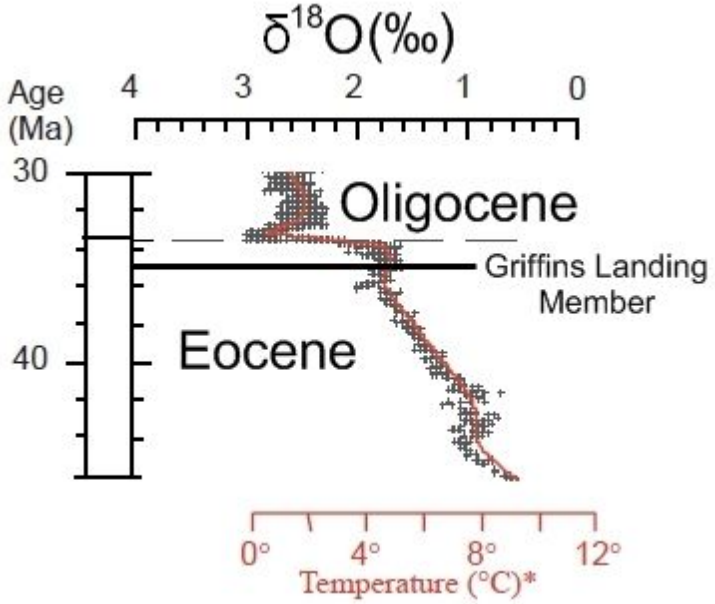

Figure 5.5 - Atlantic deep water benthic foraminifera data from deep sea cores displaying a steady cooling trend from the middle Eocene to the late Eocene. Adapted from Zachos et al. (2001).

Figure 5.6

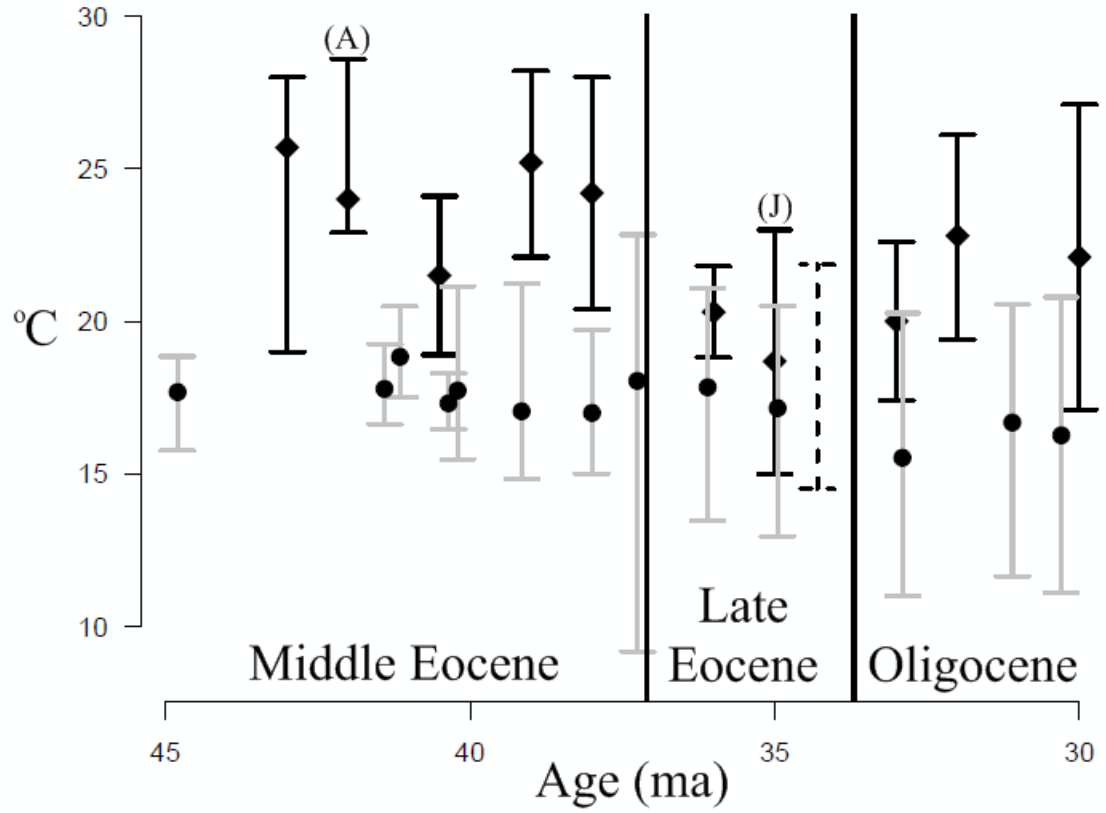

Figure 5.6 - Comparison of paleotemperature data from the unaltered shells (1,2,3) in this study (J) with data from Andreasson and Schmitz, (2000) (A), Kobashi et al. (2001) (all other black bars), and Ivany et al. (2003) (gray bars). Dotted line represents Ivany data corrected for age and latitude. All bars shown represent ranges in temperature as detailed in Table 5.4. Black dots and diamonds shown within range bars represent average temperatures from fish otoliths and mollusks, respectively.

Table 5.4 - Paleotemperature data from Andreasson and Schmitz (2000) and Kobashi et al. (2001) from serially sampled mollusk shells collected from the southeastern U.S. Gulf Coastal plain. Mollusk temperature ranges were calculated by averaging the warmest summer temperature and coolest winter temperature from different specimens to obtain a single summer and winter temperature for a given time period. Otolith paleotemperatures are provided by Ivany with paleotemperatures corrected for age and latitude at 35 Ma (in parentheses) when possible.

Epoch	Reference	Material	Age (ma)	Summer (ºC)	Winter (ºC)	Average-T (ºC)
Oligocene	Kobashi et al. (2001)	Mollusk	30.0	27.1	17.1	22.1
	Kobashi et al. (2001)	Mollusk	32.0	26.1	19.4	22.8
	Kobashi et al. (2001)	Mollusk	33.0	22.6	17.4	20.0
Late Eocene	This Study	Mollusk	35.0	22.8	15.1	18.7
	Kobashi et al. (2001)	Mollusk	36.0	21.8	18.8	20.3
Middle Eocene	Kobashi et al. (2001)	Mollusk	38.0	28.0	20.4	24.2
	Kobashi et al. (2001)	Mollusk	39.0	28.2	22.1	25.2
	Kobashi et al. (2001)	Mollusk	40.5	24.1	18.9	21.5
	Andreasson and Schmitz (2000)	Mollusk	42.0	28.6	22.9	24.0
	Kobashi et al. (2001)	Mollusk	43.0	28.0	19.0	25.7
Oligocene	Ivany et al. (2003)	Otolith	30.3	20.8	11.1	16.3
	Ivany et al. (2003)	Otolith	31.1	20.6	11.6	16.7
	Ivany et al. (2003)	Otolith	32.9	20.3	11.0	15.5
Late Eocene	Ivany et al. (2003)	Otolith	35.0	20.5 (21.9)	13.00 (14.5)	17.2
	Ivany et al. (2003)	Otolith	36.1	21.1	13.5	17.9
	Ivany et al. (2003)	Otolith	37.3	22.8	9.2	18.1
Middle Eocene	Ivany et al. (2003)	Otolith	38.0	19.7	15.0	17.0
	Ivany et al. (2003)	Otolith	39.2	21.2	14.8	17.1
	Ivany et al. (2003)	Otolith	40.2	21.2	15.5	17.8
	Ivany et al. (2003)	Otolith	40.4	18.3	16.5	17.3
	Ivany et al. (2003)	Otolith	41.2	20.5	17.5	18.8
	Ivany et al. (2003)	Otolith	41.4	19.3	16.6	17.8
	Ivany et al. (2003)	Otolith	44.8	18.9	15.8	17.7

Late Eocene temperature data from Kobashi et al. (2001) indicate that temperature in the GCP was ~19º to 22ºC, while our data show a range of temperatures from 15º to 23ºC. Kobashi et al. (2001) interpreted the narrow range (~3ºC) of Late Eocene temperatures as resulting from the collection of samples that lived in a relatively deep water habitat compared to other samples from their study. The average temperature for the Late Eocene from Kobashi et al. (2001) is 20.3ºC, which is close to the average temperature reported here (18.7ºC). Despite the collection sites being chronologically separated by ~1 Ma, the similarity of summer climates during the Late Eocene for the GCP and the ACP is striking with winter temperatures being slightly cooler in the ACP than the GCP (Figure 5.6).

Data from this study as well as Kobashi et al. (2001) suggest cooler temperatures in the Late Eocene in comparison to the Middle Eocene. Early Middle Eocene GCP paleotemperature data from Kobashi et al. (2001) and Andreasson and Schmitz (2000) are reported at ~19º to 28ºC, and 23 to 29ºC, respectively. Comparison of these temperatures to our calculated temperatures (see Table 4.1) represents 4º to 8ºC of winter cooling, 4º to 5ºC summer cooling, and a ~6ºC decrease in average temperatures during the cooling trend from the Middle to the Late Eocene. This pattern seen in the mollusk record is consistent with the record of benthic foraminifera reported by Zachos et al. (2001) (Figure 5.5).

Comparing temperature data for the Late Eocene with Oligocene data from Kobashi et al. (2001) reveals an interesting pattern. Our Late Eocene data range from ~15º to 23ºC whereas Eocene/Oligocene boundary (32 Ma) temperature data range from ~17º to 23ºC. There does not appear to be much of a change in summer temperatures

across the boundary while winter temperatures became ~2ºC warmer. This suggests that the 1‰ negative shift in the $\delta^{18}O$ value of benthic foraminifera at the Eocene/Oligocene boundary (Figure 5.5) is primarily due to an increase in the $\delta^{18}O$ of seawater, probably due to the formation of polar ice. Moving into the later portion of the Oligocene, data from Kobashi et al. (2001) suggest that summer temperatures warmed further to a steady ~26ºC, while winter temperatures increased ~2ºC (17º to 19ºC) (Figure 5.6).

Comparison to Fish Otolith Data

To test the hypothesis that cooling temperatures played an important role in the loss of warm-water molluscan taxa of the GCP in the Eocene/Oligocene transition, Ivany et al. (2003) analyzed fossil fish otoliths in the Gulf Coast Paleogene. Their data are plotted in Figure 5.6. It is clear there are some significant differences between the mollusk and fish otolith climate record: 1) fish otoliths do not indicate steady cooling from the Middle Eocene to the Late Eocene and 2) the otolith data predict cooler temperatures than the mollusk data. One important caveat is that the otolith temperature data were not calculated using a $\delta^{18}O$ value for seawater that is consistent with that used for the mollusk temperature data [i.e. Lear et al. (2000) and Zachos et al. (1994)]. Ivany et al. (2003) used estimated global averages for the $\delta^{18}O$ value of seawater reported through the Paleogene by Zachos et al. (1994) without applying a latitude correction.

To facilitate a more meaningful comparison, corrections based on Lear et al. (2000) and Zachos et al. (1994), were made to the otolith data for 35 Ma and the results are shown in Figure 5.6 by the dashed bar to the right of the data. Application of this correction to the otolith data for 35 Ma results in corrected data that are consistent with our data at 35 Ma (Figure 5.6). This correction could not be applied to all data reported

by Ivany et al. (2003) as the contributed dataset did not include latitudes for each collection site.

It should be noted that there are significant lifestyle differences between fish and mollusks as well. Whereas mollusks are generally sessile creatures, recording temperatures in place throughout ontogeny, fish are vagile, and they may record water temperatures throughout the water column in which they lived.

Paleotemperatures aquired in this study fit well within the framework established by other studies. Our data support the contention that the overall trend in climate from Middle to Late Eocene was cooling with a steady decrease in both average and winter temperatures (Figure 5.6). In addition, when our data are paired with Kobashi et al. (2001) and Ivany et al. (2003), the implication is that while summer temperatures remained constant across the Eocene/Oligocene boundary, winter temperatures became warmer.

Concluding Remarks Regarding Extinctions

Beginning in the Late Eocene, molluscan populations decreased due to extinctions at the boundary between the Middle and Late Eocene that are measureable in the GCP (Dockery, 1986; Hansen, 1987; Haasl and Hansen, 1996). The boundary is marked by a 72% and 63% decline in gastropods and bivalves, respectively, and it is followed by yet a second decline in the early Late Eocene when gastropods and bivalves further declined 89% and 84%, respectively (Hansen, 1987; Prothero, 1994). When these extinction events are placed within the framework of data from this and prior studies, the possibility exists that the extinctions were most likely the result of changes in winter temperatures and not summer temperature for most species.

Chapter 6

Conclusions

1. Some shell material within the chondrophore of fossil *C. gigantissima* shells of Griffins Landing (35 ma) is primary and may be used for paleoclimate analysis. This is supported by a lack of luminescence and intact shell microstructure although these data do not provide conclusive evidence for unaltered material. A comparison of $\delta^{13}C$ and $\delta^{18}O$ values with diagenetic carbonates and known fields for primary and secondary carbonates facilitated the recognition of primary from altered material. Given these conclusions, Shells 1,2, and 3 were unaltered while Shells 4,5, and 6 were influenced by diagenetic fluids.
2. Based on the isotope evidence, the environment of deposition for Griffins Landing was normal marine.
3. Morphological ridges and valleys within the chondrophore of *C. gigantissima* formed annually, with ridges occurring generally in summer months.
4. Based on three shells the MAT for waters of the Late Eocene, at Griffins Landing was 18.7ºC while the MART was ~8ºC (~15º to 23ºC).
5. Paleotemperatures from the ACP are similar to those from the GCP for the Late Eocene.
6. The mollusk record of Eocene climate, shows steady cooling from the Middle Eocene to Late Eocene, with most cooling occurring in winter months.

Data from this study agree well with this trend and suggest that Late Eocene molluscan extinctions were due to winter cooling.

Implications for Future Study

Based on this study, *Crassostrea gigantissima* collected from Griffins Landing is an acceptable source of paleoclimate data. There are other sites within the state of Georgia where *C. gigantissima* have been reported including the Clinchfield Sand which is older than the Griffins Landing member. If a suitable collection site was located, the potential exists for additional paleoclimate data to be obtained over a broader time interval.

As well, the paleoecology of other fossil *Crassostrea* species within the Paleogene of the southeastern US should be explored. Currently it is believed that *C. virginica* is much smaller than *C. gigantissima* due to differences in paleoecology. There are other small fossil *Crassostrea* within the Gulf Coastal Plain such as *C. alabamiensis* (Toulmin, 1977) which could potentially be estuarine. Understanding the paleoecology of other fossil *Crassostrea* in the paleogene of the southeastern US would help to better constrain the evolutionary history of *Crassostrea* in the southeastern US.

Works Cited

Auclair, Anne-Cecile, Christophe Lecuyera, Hugo Bucherb, Simon M.F. Sheppard. 2004. Carbon and oxygen isotope composition of *Nautilus macromphalus*: a record of thermocline waters off New Caledonia. Chemical Geology, Vol. 207 pp. 91-100.

Al-Aasm, Ihsan S., and Jan Veizer. 1986. Diagenetic Stabilization of Aragonite and low-Mg Calcite, I. Trace Elements in Rudists. Journal of Sedimentary Petrology, Vol. 56, No. 1, pp. 138-152.

Allison, P.A. 2001. Decay *in* Palaeobiology II, Derek E. Briggs and Peter R. Crowther Eds. Blackwell, Massachusetts, pp. 270-273.

Andreasson, Fredrick P., Birger Schmitz, and Emma Jönsson. 1999. Surface-Water Seasonality from Stable Isotope Profiles of Littorina littorea Shells: Implications for Paleoenvironmental Reconstructions of Coastal Areas, Palaios, Vol. 14, pp. 273-281.

Andreasson, F.P., and Schmitz, B., 2000. Temperature Seasonality in the early middle eocene North Atlantic region: evidence from stable isotope profiles of marine gastropod shells: Geological Society of America Bulletin, Vol. 112, pp. 628-640.

Andrus, C. Fred T., and Doug E. Crowe, 2000. Geochemical Analysis of Crassostrea virginica as a Method to Determine Season of Capture. Journal of Archaeological Science, Vol. 27, pp. 33-42.

Andrus, C. Fred T., and Kelley Whatley Rich. 2008. A Preliminary Assessment of Oxygen Isotope Fractionation and Growth Increment Periodicity in the Estuarine Clam Rangia cuneata. Geo-Marine Letters, Vol. 28, pp. 301-308.

Bemis, Bryan E., and Dana H. Geary. 1996. The Usefulness of Bivalve stable Isotope Profiles as Environmental Indicators: Data from the Eastern Pacific Ocean and the Southern Caribbean Sea. Palaios, Vol. 11, pp. 328-339.

Berggren, W.A., D.V. Kent, C.C. Swisher, and M.P. Aubry. 1995. A Revised Cenozoic Geochronology and Chronostratigraphy. SEPM Special Publication 54, pp. 140.

Budd, David A., Ursula Hammes, and W. Bruce Ward. 2000. Cathodoluminescence in Calcite Cements: New Insights on Pb and Zn Sensitizing, Mn Activation, and Fe Quenching at Low Trace-Element Concentrations. Journal of Sedimentary Research. Vol. 70, No. 1. pp. 217-226.

Brand, Uwe, and Jan Veizer. 1980. Chemical Diagenesis of a Multicomponent Carbonate System; 1, Trace Elements. Journal of Sedimentary Research. Vol. 50, No. 4. pp. 1219-1236.

Campbell, David C., and Matthew R. Campbell. 2003. Biotic Patterns in Eocene-Oligocene Mollusks of the Atlantic Coastal Plain, U.S.A. in Prothero, D.R., Ivany, L.C., and Elizabeth A. Nesbitt, eds., From Greenhouse to Icehouse: The Marine Eocene-Oligocene transition. New York, Columbia U.P., pp. 232-251.

Carre, Matthieu, Ilhem Bentaleb, Dominique Blamart, Neil Ogle, Freddy Cardenas, Sheyla Zevallos, Robert M. Kalin, Luc Ortlieb, Michel Fontugne. 2005. Stable isotopes and sclerochronology of the bivalve *Mesodesma donacium*: Potential application to Peruvian paleoceanographic reconstructions. Palaeoceanography, Palaeoclimatology, Palaeoecology, Vol. 228, pp. 4-25.

Carriker, M.R., 1996. Chapter 3. The Shell and Ligament. in Kennedy, V.S., R.I.E. Newell, A.F. Eble (Eds.), The Eastern Oyster, Crassostrea virginica. Maryland Sea Grant, 105p.

Carriker, M.R. and R.E. Palmer. 1979. A New Mineralized Layer in the Hinge of the Oyster. Science, Vol. 206, pp. 627-629.

Cerajewski, Rebecca J., 2002 Paleoclimate Reconstruction Using Isotopic Analysis of Tropical Bivalves from the Pigeon Creek Archaeological Site, San Salvador Island, Bahamas, Unpublished Masters Thesis. University of Georgia, 109p.

Craig, Harmon. 1957. Isotopic standards for carbon and oxygen and correction factors for mass-spectrometric analysis of carbon dioxide. Geochimica et Cosmochimica Acta. Vol. 12, Issue 1-2, pp. 133-149.

Custer, Jay F. and Keith R. Doms. 1990. Analysis of Microgrowth Patterns of the American Oyster (Crassostrea virginica) in the Middle Atlantic Region of Eastern North America: Archaeological Applications. Journal of Archaeological Science, Vol. 17, pp. 151-160.

Dettman, D.L., and Kyger C. Lohmann. 1995. Microsampling Carbonates for Stable Isotope and Minor Element Analysis; Physical Separation of Samples on a 20 Micrometer Scale. Journal of Sedimentary Research. Vol. 65, No. 3a pp. 566-569.

Dockery, D.T. III. 1986. Punctuated Succession of Paleogene Mollusks in the Northern Gulf Coastal Plain: Palaios. Vol. 1, pp. 582-589.

Eby, G. Nelson. 2004. Principles of Environmental Geochemistry. Brooks/Cole, California. 514p.

Edinger, E.N. 2001. Bioerosion *in* Palaeobiology II, Derek E. Briggs and Peter R. Crowther Eds. Blackwell, Massachusetts, pp. 273-277.

Emiliani, Cesare. 1955. Pleistocene Temperatures. Journal of Geology. Vol. 63, No. 6, pp. 538-578.

Epstein, S., R. Buchsbaum, H.A. Lowenstam and H.C. Urey. 1953. Revised Carbonate-water Isotopic Temperature Scale. Bulletin of the Geological Society of America. Vol. 64, pp. 1315-1326.

Epstein, S. and T. Mayeda. 1953. Variation of O^{18} Content of Waters from Natural Sources. Geochimica et Cosmochimica Acta. Vol. 4, pp. 213-224.

Fallaw, Wallace C., and Van Price. 1992. Outline of Stratigraphy at the Savannah River Site in Fallaw And Price, Geological Investigations of the Central Savannah River Area, South Carolina and Georgia. Carolina Geological Society Field Trip Guidebook.

Faure, Gunter. 1998. Principles and Applications of Geochemistry 2nd ed. Prentice Hall, New Jersey, 600p.

Fenger, Tracy, Donna Surge, Bernd Schöne, and Nicky Milner. 2007. Sclerochronology and Geochemical Variation in Limpet Shells (Patella vulgata): A New Archive to Reconstruct Coastal Sea-Surface Temperature, Geochemistry, Geophysics, Geosystems: An Electronic Journal of the Earth Sciences, Vol. 8, No. 7, 17p.

Frakes, L.A. 1979. Climates Throughout Geological Time. New York. Elsevier.

Fry, Brian. 2006. Stable Isotope Ecology. Springer, New York. 308p.

Galtsoff, P.J. 1964. The American Oyster Crassostrea virginica Gmelin. U.S. Fish and Wildlife Service, Fisheries Bulletin, Vol 64, 480p.

Geary, Dana H., Timothy A. Brieske, and Bryan E. Bemis. 1992. The Influence and Interaction of Temperature, Salinity, and Upwelling on the Stable Isotopic Profiles of Strombid Gastropod Shells. Palaios. Vol. 7, pp. 77-85.

Gillikin, David Paul, Fjo De Ridder, Hans Ulens, Marc Elskens, Eddy Keppens, Willy Baeyens, Frank Dehairs. 2005. Assessing the reproducibility and reliability of estuarine bivalve shells (*Saxidomus giganteus*) for sea surface temperature reconstruction: Implications for paleoclimate studies. Palaeogeography, Palaeoclimatology, Palaeoecology, Vol. 228, pp. 70-85.

Goodwin, David H., Bernd R. Schone, and David L. Dettman., 2003. Resolution on and Fidelity of Oxygen Isotopes as Paleotemperature Proxies in Bivalve Mollusk Shells: Models and Observations. Palaios, Vol. 18, pp. 110-125.

Greenwood, David R. and Scott L. Wing. 1995. Eocene Continental Climates and Latitudinal Temperature Gradients. Geology. Vol. 23, No. 11, pp. 1044-1048.

Griffiths, H. 2006. Stable Isotopes: The Integration of Biological, Ecological and Geochemical Processes (Environmental Plant Biology Series). Garland Science. 460p.

Grossman E.L. and T.L. Ku. 1986. Oxygen and Carbon Isotope Fractionation in Biogenic Aragonite: Temperature Effects. Chemical Geology, Vol. 59, pp. 59-74.

Haasl, David M., and Thor A. Hansen. 1996. Timing of Late Eocene Molluscan Extinction Patterns in Mississippi. Palaios. Vol. 11, pp. 487-494.

Hansen, Thor A. 1987. Extinction of Late Eocene to Oligocene Molluscs: Relationship to Shelf Area, Temperature Changes, and Impact Events. Palaios. Vol. 2, pp. 69-75.

Harris, W.B., V.A. Zullo and R.A. Laws. 1993. Sequence Stratigraphy of the Onshore Palaeogene, Southeastern Atlantic Coastal Plain, USA, Spec. Pubs. Int. Ass. Sediment. Vol. 18, pp. 537-561.

Hendry, James P., and Robert M. Kalin. 1997. Are Oxygen and Carbon Isotopes of Mollusc Shells Reliable Palaeosalinity Indicators in Marginal Marine Environments? A Case Study from the Middle Jurassic of England. Journal of the Geological Society, London, Vol. 154, pp. 321-333.

Herrick, S.M., and Counts, H.B. 1968. Late Tertiary Stratigraphy of Eastern Georgia: Georgia Geol. Soc. Guidebook, 3rd Annual Field Trip, 88p.

Hickson, Jon A., Andrew L.A. Johnson, Tim H.E. Heaton, and Peter S. Balson. 1999. The Shell of the Queen Scallop Aequipecten opercularis (L.) as a Promising Tool for Palaeoenvironmental Reconstruction: Evidence and Reasons for Equilibrium Stable-Isotope Incorporation. Palaeogeography, Palaeoclimatology, Palaeoecology. Vol. 154, pp. 325-337.

Hoefs, Jochen. 1997. Stable Isotope Geochemistry. Springer-Verlag, Berlin, 201p.

Howe, H.V. 1937. Large Oysters from the Gulf Coast Tertiary. Journal of Paleontology, Vol. 11, pp. 355-366.

Huddlestun P.F. and J.H. Hetrick. 1986. Upper Eocene Stratigraphy of Central and Eastern Georgia: Georgia Geologic Survey Bulletin 95, 78p.

Hudson, J.D. 1977. Stable Isotopes and Limestone Lithification. Journal of the Geological Society of London. Vol. 133, pp. 637-660.

Ivany, Linda C., Kyger C. Lohmann, and William P. Patterson., 2003. Paleogene temperature history of the U.S. Gulf Coastal Plain inferred from $\delta^{18}O$ of Fossil Otoliths *in* Prothero, D.R., Ivany, L.C., and Elizabeth A. Nesbitt, eds., From Greenhouse to Icehouse: The marine Eocene-Oligocene transition. New York, Columbia U.P., pp. 232-251.

James, N.P., Choquette, P.W. 1990. Limestones - the Meteoric Diagenetic Environment. *In*: Mcllreath, I.A., Morrow, D.W. (Eds.), Diagenesis. Geosci. Can. Repr. Ser., Vol. 4, pp. 35-73.

Jones, Douglas S., Douglas F. Williams, and Michael A. Arthur. 1983. Growth History and Ecology of the Atlantic Surf Clam, Spissula solidissima (Dillwyn), as Revealed by Stable Isotopes and Annual Shell Increments. J. Exp. Mar. Biol. Ecol., Vol. 73, pp. 225-242.

Jones, D.S. and S.J. Gould. 1999. Direct measurement of age in fossil Gryphaea: the solution to a classic problem in heterochrony. Paleobiology. Vol. 25, No. 2, pp. 158-187.

Jones, Douglas S. and Irvy R Quitmyer., 1996. Marking Time with Bivalve Shells: Oxygen Isotopes and Season of Annual Increment Formation. Palaios. Vol. 11, pp. 340-346.

Jones DS, Bill Arnold, Irvy Quitmyer, Bernd Schöne, and Donna Surge. 2007. 1st International Sclerochronology Conference. http://conference.ifas.ufl.edu/sclerochronology. Accessed 15 July 2009.

Keith, M.L., G.M. Anderson and R. Eichler. 1964. Carbon and Oxygen Isotopic Composition of Mollusk Shells from Marine and Fresh-Water Environments. Geochimica et Cosmochimica Acta. Vol. 28, pp. 1757-1786.

Keller, Gerta. 1982. Biochronology and Paleoclimatic Implications of Middle Eocene to Oligocene Planktonic Foraminiferal Faunas. Marine Micropaleontology. Vol. 7, pp. 463-486.

Kennet, J.P. 1977. Cenozoic Evolution of Antarctic Glaciation, the Circum-Antarctic Ocean and Their Impact on Paleoceanography, Journal of Geophysical Research, Vol. 82, pp. 3843-3860.

Kent, Bretton W. 1988. Making Dead Oysters Talk: Techniques for Analyzing Oysters from Archaeological Sites. Crownsville, Maryland. Maryland Historical & Cultural Publications. 76 p.

Kharaka and J.J. Thorsden. 1992. Stable Isotope Geochemistry and Origin of Waters in Sedimentary Basins in Lecture Notes in Earth Sciences 43: Isotope Signatures and Sedimentary Records. Norbert Clauer and Sambhu Chaudhuri (Eds.). Springer-Verlag, Berlin, pp. 411-466.

Kirby, Michael Xavier. 2000. Paleoecological Differences Between Tertiary and Quaternary Crassostrea Oysters, as Revealed by Stable Isotope Sclerochronology. Palaios. Vol. 15, pp. 132-141.

Kirby, Michael Xavier. 2001. Differences in growth rate and environment between Tertiary and Quaternary Crassostrea oysters. Paleobiology. Vol. 27 no. 1 pp.84-103.

Kirby, M.X.. Soniat, T.M., and Spero, H.J., 1998. Stable Isotope sclerochronology of Pleistocene and Recent oyster shells (*Crassostrea virginica*): PALAIOS, v. 13 pp. 560-569.

Klein, Robert T., Kyger C. Lohmann, and Charles W. Thayer. 1996. Sr/Ca and 13C/12C ratios in skeletal calcite of *Mytilus trossulus*: Covariation with metabolic rate, salinity, and carbon isotopic composition of seawater. Geochimica et Cosmochimica Acta. Vol. 60, No. 21, pp. 4207-4221.

Krantz, David E., Douglas F. Williams, and Douglas S. Jones. 1987. Ecological and Paleoenvironmental Information Using Stable Isotope Profiles from Living and Fossil Molluscs. Palaeogeography, Palaeoclimatology, Palaeoecology. Vol. 58, pp. 249-266.

Kobashi, Takuro, Ethan L. Grossman, Thomas E. Yancey, David T. Dockery III. 2001. Reevaluation of Conflicting Eocene Tropical Temperature Estimates: Molluskan Oxygen Isotope Evidence for Warm Low Latitudes. Geology, Vol. 29, No. 11, pp. 983-986.

Kobashi, Takuro, and Ethan L. Grossman. 2003. The Oxygen Isotopic Record of Seasonality in *Conus* Shells and its Application to Understanding Middle Eocene (38 Ma) Climate. Paleontological Research. Vol. 7, No. 4, pp. 343-355.

Lawrence, David R. 1988. Oysters as Geoarchaeologic Objects. Geoarchaeology, Vol. 3, No. 4, pp. 267-274.

Lawrence, David R. 1995. Diagnosis of the Genus Crassostrea (Bivalvia, Ostreidae). Malacologia, Vol 36, pp. 185-202.

Laws, Richard A., W. Burleigh Harris and Victor A. Zullo. 1992. Nannofossil Biostratigraphy and Sequence Stratigraphy of Middle to Upper Eocene Strata in the Southwestern Savannah River Site and Adjacent Areas of Georgia in Fallaw, Wallace and Van Price. Geological Investigations of the Central Savannah River Area, South Carolina and Georgia. Carolina Geological Society Field Trip Guidebook 1992. pp. 59-66.

Lear, C.H., H. Elderfield, P.A. Wilson. 2000. Cenozoic Deep-Sea Temperatures and Global Ice Volumes from Mg/Ca in Benthic Foraminiferal Calcite. Science. Vol. 287, pp. 269-272.

Libes, Susan M. 1992. An Introduction to Marine Biogeochemistry, Wiley, New York, 734p.

Martin, Gale D., Bruce H. Wilkinson and Kyger C Lohmann. 1986. The Role of Skeletal Porosity in Aragonite Neomorphism - *Strombus* and *Montastrea* from the Pleistocene Key Largo Limestone, Florida. Journal of Sedimentary Petrology. Vol. 56, No. 2, pp. 194-203.

McConnaughey, Ted. 1989. ^{13}C and ^{18}O Isotopic Disequilibrium in Biological Carbonates: II. In vitro Simulation of Kinetic Isotope Effects. Geochimica et Cosmochimica Acta. Vol. 53. pp. 163-171.

Miller, Kenneth G., Richard G. Fairbanks and Gregory S. Mountain. 1987. Tertiary Oxygen Isotope Synthesis, Sea Level History, and Continental Margin Erosion. Paleoceanography. Vol. 2, No. 1, pp. 1-19.

Miller, Kenneth G. 1992. Middle Eocene to Oligocene Stable Isotopes, Climate, and Deep-Water History: The Terminal Eocene Event? in Prothero, D.R., and William A. Berggren Ed. Eocene-Oligocene Climatic and Biotic Evolution. Princeton U.P., pp. 161-177.

Mook, W.G. 1971. Paleotemperatures and Chlorinities from Stable Carbon and Oxygen Isotopes in Shell Carbonate. Palaeogeography, Palaeoclimatology, Palaeoecology. Vol. 9, pp. 245-263.

Morley, R.J. 2000. Origin and Evolution of Tropical Rain Forests: New York, Wiley, 362p.

O'Leary, Marion H. 1988. Carbon Isotopes in Photosynthesis. Bioscience. Vol. 38, No. 5. pp. 328-336.

Palmer, K. V. W. 1937, The Claibornian Scaphopoda, Gastropoda, and dibranchiate Cephalopoda of the southern United States: Bulletin of American Paleontology, Vol.7, No. 32, pt. 1, pp. 548., pt. 2, 90 plts.

Palmer, K. V. W., and Brann D. C., 1965, Catalogue of the Paleocene and Eocene Mollusca of the Southern and Eastern United States: Part I. Pelecypoda, Amphineura, Pteropoda, Scaphopoda, and Cephalopoda, Bulletins of American Paleontology, V. 48, No. 218, 443p. 3 plts.

Palmer, K. V. W., and Brann D. C., 1966, Catalogue of the Paleocene and Eocene Mollusca of the Southern and Eastern United States: Part II. Gastropoda, Bulletins of American Paleontology, V. 48, No. 218, 556p. 5 plts.

Ponder, Winston F. and David R. Lindberg. 2008. Phylogeny and Evolution of the Mollusca. Berkley, Los Angeles. University of California Press.

Prothero, Donald R. 1994. "The Eocene-Oligocene transition: Paradise Lost". New York. Columbia U.P. 291 p.

Prothero, Donald R., and Fred Schwab. 2004. "Sedimentary Geology: An Introduction to Sedimentary Rocks and Stragigraphy 2nd ed." New York. W.H. Freeman Co. 557 p.

Railsback, L. Bruce, Bouker, Polly A., Feeney, Thomas P., Goddard, Ethan A., Goggin, Keith E., Hall, A. Shawn, Jackson, Brian P., McLain, Angela A., Orsega, Michael C., Rafter, Margaret A., and Webster, James W., 1996, A survey of the major-element geochemistry of Georgia groundwater: Southeastern Geology, v. 36, No. 3, pp. 99-102.

Rhoads, Donald C., and Richard A. Lutz Eds. 1980. Skeletal Growth of Aquatic Organisms: Biological Records of Environmental Change. Plenum Press. NY and London. pp. 185-186.

Romanek, Christopher S. and Ethan L. Grossman. 1989. Stable Isotope Profiles of *Tridacna maxima* as Environmental Indicators. Palaios. Vol. 4, pp. 402-413.

Romanek, Christopher S., Grossman, E.L., and Morse, J.W. 1992. Carbon Isotopic Fractionation in Synthetic Aragonite and Calcite: Effects of Temperature and Precipitation Rate. Geochimica et Cosmochimica Acta, Vol. 56, pp. 419-430.

Scholle, Peter A., and Dana S. Ulmer-Scholle. 2003. A Color Guide to the Petrography of Carbonate Rocks: Grains, Textures, Porosity, Diagenesis. AAPG Memoir 77, The American Association of Petroleum Geologists. Tulsa, OK, 474p.

Shackleton, N.J. and Neil D. Opdyke. 1973. Oxygen Isotope and Paleomagnetic Stratigraphy of Equatorial Pacific Core V28-238: Oxygen Isotope Temperatures and Ice Volumes on a 10^5 Year and 10^6 Year Scale. Quaternary Research. Vol. 3, pp. 39-55.

Shanahan, Timothy M., Jeffrey S. Pigati, David L. Dettman, and Jay Quade. 2005. Isotopic Variability in the Aragonite Shells of Freshwater Gastropods Living in Springs with Nearly Constant Temperature and Isotopic Composition. Geochimica et Cosmochimica Acta, Vol. 69, No. 16, pp. 3949-3966.

Sloan, L. Cirbus, and Eric J. Barron. 1992. A Comparison of Eocene Climate Model Results to Quantified Paleoclimatic Interpretatons. Palaeogeography, Palaeoclimatology, Paleoecology. Vol. 93, pp. 183-202.

Sloan, L.C. 1994. Equable Climates During the Early Eocene: Significance of Regional Paleogeography for North American Climate. Geology. Vol. 22, pp. 881-884.

Sloan, L.C., and Rea, D.K. 1995. Atmospheric Carbon Dioxide and Early Eocene Climate: A General Circulation Modeling Sensitivity Study. Palaeogeography, Palaeoclimatology, palaeoecology. Vol. 119, pp. 275-292.

Stenzel, H.B. 1963. Aragonite and Calcite as Constituents of Adult Oyster Shells. Science. Vol. 47, pp. 232-233.

Surge, Donna. K.C. Lohmann, and David L. Dettman. 2001. Controls on isotopic chemistry of the American oyster, *Crassostrea virginica*: implications for growth patterns. Palaeogeography, Palaeoclimatology, Palaeoecology. Vol. 172, pp. 283-286.

Surge, Donna M., Kyger C. Lohmann, Glenn A. Goodfriend. 2003. Reconstructing Estuarine Conditions: Oyster Shells as Recorders of Environmental Change, Southwest Florida. Estuarine, Coastal and Shelf Science. Vol. 57, pp. 737-756.

Surge, Donna and Karen J. Walker. 2006. Geochemical variation in microstructural shell layers of the southern quahog (*Mercenaria campechiensis*): Implications for reconstructing seasonality. Palaeogeography, Palaeoclimatology, Palaeoecology. Vol. 237, pp. 182-190.

Surge, Donna, Ginger Kelley, William S. Arnold, Stephen P. Geiger, Anne E. Goewert, and Karen Jo Walker. 2008. Isotope Sclerochronology of Mercenaria mercenaria, M. campechiensis, and their Natural Hybrid Form: Does Genotype Matter? Palaios. Vol. 23, pp. 559-565.

Swart, P.K., A.F. Wilson, and J.S. Jell. 1983. Oxygen Isotope Variation in a Lagoonal Platform Reef, Heron Island, Great Barrier Reef. Australian Journal of Marine and Freshwater Research, Vol. 34, pp. 813-819.

Taylor, J.D., W.J. Kennedy, and A. Hall. 1969. The Shell Structure and Mineralogy of the Bivalvia; Introduction; Nuculacea-Trigonacea: London, British Museum (Natural History), 115p.

Thayer, Paul A., and Mary K Harris. 1992. Petrology and Reservoir Characteristics of Middle and Late Eocene Carbonate Strata in Downdip Wells at the Savannah River Site, South Carolina, in Fallaw, Wallace and Van Price. Geological Investigations of the Central Savannah River Area, South Carolina and Georgia. Carolina Geological Society Field Trip Guidebook 1992. pp. 49-55.

Toulmin, Lyman Dorgan. 1977. Stratigraphic Distribution of Paleocene and Eocene Fossils in the Eastern Gulf Coast Region (Monograph – Geological Survey of Alabama, Geologic Division; 13). Geological Survey of Alabama. 350p.

Valentine, J.W. 1973. Evolutionary Paleoecology of the Marine Biosphere: Englewood Cliffs, New Jersey, Prentice-Hall, Inc., 511p.

Vermeij, G.J. 1978. Biogeography and Adaptation: Cambridge, Massachusetts, Harvard UP, 332p.

Veizer, Jan. 1983. Chemical Diagenesis of Carbonates: Theory and Application of Trace Element Technique. in Arthur, Michael A., Thomas F. Anderson, Isaac R. Kaplan, Jan Veizer, and Lynton S. Land. Stable Isotopes in Sedimentary Geology. SEPM Short Course No. 10, Dallas. U.S.A.

Veizer, Jan, Davin Ala, Karem Azmy, Peter Bruckschen, Dieter Buhl, Frank Bruhn, Giles A.F. Carden, Andreas Diener, Stefan Ebneth, Yves Godderis, Torsten Jasper, Christoph Korte, Frank Pawelleck, Olaf G. Podlaha, and Harald Strauss. 1999. $^{87}Sr/^{86}Sr$, $\delta^{13}C$ and $\delta^{18}O$ Evolution of Phanerozoic Seawater. Chemical Geology. Vol. 161, pp. 59-88.

Wolfe, J.A., 1978. A Paleobotanical Interpretation of Tertiary Climates in the Northern Hemisphere. American Scientist, Vol. 66, pp. 694-703.

Zachos, James C., Lowell D. Scott, Kyger C. Lohmann. 1994. Evolution of Early Cenozoic Marine Temperatures. Paleoceanography. Vol. 9, No. 2, pp. 353-387.

Zachos, J.C., Quinn, T.M., and Salamy, K.A. 1996. High-Resolution (10^4 years) Deep-Sea Foraminiferal Stable Isotope Records of the Eocene-Oligocene Climate Transition. Paleoceanography, Vol. 11, pp. 251-266.

Zalasiewicz, Jan. 2006. In Deep Water. The Palaeontological Association Newsletter Number 61. pp. 27-32.

Zullo, Victor A., and Lucille E. Kite. 1985. Barnacles of the Jacksonian (Upper Eocene) Griffins Landing Member, Dry Branch Formation in South Carolina and Georgia. South Carolina Geology. Vol. 28, No. 1, pp. 1-21.

Appendix 1

Measured Stratigraphic Section

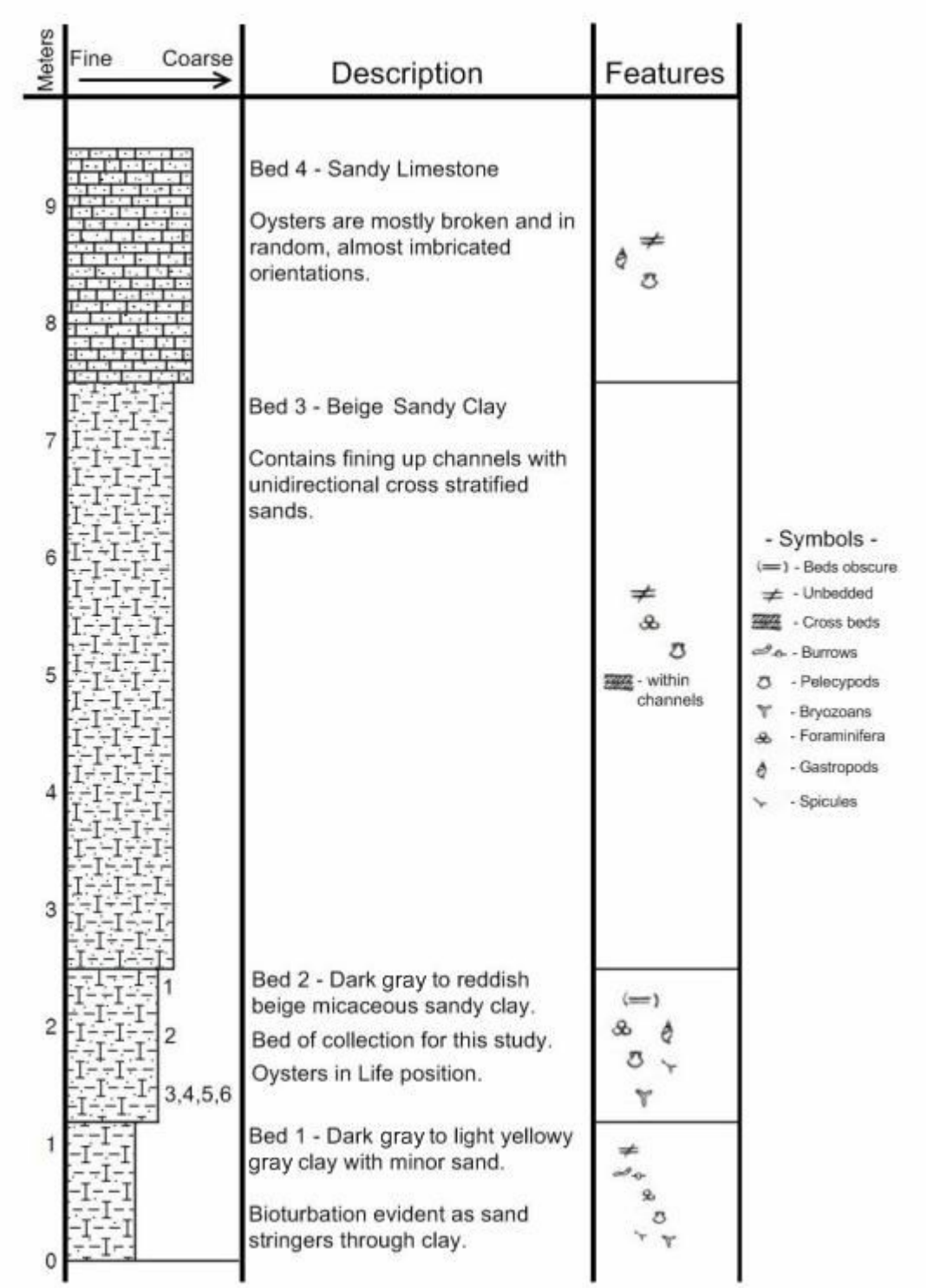
Meters
Fine
Coarse
Description
Features
9
8
7
6
5
4
3
2
1
0
Bed 4 - Sandy Limestone
Oysters are mostly broken and in random, almost imbricated orientations.
Bed 3 - Beige Sandy Clay
Contains fining up channels with unidirectional cross stratified sands.
- within channels
Bed 2 - Dark gray to reddish beige micaceous sandy clay.
Bed of collection for this study.
Oysters in Life position.
1
2
3,4,5,6
Bed 1 - Dark gray to light yellowy gray clay with minor sand.
Bioturbation evident as sand stringers through clay.
- Symbols -
(=) - Beds obscure
- Unbedded
- Cross beds
- Burrows
- Pelecypods
- Bryozoans
- Foraminifera
- Gastropods
- Spicules

Beds are mostly clay and dip to the south. 50 – 60 yards south of the boatramp at Griffins Landing, the lower beds begin to interfinger and eventually grade into the Utley Limestone Member of the underlying Clinchfield Formation. The Utley Limestone is easily distinguished by a more diverse bivalve fauna, presence of corals, and large (~1mm) angular quartz grains. Numerous ray teeth, hermit crab domiciles, and commatulid crinoids have been recovered but from talus scattered near river level making bed of origin uncertain. Beds are defined here as laterally continuous clay lithology and are divided based primarily on sedimentary structures and color.

Bed 4 - 2+m - Composed of a loosely indurated massively bedded very sandy limestone shell hash. Size of sand grains ranges from fine to coarse. The upper part of the bed contains abundant *Crassostrea gigantissima* shells often broken and in random almost imbricated orientation. In places, small broken shell fragments are parallel in orientation to each other displaying localized bedding (Figure 1E). Fossils include, abundant *Crassostrea gigantissima*, Balanoid barnacles, and Turritelid gastropods. The top of the bed caps the bluffs along the river at Griffins Landing.

Bed 3 - 5m - Massive calcareous buff white kaolinitic sandy clay. Contains channel deposits consisting of well stratified clay that show bioturbation between bedding planes as well as unidirectional cross bedded sands (Figure 1D). Few shark teeth were found at the base of this bed along with a well preserved clay gastropod cast. Numerous mussel casts have been recovered as well. No shells were collected from this bed.

Bed 2 – 1-1.3m - Dark gray to light yellowy gray clay with minor sand, grades upward into a reddish to beige clay at the upper contact with bed 3. Carbonized bioturbation abundant in places make the base easily distinguished from the upper part of bed 1 (Figure 1B). Mottled bedding is present along most of the exposure especially where oyster reefs of *C. gigantissima* exist in life position. Micah content is greater than that of bed 1 and is abundant between mottled bedding planes. Some oysters present and in life position. Some of the oysters show evidence of bioerosion by boring bivalves and clionid sponges. Contact is sharp at places between bed 2 and the overlying bed 3 (Figure 1C). This was the bed from which shells were acquired for Stable Isotope Analysis.

Bed 1 - 1.2m - Dark grey to light yellowy grey micaceous sandy clay. No apparent bedding present. Bioturbation is distinctly seen as highly sandy paths through clay (Figure 1A). Content of sand within the bed varies from almost no sand present to very sandy clay. Observations of deflocculated material showed quartz grains to be very angular. Where there is little sand, clay sometimes displays conchoidal fracture when broken. Contains *Crassostrea gitantissima* in life position, balanoid barnacles both loose and on oyster shells, as well as clay mussel casts and evidence of boring bivalves living within oyster shells. Bed was not sampled for shells containing isotope data because proximity to river level greatly increases the potential of meteoric diagenetic alteration of shells.

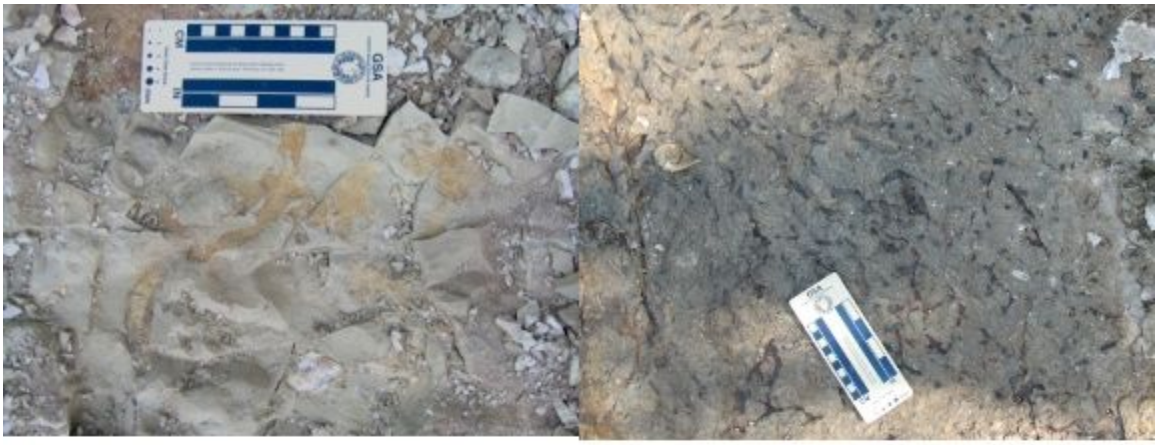

a) b)

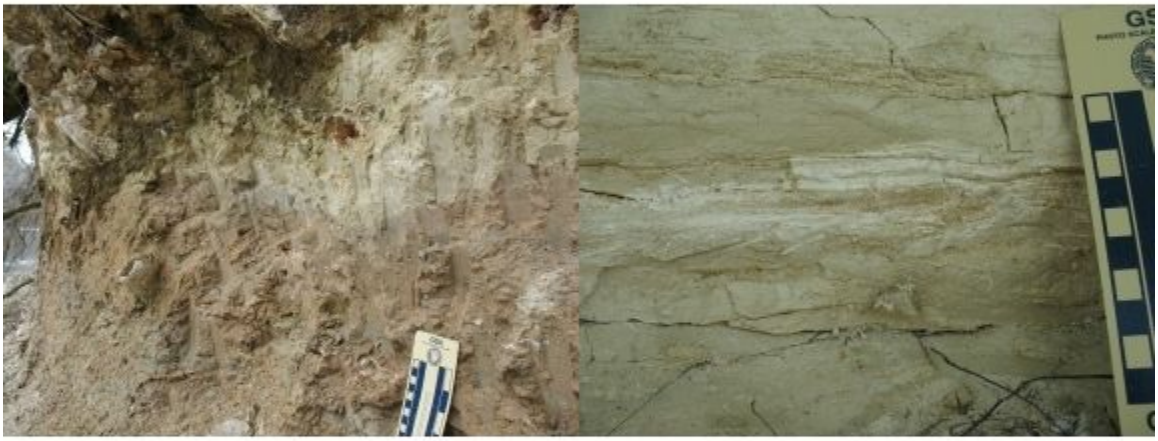

c) d)

e)

Appendix 2

Raw Isotope and Temperature Data

Shell 1 -

Sample #	mm	$\delta^{13}C$	$\delta^{18}O$	TºC
1	2.32	-0.53	-0.47	17.05
2	2.65	-0.67	-0.89	18.89
3	2.98	-0.51	-1.10	19.83
4	3.31	-0.40	-0.61	17.69
5	3.64	-1.10	-1.49	21.61
6	3.97	-0.58	-1.41	21.25
7	4.30	-0.98	-1.16	20.10
8	4.63	-0.62	-0.99	19.37
9	4.96	-0.69	-0.71	18.13
10	5.29	-1.01	-0.33	16.46
11	5.62	-0.75	-0.69	18.03
12	5.95	-0.86	-1.04	19.58
13	6.26	-1.21	-0.83	18.64
14	6.61	-0.80	-1.00	19.39
15	6.94	-1.17	-0.76	18.32
16	7.27	-1.06	-1.00	19.40
17	7.60	-1.30	-0.96	19.21
18	7.93	-1.25	-1.07	19.72
19	8.26	-1.37	-0.88	18.84
20	8.59	-1.60	-0.67	17.92
21	8.92	-1.15	-0.47	17.08
22	9.25	-0.86	0.20	14.24
23	9.58	-1.32	-0.13	15.62
24	9.91	-1.44	-0.86	18.79
25	10.24	-1.60	-0.87	18.82
26	10.57	-1.44	-0.76	18.31
27	10.90	-1.45	-0.75	18.31
28	11.23	-1.27	-0.61	17.68
29	11.56	-0.77	-0.54	17.36
30	11.69	-0.82	-0.46	17.01
31	12.22	-0.94	-0.58	17.56
32	12.55	-1.04	0.49	13.04
33	12.88	-0.94	0.57	12.68
34	13.21	-0.98	-0.82	18.60
35	13.54	-1.00	-0.69	18.03
36	13.87	-0.52	-0.55	17.43
37	14.20	-0.36	-0.26	16.14
38	14.53	-0.45	-1.08	19.77
39	14.86	-0.43	-1.09	19.82
40	15.19	-0.72	-1.73	22.73
41	15.52	-0.66	-1.56	21.96
	Min =	-1.60	-1.73	12.68
	Max =	-0.36	0.57	22.73
	Range =	1.24	2.30	10.04
	Avg =	-0.94	-0.75	18.30
	StDev=	0.35	0.47	2.07

Shell 2 -

Sample #	mm	$\delta^{13}C$	$\delta^{18}O$	TºC
1	2.1	-1	-0.88	19.4
2	2.38	-1.02	-1.03	19.49
3	2.66	-0.91	-1.02	19
4	2.94	-0.89	-1.43	18.91
5	3.22	-0.78	-0.95	18.42
6	3.5	-0.72	-0.95	18.15
7	3.78	-0.8	-1.35	18.51
8	4.06	-0.9	-0.76	18.95
9	4.34	-1.02	-1.11	19.49
10	4.62	-0.71	-1.01	18.11
11	4.9	-0.36	-0.74	16.59
12	5.18	-0.51	-0.84	17.24
13	5.46	-0.21	-0.85	15.94
14	5.74	-1.11	-2.17	19.89
15	6.02	-0.25	-1.17	16.11
16	6.3	-0.35	-1.08	16.54
17	6.58	-0.26	-0.99	16.16
18	6.86	-0.41	-1.23	16.8
19	7.14	-0.49	-1.13	17.15
20	7.42	-0.91	-0.92	19
21	7.7	-0.66	-0.99	17.89
22	7.98	-0.88	-0.97	18.86
23	8.26	-1.26	-1.44	20.57
24	8.54	-1.02	-0.83	19.49
25	8.82	-0.96	-1.53	19.22
26	9.1	-1.05	-0.87	19.62
27	9.38	-1.01	-0.82	19.44
28	9.66	-1.01	-0.85	19.44
29	9.94	-1	-0.83	19.4
30	10.22	-0.71	-0.71	18.11
31	10.5	-0.86	-0.77	18.77
32	10.78	-0.84	-0.86	18.69
33	11.06	-0.76	-1.63	18.33
34	11.34	-0.64	-0.93	17.8
35	11.62	-0.8	-0.91	18.51
36	11.9	-0.55	-0.64	17.41
37	12.18	-0.32	-0.64	16.41
38	12.46	-0.41	-0.66	16.8
39	12.74	-0.71	-0.89	18.11
40	13.02	-0.46	-1.37	17.02
41	13.3	-0.51	-1.44	17.24
42	13.58	-0.32	-0.67	16.41
43	13.86	-0.35	-0.63	16.54
44	14.14	-0.6	-0.88	17.63
45	14.42	-0.55	-0.49	17.41
46	14.7	-0.33	-1.01	16.46

47	14.98	-0.43	-0.70	16.89
48	15.26	-0.84	-0.95	18.69
49	15.54	-0.83	-0.86	18.64
50	15.82	-0.66	-0.82	17.89
51	16.1	-0.72	-0.96	18.15
52	16.38	-0.49	-0.95	17.15
53	16.66	-0.33	-0.76	16.46
54	16.94	-0.33	-1.01	16.46
55	17.22	-0.36	-0.83	16.59
56	17.5	-0.28	-0.68	16.24
57	17.78	-0.38	-0.70	16.67
58	18.06	-0.44	-0.74	16.93
59	18.34	-0.55	-1.04	17.41
60	18.62	-0.69	-1.06	18.02
61	18.9	-0.64	-0.93	17.8
62	19.18	-0.94	-0.72	19.13
63	19.46	-0.85	-0.89	18.73
64	19.74	-0.79	-0.72	18.46
65	20.02	-0.96	-0.41	19.22
66	20.3	-0.89	-0.69	18.91
67	20.58	-0.92	-0.92	19.04
68	20.86	-1.13	-1.03	19.98
69	21.14	-0.79	-1.04	18.46
70	21.42	-0.79	-1.04	18.46
71	21.7	-0.58	-0.24	17.54
72	21.98	-0.74	-0.43	18.24
73	22.26	-0.6	-0.34	17.63
74	22.54	-0.46	-0.33	17.02
	Min =	-1.26	-2.17	15.94
	Max =	-0.21	-0.24	20.57
	Range =	1.05	1.93	4.63
	Avg =	-0.68	-0.91	18
	StDev=	0.26	0.3	1.14

Shell 3 -

Sample #	mm	$\delta^{13}C$	$\delta^{18}O$	TºC
1	4.8	-1.7	-1.8	23.28
2	5.13	-2.0	-2.1	24.45
3	5.46	-2.3	-2.4	26.18
4	5.79	-2.2	-2.0	24.21
5	6.12	-1.7	-1.9	23.72
6	6.45	-1.4	-1.7	22.81
7	6.78	-0.9	-2.0	24.13
8	7.11	-0.1	-2.2	25.15
9	7.44	-0.2	-1.8	23.01
10	7.77	-0.5	-1.5	21.86
11	8.1	-0.3	-1.1	19.82
12	8.43	-0.4	-1.2	20.31
13	8.76	-0.3	-1.0	19.44
14	9.09	-0.2	-1.0	19.32
15	9.42	-0.3	-0.8	18.72
16	9.75	-0.5	-0.6	17.68
17	10.08	-0.6	-0.9	18.77
18	10.41	-0.6	-1.1	19.74
19	10.74	-0.8	-1.5	21.48
20	11.07	-0.3	-1.3	20.96
21	11.4	-0.5	-1.4	21.09
22	11.73	-1.1	-1.8	23.24
23	12.06	-1.6	-1.6	21.99
24	12.39	-1.3	-1.1	19.88
25	12.72	-1.6	-1.5	21.68
26	13.05	-1.5	-1.3	20.71
27	13.38	-1.8	-1.1	19.87
28	13.71	-1.3	-0.7	18.14
29	14.04	-1.2	-0.7	17.9
30	14.37	-1.1	-0.8	18.49
31	14.7	-1.2	-0.8	18.3
32	15.03	-1.3	-0.6	17.72
33	15.36	-1.2	-0.7	17.99
34	15.69	-1.3	-0.4	16.78
35	16.02	-1.0	-0.4	16.94
36	16.35	-1.2	-0.5	17.37
37	16.68	-1.1	-0.5	17.27
38	17.01	-1.4	-0.8	18.66
39	17.34	-2.2	-1.0	19.46
40	17.67	-2.2	-1.1	19.75
41	18	-2.2	-1.1	19.98
42	18.33	-2.0	-1.0	19.22
43	18.66	-1.4	-0.9	18.77
44	18.99	-1.6	-1.1	19.64
45	19.32	-1.4	-0.8	18.5
46	19.65	-1.6	-1.0	19.48

47	19.98	-1.4	-0.9	19.14
48	20.31	-1.1	-0.9	18.8
49	20.64	-1.4	-1.2	20.36
50	20.97	-1.5	-1.0	19.38
51	21.3	-1.7	-1.1	19.9
52	21.63	-1.3	-1.1	19.78
53	21.96	-1.0	-0.8	18.31
54	22.29	-1.0	-0.5	17.35
55	22.62	-0.9	-0.6	17.7
56	22.95	-0.7	-0.6	17.67
57	23.28	-0.7	-0.8	18.37
58	23.61	-2.4	-1.0	19.25
59	23.94	-1.2	-0.8	18.4
60	24.27	-2.7	-1.2	20.39
61	24.6	-2.6	-0.9	19.09
62	24.93	-2.5	-1.4	21.44
63	25.26	-1.7	-1.5	21.78
64	25.59	-1.3	-1.5	21.64
65	25.92	-1.5	-1.1	19.68
66	26.25	-0.8	-0.7	18.28
67	26.58	-2.6	-1.1	19.78
68	26.91	-2.0	-1.0	19.22
69	27.24	-1.2	-1.1	20.03
	Min =	-2.68	-2.45	16.78
	Max =	-0.09	-0.4	26.18
	Range =	2.59	2.04	9.4
	Average =	-1.31	-1.13	19.99
	StDev =	0.65	0.46	2.1

Shell 4 -

Sample #	mm	$\delta^{13}C$	$\delta^{18}O$	TºC
1	4.8	-1.1	-0.6	17.66
2	5.13	-2.5	-1.0	19.44
3	5.46	-3.3	-1.6	22.02
4	5.79	-4.0	-1.8	23.28
5	6.12	-4.3	-2.3	25.33
6	6.45	-4.5	-2.0	24.08
7	6.78	-3.5	-1.4	21.16
8	7.11	-4.6	-1.9	23.71
9	7.44	-4.6	-1.9	23.44
10	7.77	-3.8	-1.4	21.32
11	8.1	-2.3	-1.1	19.71
12	8.43	-1.0	-0.6	17.64
13	8.76	-2.0	-0.6	17.75
14	9.09	-3.0	-1.0	19.49
15	9.42	-4.1	-1.5	21.62
16	9.75	-4.9	-1.9	23.45
17	10.08	-3.0	-0.9	18.97
18	10.41	-3.2	-1.1	19.9
19	10.74	-3.3	-0.9	18.97
20	11.07	-3.3	-1.2	20.09
21	11.4	-4.1	-1.4	21.2
22	11.73	-4.0	-1.7	22.64
23	12.06	-4.0	-1.8	22.99
24	12.39	-4.5	-2.3	25.27
25	12.72	-3.8	-2.2	25.01
26	13.05	-1.2	-1.0	19.22
27	13.38	-3.8	-1.8	22.89
28	13.71	-3.1	-1.6	22.18
29	14.04	-2.2	-1.3	20.94
30	14.37	-1.4	-1.5	21.47
31	14.7	-1.2	-1.5	21.51
32	15.03	-0.7	-0.7	17.98
33	15.36	-0.9	-0.8	18.37
34	15.69	-1.3	-0.8	18.57
35	16.02	-2.1	-0.8	18.61
36	16.35	-3.1	-1.3	20.68
37	16.68	-3.1	-1.3	20.7
38	17.01	-3.3	-1.5	21.49
39	17.34	-3.3	-1.5	21.84
40	17.67	-3.3	-1.7	22.54
41	18	-3.7	-1.8	23.18
42	18.33	-4.2	-2.2	24.96

43	18.66	-4.1	-2.1	24.42
44	18.99	-4.2	-2.0	24
45	19.32	-3.1	-1.5	21.9
46	19.65	-2.1	-0.9	18.81
47	19.98	-1.2	-0.5	17.11
	Min =	-4.86	-2.27	17.11
	Max =	-0.75	-0.48	25.33
	Range =	4.11	1.79	8.21
	Average =	-3.04	-1.4	21.27
	StDev=	1.17	0.5	2.3

Shell 5 -

Sample #	mm	$\delta^{13}C$	$\delta^{18}O$	TºC
1	0	-1.3	-1.4	21.36
2	0.3	-0.6	-1.3	20.69
3	0.6	-0.4	-1.2	20.22
4	0.9	-0.4	-1.4	21.09
5	1.2	0.1	-0.9	19
6	1.5	0.1	-0.9	18.73
7	1.8	0.2	-0.6	17.61
8	2.1	-0.1	-0.6	17.82
9	2.4	-0.5	-0.5	17.06
10	2.7	-1.7	-1.2	20.08
11	3	-1.0	-1.2	20.34
12	3.3	-2.3	-1.5	21.77
13	3.6	-2.9	-1.9	23.32
14	3.9	-3.1	-1.9	23.62
15	4.2	-2.8	-1.9	23.72
16	4.5	-3.0	-1.9	23.58
17	4.8	-2.8	-2.0	24.23
18	5.1	-3.3	-2.2	24.88
19	5.4	-3.5	-2.4	25.71
20	5.7	-3.2	-2.3	25.36
21	6	-3.2	-2.3	25.57
22	6.3	-2.9	-1.9	23.49
23	6.6	-2.3	-1.7	22.69
24	6.9	-2.5	-1.5	21.75
25	7.2	-1.4	-1.5	21.85
26	7.5	-0.9	-1.3	20.74
27	7.8	-0.4	-1.2	20.26
28	8.1	-0.4	-1.4	21.23
29	8.4	-0.2	-1.1	19.98
30	8.7	-0.1	-0.9	18.8
31	9	0.1	-0.8	18.44
32	9.3	-0.1	-0.8	18.43
33	9.6	0.0	-0.9	18.9
34	9.9	-0.2	-0.9	18.84
35	10.2	-0.3	-1.0	19.49
36	10.5	-0.3	-1.4	21.43
37	10.8	-0.1	-1.0	19.58
38	11.1	-0.4	-1.1	19.85
39	11.4	-0.4	-1.5	21.87
40	11.7	-0.4	-1.5	21.46
41	12	-0.3	-1.4	21.31
42	12.3	-0.4	-1.6	22.15
43	12.6	-0.2	-1.5	21.51
44	12.9	-0.3	-1.1	19.67
45	13.2	0.1	-0.9	18.88
46	13.5	0.3	-0.7	18.18

47	13.8	0.1	-0.7	18.25
48	14.1	0.1	-0.6	17.52
49	14.4	0.2	-0.5	17.12
50	14.7	0.0	-0.7	17.95
51	15	-0.1	-0.5	17.31
52	15.3	0.1	-0.5	17.15
53	15.6	0.1	-0.4	16.87
54	15.9	0.0	-0.6	17.58
55	16.2	0.1	-0.6	17.61
56	16.5	0.0	-0.7	17.87
57	16.8	-0.1	-0.7	18.11
58	17.1	0.0	-0.8	18.59
59	17.4	0.2	-0.8	18.31
60	17.7	-0.5	-1.0	19.3
61	18	-1.7	-1.3	20.98
62	18.3	-1.6	-1.4	21.17
63	18.6	-1.9	-1.8	22.86
64	18.9	-1.5	-1.6	22.09
65	19.2	-1.7	-1.6	21.94
66	19.5	-1.1	-1.4	21.09
67	19.8	0.2	-1.0	19.58
68	20.1	-0.2	-0.6	17.62
69	20.4	0.3	-0.5	17.02
70	20.7	0.9	-0.3	16.22
	Min =	-3.51	-2.35	16.22
	Max =	0.95	-0.27	25.71
	Range =	4.46	2.08	9.49
	Average =	-0.82	-1.18	20.24
	StDev=	1.15	0.52	2.37

Shell 6 -

Sample #	mm	$\delta^{13}C$	$\delta^{18}O$	TºC
1	1.5	-0.9	-1.7	22.69
2	1.83	-0.4	-1.6	21.93
3	2.16	-1.2	-1.7	22.44
4	2.49	-1.2	-1.7	22.73
5	2.82	-1.2	-1.7	22.8
6	3.15	-0.4	-1.6	21.92
7	3.48	0.0	-1.3	20.7
8	3.81	0.0	-1.1	19.85
9	4.14	-0.3	-1.0	19.61
10	4.47	-1.8	-1.4	21.38
11	4.8	-2.3	-1.9	23.35
12	5.13	-3.7	-1.9	23.62
13	5.46	-4.6	-2.0	24.13
14	5.79	-4.5	-2.0	24.24
15	6.12	-3.9	-1.9	23.65
16	6.45	-2.1	-1.2	20.31
17	6.78	-2.5	-1.2	20.42
18	7.11	-3.0	-1.1	19.67
19	7.44	-2.0	-1.1	20.02
20	7.77	-2.8	-1.4	21.22
21	8.1	-3.3	-1.5	21.61
22	8.43	-4.0	-1.9	23.55
23	8.76	-4.4	-2.1	24.54
	Min =	-4.61	-2.11	19.61
	Max =	0.03	-1.05	24.54
	Range =	4.65	1.06	4.93
	Avg =	-2.2	-1.57	22.02
	StDev=	1.53	0.34	1.58

Diagenetic Data -

Sample	$\delta^{13}C$	$\delta^{18}O$
Shell 1 Foliated	0.22	-0.66
Shell_3_Recryst 1	-1.0	-2.5
Shell_3_Recryst 2	-2.7	-3.1
Shell_3_Recryst 3	-3.0	-3.1
Shell_3_Recryst 4	-2.1	-2.8
Shell_3_Recryst 5	-3.9	-3.3
Shell 4_DTS1	-5.5	-2.9
Shell 4_DTS2	-4.8	-2.4
Shell 4_DTS3	-4.4	-2.2
S6lum_1	-2.3	-1.9
S6lum_2	-3.2	-2.2
S6lum_3	-4.0	-2.8
S6lum_4	-4.4	-3.1
S6lum_5	-3.9	-2.3
S6lum_6	-4.0	-2.4
S6lum_7	-3.5	-2.4
S6lum_8	-3.6	-2.3
S6lum_9	-0.6	-1.6
S6lum_10	-2.5	-1.9
Shell 6-DLMC1_175	-6.2	-2.9
Shell 6_DLMC2_148	-7.0	-3.3
Shell 6_DLMC3_170	-6.3	-3.2
Shell 6-DLMC4_162	-5.6	-2.8
Shell 6-DLMC5_177	-6.9	-3.0
Shell 6_DLMC6_175	-5.8	-2.8
Shell 6_DLMC7_180	-5.7	-3.1
Shell 6-DLMC8_159	-6.4	-3.2
Shell 6_DLMC9_153	-6.2	-3.0
Shell 6 DLMC10_175	-6.7	-3.1
Shell_6_Crys_1	-1.0	-1.4
Shell_6_Crys_2	-1.0	-1.7
Shell_6_Crys_3	-0.8	-1.4
Shell_6_Crys_4	-1.3	-1.6
Shell_6_Crys_5	-1.9	-1.9
RDTS_1	-7.9	-3.1
RDTS_2	-8.3	-3.2
RDTS_3	-7.0	-3.4
RDTS_4	-7.2	-3.3
RDTS_5	-6.6	-3.3
RDTS_6	-6.3	-3.2
RDTS_7	-7.3	-3.5
RDTS_8	-7.0	-3.5
RDTS_9	-6.1	-2.8
RDTS_10	-4.6	-2.0
Min =	-8.3	-3.47
Max =	0.22	-0.66
Range =	8.52	2.81
Avg =	-4.46	-2.61
StDev=	2.31	0.68

Shell 6 Rejected Data -

Sample	$\delta^{13}C$	$\delta^{18}O$
Shell 6 Rejected	-3.9	-1.9
Shell 6 Rejected	-4.0	-2.2
Shell 6 Rejected	-4.2	-2.0
Shell 6 Rejected	-4.0	-2.0
Shell 6 Rejected	-4.6	-2.2
Shell 6 Rejected	-4.5	-2.6
Shell 6 Rejected	-4.6	-2.4
Shell 6 Rejected	-4.6	-2.3
Shell 6 Rejected	-4.5	-2.1
Shell 6 Rejected	-4.6	-2.1
Shell 6 Rejected	-5.0	-2.3
Shell 6 Rejected	-4.7	-2.3
Shell 6 Rejected	-4.5	-2.3
Shell 6 Rejected	-4.2	-2.1
Shell 6 Rejected	-4.2	-2.1
Shell 6 Rejected	-4.1	-2.0
Shell 6 Rejected	-4.0	-2.0
Shell 6 Rejected	-4.3	-2.0
Shell 6 Rejected	-5.1	-2.5
Shell 6 Rejected	-5.1	-2.6
Shell 6 Rejected	-4.7	-2.6
Shell 6 Rejected	-5.0	-2.7
Shell 6 Rejected	-4.9	-2.8
Shell 6 Rejected	-4.8	-2.7
Shell 6 Rejected	-4.4	-2.6
Shell 6 Rejected	-4.4	-2.4
Shell 6 Rejected	-4.3	-2.3
Shell 6 Rejected	-4.3	-2.2
Shell 6 Rejected	-4.7	-2.6
Shell 6 Rejected	-4.5	-2.3
Shell 6 Rejected	-4.4	-2.4
Shell 6 Rejected	-4.5	-2.5
Shell 6 Rejected	-4.2	-2.2
Shell 6 Rejected	-4.4	-2.4
Shell 6 Rejected	-4.1	-2.2
Shell 6 Rejected	-4.3	-2.3
Shell 6 Rejected	-1.9	-1.2
Min =	-5.11	-2.77
Max =	-1.86	-1.16
Range =	3.25	1.61
Average =	-4.38	-2.28
StDev =	0.53	0.3

Appendix 3

Raw Data Used to Construct Environmental Plots

- Range Plot -

Sample	Rng $\delta^{18}O$	Rng $\delta^{13}C$	Environment	Author	Year
BW20L1	2.75	3.25	Estuarine	Surge et al	2003
BW20L2	2.22	3.05	Estuarine	Surge et al	2003
BW20L3	2.42	3.57	Estuarine	Surge et al	2003
BW20L4	2.37	3.95	Estuarine	Surge et al	2003
BW20L5	2.92	3	Estuarine	Surge et al	2003
Miss-1	4.62	3.46	Estuarine	Kirby	1998
Miss-2	5.2	3.55	Estuarine	Kirby	1998
FU90L1	3.69	3.8	Estuarine	Surge et al	2003
FU90L2	3.39	3.86	Estuarine	Surge et al	2003
FU90L3	3.5	3.82	Estuarine	Surge et al	2003
FU90L4	3.36	4.37	Estuarine	Surge et al	2003
FU90L5	4.25	4.18	Estuarine	Surge et al	2003
FU90L6	4.6	4.34	Estuarine	Surge et al	2003
Pacific	4.5	1.8	Estuarine	Geary et al	1992
BOK1	4.52	2.49	Estuarine	Surge & Walker	2006
BOK2	4.61	2.1	Estuarine	Surge & Walker	2006
A	4.45	1.65	Estuarine	Klein et al.	1996
B	5.22	0.82	Estuarine	Klein et al.	1996
M1	5.9	2	Estuarine	Andreasson & Schmitz	1999
L1	6.3	2.5	Estuarine	Andreasson & Schmitz	1999
L2	5.6	2.5	Estuarine	Andreasson & Schmitz	1999
L3	5.6	2.5	Estuarine	Andreasson & Schmitz	1999
B1	2.26	1.31	Estuarine	Gillikin et al.	2004
B2	2.34	1.81	Estuarine	Gillikin et al.	2004
B3	2.01	1.12	Estuarine	Gillikin et al.	2004
COIBA-10	1.6	1.1	Marine	Beamis & Geary	1996
COLON-10	1	1.2	Marine	Beamis & Geary	1996
CANAL-24	0.7	1.4	Marine	Beamis & Geary	1996
Carribean	1.5	1.6	Marine	Geary et al.	1992
Florida	2.8	1.7	Marine	Geary et al.	1992
DS40*	4.44	1.2	Marine	Krantz et al.	1987
DS41*	2.99	1.11	Marine	Krantz et al.	1987
DS44*	2.59	1.57	Marine	Krantz et al.	1987
DS46*	2.43	2.09	Marine	Krantz et al.	1987
PM10*	2.27	1.9	Marine	Krantz et al.	1987
PM26*	2.64	1.93	Marine	Krantz et al.	1987
PEARL-10	2.2	0.7	Marine	Beamis & Geary	1996
PEARL-99	3.1	2.2	Marine	Beamis & Geary	1996
PARITA-20(k)	1.8	1.4	Marine	Beamis & Geary	1996
PARITA-20(o)	2.8	1.5	Marine	Beamis & Geary	1996
PARITA-20(a)	3	1.2	Marine	Beamis & Geary	1996
PARITA-33	1.8	0.9	Marine	Beamis & Geary	1996
PARITA-45	1.6	0.6	Marine	Beamis & Geary	1996
MOSQ-47	0.7	0.8	Marine	Beamis & Geary	1996
CANAL-68	0.8	0.8	Marine	Beamis & Geary	1996

DARIEN-70	1.5	1.3	Marine	Beamis & Geary	1996
STMART-16	1.4	1.3	Marine	Beamis & Geary	1996
GUAJIRA-27	1.8	0.9	Marine	Beamis & Geary	1996
VENEZ-55	2.6	1.8	Marine	Beamis & Geary	1996
brmd6	0.88	0.85	Marine	Carre et al.	2005
brmd7	1.17	0.91	Marine	Carre et al.	2005
brmd21	1.88	2.17	Marine	Carre et al.	2005
brmd24	1.22	0.98	Marine	Carre et al.	2005
M3	0.87	1.57	Marine	Carre et al.	2005
pmd2	1.01	1.23	Marine	Carre et al.	2005
lmd6	1.71	1.39	Marine	Carre et al.	2005
Naut	1.28	0.77	Marine	Auclaire et al.	2004
SWN35	2.78	0.83	Marine	Hickson et al.	1999
DOGB11	2.26	1.46	Marine	Hickson et al.	1999
DOGD25	2.55	1.24	Marine	Hickson et al.	1999
Spisula solidissima	3.84	1.4	Marine	Jones et al.	1983
MOC2	2.58	1.55	Marine	Kobashi et al.	2001
MOC3	3.06	2.32	Marine	Kobashi et al.	2001
MOC5	2.51	2.14	Marine	Kobashi et al.	2001
MOC6	3.1	1.53	Marine	Kobashi et al.	2001
MOC1	1.98	2.96	Marine	Kobashi et al.	2001
MOC4	2.56	2.69	Marine	Kobashi et al.	2001
C8	5.33	4.32	Marine	Mitchell et al.	1994
PCL-UN2	1.73	1.73	Lagoonal	Cerajewski	2002
PCL-BO2	2.05	1.7	Lagoonal	Cerajewski	2002
PCM-UN21	1.74	2.12	Lagoonal	Cerajewski	2002
PCM-UN22	1.43	3.29	Lagoonal	Cerajewski	2002
Rangia cuneata	1.51	3.56	Estuarine	Andrus and Rich	2008
P1006Mm	3.19	1.47	Estuarine	Surge et al.	2008
P1017Mm	3.52	1.89	Estuarine	Surge et al.	2008
P1048Mm	3.46	1.56	Estuarine	Surge et al.	2008
P1021Mc	3.27	2.84	Estuarine	Surge et al.	2008
P1036Mc	3.56	2.68	Estuarine	Surge et al.	2008
P1045Mc	3.41	2.43	Estuarine	Surge et al.	2008
P1002Mhy	2.93	2.21	Estuarine	Surge et al.	2008
P1038Mhy	3.11	1.59	Estuarine	Surge et al.	2008
P1046Mhy	3.08	1.06	Estuarine	Surge et al.	2008
NL-0101-2	1.82	1.07	Marine	Fenger et al.	2007
NL-0601-2	2.49	1.12	Marine	Fenger et al.	2007
NL-0601-3	2.8	2.07	Marine	Fenger et al.	2007

- Average Plot -

Sample	Environment	Avg $\delta^{18}O$	Avg ^{13}C	Author	Year
B1	Estuarine	-1.29	-0.67	Gillikin et al.	2004
B2	Estuarine	-1.1	-0.81	Gillikin et al.	2004
B3	Estuarine	-1.16	-0.44	Gillikin et al.	2004
BW1	Estuarine	-0.05	-6.21	Surge et al.	2003
BW2	Estuarine	-0.14	-6.96	Surge et al.	2003
BW3	Estuarine	-0.54	-7.11	Surge et al.	2003
BW4	Estuarine	-0.98	-7.07	Surge et al.	2003
BW5	Estuarine	-0.51	-7.13	Surge et al.	2003
FUL1	Estuarine	-0.91	-7.44	Surge et al.	2003
FUL2	Estuarine	-0.96	-7.09	Surge et al.	2003
FUL3	Estuarine	-1.39	-7.28	Surge et al.	2003
FUL4	Estuarine	-1.02	-7.24	Surge et al.	2003
FUL5	Estuarine	-0.8	-7.19	Surge et al.	2003
A	Estuarine	-2.54	-1.9	Klein et al.	1996
B	Estuarine	-2.22	-2.27	Klein et al.	1996
Florida	Marine	-0.8	0.4	Geary et al.	1992
Carribean	Marine	-1.1	2.2	Geary et al.	1992
RAJ-1 (jouvenile)	Marine	1.8	-1.92	Romanek & Grossman	1989
RAA-1	Marine	1.4	-1.22	Romanek & Grossman	1989
RAA-9	Marine	2.03	-0.97	Romanek & Grossman	1989
Terebra areolata	Marine	3.35	-1.32	Romanek & Grossman	1989
Chama cf. savignyi	Marine	1.81	-1.59	Romanek & Grossman	1989
brmd6	Marine	0.19	-0.04	Carre et al.	2005
brmd17	Marine	-0.14	0.1	Carre et al.	2005
brmd21	Marine	0.57	0.22	Carre et al.	2005
brmd24	Marine	0.3	0.26	Carre et al.	2005
M3	Marine	0.31	0.48	Carre et al.	2005
Pmd2	Marine	0.61	0.65	Carre et al.	2005
Lmd6	Marine	1.07	0.56	Carre et al.	2005
Spisula solidissima	Marine	-0.03	0.41	Jones et al.	1983
Nautilus macromphalus	Marine	0.37	1.3	Auclair et al.	2004
Coiba-10	Marine	-3.1	0.95	Beamis and Geary	1996
Pearl-10	Marine	-2.32	1.16	Beamis and Geary	1996
Colon-10	Marine	-0.07	-2.22	Beamis and Geary	1996
Stmart-16	Marine	-0.11	-1.45	Beamis and Geary	1996
Parita-20a	Marine	-0.21	-2	Beamis and Geary	1996
Parita-20k	Marine	-0.18	-2.95	Beamis and Geary	1996
Parita-20o	Marine	-0.18	-1.71	Beamis and Geary	1996
Canal-24	Marine	0.44	-1.83	Beamis and Geary	1996
Guajira-27	Marine	-1.4	0.07	Beamis and Geary	1996
Parita-33	Marine	-1.8	0.38	Beamis and Geary	1996
Parita-45	Marine	-1.01	-0.19	Beamis and Geary	1996
Mosq-47	Marine	-1.69	0	Beamis and Geary	1996
Venez-55	Marine	0.03	-1.17	Beamis and Geary	1996
Canal-68	Marine	-1.91	0.05	Beamis and Geary	1996
Darien-70	Marine	-1.77	0.08	Beamis and Geary	1996
Pearl-99	Marine	-0.52	-1.96	Beamis and Geary	1996

Pacific Shell	Marine	-2.29	0.02	Geary et al.	1992
SWN 35	Marine	-0.38	-0.13	Hickson et al.	1999
DOGB	Marine	0.5	0.01	Hickson et al.	1999
DOGD	Marine	0.35	0.01	Hickson et al.	1999
Miss-1	Estuarine	-2.58	-3.78	Kirby et al.	1998
Miss-2	Estuarine	-2.45	-4.04	Kirby et al.	1998
MOC2	Marine	0.19	1.88	Kobashi et al.	2001
Moc3	Marine	-0.59	1.11	Kobashi et al.	2001
Moc5	Marine	-0.73	1.4	Kobashi et al.	2001
MOC6	Marine	-0.7	2.45	Kobashi et al.	2001
MOC1	Marine	0.32	1.38	Kobashi et al.	2001
MOC4	Marine	0.56	1.6	Kobashi et al.	2001
DS40	Marine	0.92	0.78	Krantz et al.	1987
DS41	Marine	0.68	0.74	Krantz et al.	1987
DS44	Marine	1.09	0.54	Krantz et al.	1987
DS46	Marine	0.97	0.68	Krantz et al.	1987
PM10	Marine	1.65	1.45	Krantz et al.	1987
PM26	Marine	1.35	1.54	Krantz et al.	1987
PCL-UN2	Lagoonal	-0.26	0.09	Cerajewski	2002
PCL-BO2	Lagoonal	-0.58	1.05	Cerajewski	2002
PCM-UN21	Lagoonal	-0.04	2.39	Cerajewski	2002
PCM-UN22	Lagoonal	0.04	2.84	Cerajewski	2002
Rangia cuneata	Estuarine	-5.03	-8.71	Andrus and Rich	2008
P1006Mm	Estuarine	-0.65	-2.79	Surge et al.	2008
P1017Mm	Estuarine	-0.58	-2.44	Surge et al.	2008
P1048Mm	Estuarine	-1.1	-3.41	Surge et al.	2008
P1021Mc	Estuarine	-0.3	-2.58	Surge et al.	2008
P1036Mc	Estuarine	-0.68	-2.69	Surge et al.	2008
P1045Mc	Estuarine	-0.82	-2.56	Surge et al.	2008
P1002Mhy	Estuarine	-1.1	-2.78	Surge et al.	2008
P1038Mhy	Estuarine	-0.52	-2.88	Surge et al.	2008
P1046Mhy	Estuarine	-0.43	-2.57	Surge et al.	2008
NL-0101-2	Marine	1.93	0.99	Fenger et al.	2007
NL-0601-2	Marine	2.02	0.25	Fenger et al.	2007
NL-0601-3	Marine	1.96	-0.15	Fenger et al.	2007

Appendix 4

R-Code Used to Construct Plots

```
## Figure 2.2 ##

environplot <- function(x)
{
 plot(x$rng18o,x$rng13c, type="n", ylim=c(0.45,4.75),
    xlab=expression(delta^18*O), ylab=expression(delta^13*C),las=0)
 points((max(shell6[1:23,2])-min(shell6[1:23,2])),
    (max(shell6[1:23,1])-min(shell6[1:23,1])), pch=4, cex=1.4, col="RED")
 points((max(shell1[,2])-min(shell1[,2])),
    (max(shell1[,1])-min(shell1[,1])), pch=4, cex=1.4, col="RED")
 points((max(shell2[,2])-min(shell2[,2])),
    (max(shell2[,1])-min(shell2[,1])), pch=4, cex=1.4, col="RED")
 points((max(shell3[,2])-min(shell3[,2])),
    (max(shell3[,1])-min(shell3[,1])), pch=4, cex=1.4, col="RED")
 points((max(shell4[,2])-min(shell4[,2])),
    (max(shell4[,1])-min(shell4[,1])), pch=4, cex=1.4, col="RED")
 points((max(shell5[,2])-min(shell5[,2])),
    (max(shell5[,1])-min(shell5[,1])), pch=4, cex=1.4, col="RED")
 points(x$rng18o[x$Environment=="Marine"],
    x$rng13c[x$Environment=="Marine"], pch=16, col="BLUE")
 points(x$rng18o[x$Environment=="Estuarine"],
    x$rng13c[x$Environment=="Estuarine"], pch=17, col="GREEN")
 points(x$rng18o[x$Environment=="Lagoonal"],
    x$rng13c[x$Environment=="Lagoonal"], pch=1, cex=1.2)
 points(3.80,1.88, pch=8, cex=1.2)
 points(4.48,2.26, pch=8, cex=1.2)
}

##  Figure 2.3  ##

avgplot <- function(x)
{
 plot(x$avg18o,x$avg13c, type="n", xlim=c(min(x$avg18o),max(x$avg18o)),
    ylim=c(min(x$avg13c),max(x$avg13c)),
  xlab=expression(delta^18*O), ylab=expression(delta^13*C), las=0)
 points(x$avg18o[x$Environment=="Marine"],x$avg13c[x$Environment=="Marine"],
    pch=16, col="BLUE")
 points(x$avg18o[x$Environment=="Estuarine"],
    x$avg13c[x$Environment=="Estuarine"], pch=17, col="GREEN")
 points(x$avg18o[x$Environment=="Lagoonal"],
    x$avg13c[x$Environment=="Lagoonal"], pch=1, cex=1.2)
 points((mean(shell1[,2])+0.9),mean(shell1[,1]), pch=4, cex=1.4, col="RED")
 points((mean(shell2[,2])+0.9),mean(shell2[,1]), pch=4, cex=1.4, col="RED")
 points((mean(shell3[,2])+0.9),mean(shell3[,1]), pch=4, cex=1.4, col="RED")
 points((mean(shell4[,2])+0.9),mean(shell4[,1]), pch=4, cex=1.4, col="RED")
 points((mean(shell5[,2])+0.9),mean(shell5[,1]), pch=4, cex=1.4, col="RED")
```

```
  points((mean(shell6[1:23,2])+0.9),mean(shell6[1:23,1]), pch=4, cex=1.4,
     col="RED")
  points((-0.95+0.4),-0.32, pch=8, cex=1.2)
  points((-0.98+0.4),-0.69, pch=8, cex=1.2)
  abline(h=0)
  abline(v=0)
}

##  Figure 4.4  ##

isographox <- function(x, ttl="", sm=0.5, dw=-0.34, vertlns=NULL)
{
  par(las=1, mar=c(4.5,5.5,4,4.5), font.main=2)
  plot(x[,2], pch=8, cex=2, ylim=c(max(x[,2]), min(x[,2])), xlab=NA,
     ylab=NA, frame=FALSE, axes=FALSE)
  oxmin <- min(x[,2])
  oxrng <- (max(x[,2])-min(x[,2]))
  oxax <- c(oxmin,(oxmin+(oxrng*0.2)),(oxmin+(oxrng*0.4)),
     (oxmin+(oxrng*0.6)),(oxmin+(oxrng*0.8)),(oxmin+oxrng))
  oxax <- round(oxax, digits=2)
  axis(2, at=oxax, labels=oxax)
  #xspline(x[,2], lwd=1.5, shape=-0.5)
  g <- smooth.spline(x[,2], spar=sm)
  yvals <- g$y
  xvals <- g$x
  set <- c()
  for(i in 1:(length(yvals)-1))
  {
   inc <- i
   curry <- yvals[inc]
   prevy <- yvals[inc-1]
   nexty <- yvals[inc+1]
   if(i == 1)
   {
    prevy <- min(g$y)
   }
   if((curry > prevy) && (curry > nexty))
   {
    set[length(set)+1] <- xvals[i]
   }
  }
  shmean <- mean(x[,2])
  sdev <- sd(x[,2])
  cyc <- c()
  for(i in 1:length(set))
  {
```

```
  if(x[,2][set[i]] > (shmean + (sdev/2)))
  {
   cyc[length(cyc) + 1] <- set[i]
  }
 }
 abline(v=cyc, lwd=3)
 lines(g, lty=2, col="BLUE", lwd=2)
 points(g, pch=20, col="Blue", cex=2)
 abline(h=mean(x[,2]), lwd=2, col="RED")
 abline(h=(mean(x[,2])+(sd(x[,2])/2)), lwd=2, lty=2, col="RED")
 t <- c()
 for(i in 1:length(oxax))
 {
   t[i] <- 16.5 - (4.3*(oxax[i]-dw)) + (0.14*((oxax[i]-dw)^2))
 }
 t <- round(t, digits=1)
 axis(4, at=oxax, labels=t)
 mtext(ttl, cex=2.25, side=3, line=2, las=1, font=2)
 mtext(expression(delta^18*O), cex=1.5, side=2, line=2.8, las=1, font=2)
 mtext(expression(degree*C), cex=1.5, side=4, line=2.8, las=1, font=2)
 interv <- round((length(x[,1])/6), digits=0)
 mmax <- c(1, interv, (interv*2), (interv*3), (interv*4), (interv*5),
   (length(x[,1])))
 f <- row.names(x[mmax,])
 axis(1, at=mmax, labels=f)
 mtext("mm", cex=1.3, side=1, line=2.75, las=1, font=2)
}

##  Figures 4.5-4.10  ##

isograph <- function(x, ttl="", sm=0.5, dw=0, vertlns=NULL)
{
 windows(height=8.5,width=11)
 par(mfrow=c(2,1), las=1, mar=c(0,5.5,4,4.5), font.main=2)
 plot(x[,2], pch=20, cex=2, ylim=c(max(x[,2]), min(x[,2])), xlab=NA,
   ylab=NA, frame=FALSE, axes=FALSE)
 oxmin <- min(x[,2])
 oxrng <- (max(x[,2])-min(x[,2]))
 oxax <- c(oxmin,(oxmin+(oxrng*0.2)),(oxmin+(oxrng*0.4)),(oxmin+(oxrng*0.6)),
   (oxmin+(oxrng*0.8)),(oxmin+oxrng))
 oxax <- round(oxax, digits=2)
 axis(2, at=oxax, labels=oxax)
 xspline(x[,2], lwd=2, shape=-0.5)
 g <- smooth.spline(x[,2], spar=sm)
 yvals <- g$y
 xvals <- g$x
```

```
set <- c()
for(i in 1:(length(yvals)-1))
{
 inc <- i
 curry <- yvals[inc]
 prevy <- yvals[inc-1]
 nexty <- yvals[inc+1]
 if(i == 1)
 {
  prevy <- min(g$y)
 }
 if((curry > prevy) && (curry > nexty))
 {
  set[length(set)+1] <- xvals[i]
 }
}
shmean <- mean(x[,2])
sdev <- sd(x[,2])
cyc <- c()
for(i in 1:length(set))
{
 if(x[,2][set[i]] > (shmean + (sdev/2)))
 {
  cyc[length(cyc) + 1] <- set[i]
 }
}
abline(v=vertlns, lwd=2, lty=2, col="RED")
abline(v=cyc, lwd=3)
#lines(g, lty=2, col="BLUE", lwd=2)
#abline(h=mean(x[,2]), lty=2, lwd=2.5)
t <- c()
for(i in 1:length(oxax))
{
  t[i] <- 16.5 - (4.3*(oxax[i]-dw)) + (0.14*((oxax[i]-dw)^2))
}
t <- round(t, digits=1)
axis(4, at=oxax, labels=t)
mtext(ttl, cex=2.25, side=3, line=2, las=1, font=2)
mtext(expression(delta^18*O), cex=1.5, side=2, line=2.8, las=1, font=2)
mtext(expression(degree*C), cex=1.5, side=4, line=2.8, las=1, font=2)
#abline(h=max(x[,2]), lty=2, lwd=2.5)
#abline(h=min(x[,2]), lty=2, lwd=2.5)
par(mar=c(4.5,5.5,0,4.5))
plot(x[,1], pch=20, cex=2, frame=FALSE, axes=FALSE, ylab=NA, xlab=NA)
cmin <- min(x[,1])
crng <- (max(x[,1])-min(x[,1]))
```

```
  cax <- c(cmin,(cmin+(crng*0.2)),(cmin+(crng*0.4)),(cmin+(crng*0.6)),
     (cmin+(crng*0.8)),(cmin+crng))
  cax <- round(cax, digits=2)
  axis(2, at=cax, labels=cax)
  xspline(x[,1], lwd=2, shape=-0.5)
  abline(v=vertlns, lwd=2, lty=2, col="RED")
  abline(v=cyc, lwd=3)
  #abline(h=mean(x[,1]), lty=2, lwd=2.5)
  #abline(h=max(x[,1]), lty=2, lwd=2.5)
  #abline(h=min(x[,1]),lty=2, lwd=2.5)
  interv <- round((length(x[,1])/6), digits=0)
  mmax <- c(1, interv, (interv*2), (interv*3), (interv*4), (interv*5),
     (length(x[,1])))
  f <- row.names(x[mmax,])
  axis(1, at=mmax, labels=f)
  mtext(expression(delta^13*C), cex=1.5, side=2, line=2.8, las=1, font=2)
  mtext("mm", cex=1.3, side=1, line=2.75, las=1, font=2)
}

##  Figure 4.11  ##

plot(x=NULL, asp=0, xlim=c(-2.8, 0.8), ylim=c(-5.1, 0.9),
    xlab=expression(delta^18*O),
  ylab=expression(delta^13*C), axes=FALSE)
axis(2, at=c(-5,-4,-3,-2,-1,0,1),
    labels=c("-5.0","-4.0","-3.0","-2.0","-1.0","0.0","1.0"))
axis(1, at=c(-2.5,-2,-1.5,-1,-0.5,0,0.5),
    labels=c("-2.5","-2.0","-1.5","-1.0","-0.5","0.0","0.5"))
abline(h=0)
abline(v=0)
points(shell1[,2], shell1[,1], pch=15, cex=0.8)
sh1reg <- lm(shell1)
abline(sh1reg, lty=2, lwd=2)
points(shell2[,2], shell2[,1], pch=16, cex=0.8)
sh2reg <- lm(shell2)
abline(sh2reg, lty=2, lwd=2)
points(shell3[,2], shell3[,1], pch=17, cex=0.8)
sh3reg <- lm(shell3)
abline(sh3reg, lty=2, lwd=2)
points(shell4[,2], shell4[,1], pch=18, cex=0.8)
sh4reg <- lm(shell4)
abline(sh4reg, lty=2, lwd=2)
points(shell5[,2], shell5[,1], pch=19, cex=0.8)
sh5reg <- lm(shell5)
abline(sh5reg, lty=2, lwd=2)
points(shell6[1:23,2], shell6[1:23,1], pch=20, cex=0.8)
```

```
sh6reg <- lm(shell6[1:23,])
abline(sh6reg, lty=6, lwd=2)

## Figure 5.2 ##

spar <- read.csv(file="spar.csv", header=TRUE)
rec <- read.csv(file="rec.csv", header=TRUE)

plot(x=NULL, asp=0,las=3, xlim=c(-4, 1), ylim=c(-8.6, 1),
     xlab=expression(delta^18*O),
  ylab=expression(delta^13*C), axes=FALSE, frame=TRUE)
axis(2, at=c(-8,-6,-4,-2,0), labels=c("-8.0","-6.0","-4.0","-2.0","0.0"))
axis(1, at=c(-4,-3,-2,-1,0,1),
   labels=c("-4.0","-3.0","-2.0","-1.0","0.0","1.0"))
abline(h=0)
abline(v=0)
sh4reg <- lm(shell4)
abline(sh4reg, lty=2, lwd=2)
sh5reg <- lm(shell5)
abline(sh5reg, lty=2, lwd=2)
sh6reg <- lm(shell6[1:23,])
abline(sh6reg, lty=2, lwd=2)
allrec <- lm(rec$d13c~rec$d18o)
abline(allrec, lty=1, lwd=2, col="RED")
allspar <- lm(spar$d13c~spar$d18o)
abline(allspar, lty=1, lwd=2, col="RED")

##  Figure 5.3  ##

kirb <- read.csv(file="kirb.csv", header=TRUE)
surg <- read.csv(file="surg.csv", header=TRUE)

plot(x=NULL, asp=0,las=2, ylim=c(-10.0, 1.0), xlim=c(-5.6, 1.0),
   xlab=expression(delta^18*O),
  ylab=expression(delta^13*C))
points(kirb[,3], kirb[,2], pch=13)
kirbreg <- lm(kirb[,2]~kirb[,3])
abline(kirbreg)
points(surg[,3], surg[,2], pch=10)
surgreg <- lm(surg[,2]~surg[,3])
abline(surgreg)
points(shell1[,2], shell1[,1], pch=20)
sh1reg <- lm(shell1)
abline(sh1reg, lty=2, lwd=2)
points(shell2[,2], shell2[,1], pch=20)
sh2reg <- lm(shell2)
```

```
abline(sh2reg, lty=2, lwd=2)
points(shell3[,2], shell3[,1], pch=20)
sh3reg <- lm(shell3)
abline(sh3reg, lty=2, lwd=2)
points(shell4[,2], shell4[,1], pch=20)
sh4reg <- lm(shell4)
abline(sh4reg, lty=2, lwd=2)
points(shell5[,2], shell5[,1], pch=20)
sh5reg <- lm(shell5)
abline(sh5reg, lty=2, lwd=2)
points(shell6[1:23,2], shell6[1:23,1], pch=20)
sh6reg <- lm(shell6[1:23,])
abline(sh6reg, lty=2, lwd=2)

## Figure 5.6 ##

tcomp <- read.csv(file="tcomp.csv", header=TRUE)
mytcomp <- read.csv(file="mytcomp.csv", header=TRUE)
molltcomp <- read.csv(file="molltcomp.csv", header=TRUE)
ototcomp <- read.csv(file="ototcomp.csv", header=TRUE)

complot <- function(x, pect=NA)
{
 {
 plot(NULL, type="n", xlim=c(45, 28), asp=pect, frame=FALSE,
   ylim=c(8.5, 33), xlab="Age (ma)", ylab=expression(degree*C), las=1)
 arrows(x0=(x$Age), y0=(x$Tmin), x1=(x$Age), y1=(x$Tmax), angle=90, code=3,
 length=0.1, lwd=2)
 }
 points(x$Age, x$Tavg, pch=18, cex=2)
}
addata <- function(x)
{
 arrows(x0=(x$Age), y0=(x$Tmin), x1=(x$Age), y1=(x$Tmax), angle=90, code=3,
 col="GRAY",
   length=0.1, lwd=2)
 points(x$Age, x$Tavg, pch=20, cex=2)
}
complot(molltcomp, pect=0.5)
addata(ototcomp)
abline(v=33.7, lwd=2)
abline(v=37.1, lwd=2)
arrows(x0=(34.3), y0=(14.51), x1=(34.3), y1=(21.86), angle=90, code=3, lty=2,
length=0.1, lwd=2)
points(34.3, 19.65, pch=20, cex=2)
```